

FUJI ELECTRIC REVIEW

2014
Vol.60 No.



Power Semiconductors Contributing in Energy Management



FUJI ELECTRIC REVIEW

2014
Vol.60 No.

4

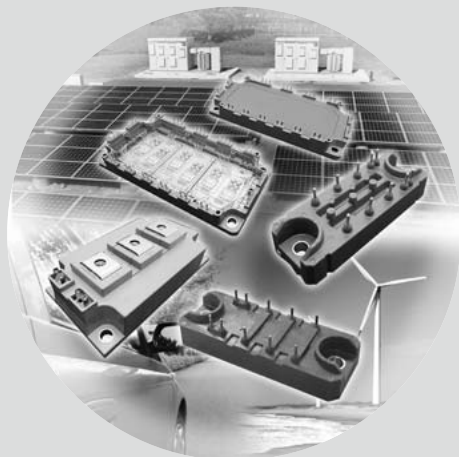
Power Semiconductors Contributing in Energy Management

Toward establishing low carbon societies, expectations are rising significantly for diffusion of renewable energy such as photovoltaic power generation and wind power generation as well as power electronics technology for using such energy efficiently. In order to meet these expectations, Fuji Electric is developing user-friendly power semiconductor products with high energy conversion efficiency and low noise for various sectors such as environment, energy, automobile, industrial machinery, social infrastructure and home appliances.

This special edition introduces the latest technology and products of power semiconductors, which are the key devices of power electronics technology.

Cover Photo (clockwise from the upper left):

SiC hybrid module (6-in-1 Package), IGBT module (6-in-1 Package), Industrial IGBT module (2-in-1 Package), All-SiC chopper module, SiC hybrid module (2-in-1 Package)



FUJI ELECTRIC REVIEW vol.60 no.4 2014

date of issue: December 30, 2014

editor-in-chief and publisher EGUCHI, Naoya

Corporate R & D Headquarters
Fuji Electric Co., Ltd.
Gate City Ohsaki, East Tower,
11-2, Osaki 1-chome, Shinagawa-ku,
Tokyo 141-0032, Japan
<http://www.fujielectric.co.jp>

editorial office Fuji Electric Journal Editorial Office
c/o Fuji Office & Life Service Co., Ltd.
1, Fujimachi, Hino-shi, Tokyo 191-8502,
Japan

Fuji Electric Co., Ltd. reserves all rights concerning the republication and publication after translation into other languages of articles appearing herein.

All brand names and product names in this journal might be trademarks or registered trademarks of their respective companies.

Contents

Power Semiconductors Contributing in Energy Management

1,200 V Withstand Voltage SiC Hybrid Module	210
KOBAYASHI, Kunio KITAMURA, Shoji ADACHI, Kazuya	

All-SiC Module for Mega-Solar Power Conditioner	214
NASHIDA, Norihiro NAKAMURA, Hideyo IWAMOTO, Susumu	

RC-IGBT Module with New Compact Package for Industrial Use	219
TAKAHASHI, Misaki YOSHIDA, Soichi HORIO, Masafumi	

RC-IGBT for Mild Hybrid Electric Vehicles	224
NOGUCHI, Seiji ADACHI, Shinichiro YOSHIDA, Soichi	

Packaging Technology of 2nd-Generation Aluminum Direct Liquid Cooling Module for Hybrid Vehicles	228
GOHARA, Hiromichi SAITO, Takashi YAMADA, Takafumi	

3rd-Gen. Critical Mode PFC Control IC “FA1A00 Series”	233
SUGAWARA, Takato YAGUCHI, Yukihiro MATSUMOTO, Kazunori	

Circuit Technology of LLC Current Resonant Power Supply	238
KAWAMURA, Kazuhiro YAMAMOTO, Tsuyoshi HOJO, Kota	

High Current IPS for Vehicle	243
IWAMIZU, Morio TAKEUCHI, Shigeyuki NISHIMURA, Takeyoshi	

New Products

1,700 V Withstand Voltage SiC Hybrid Module	247
AT-NPC 3-Level High-Power IGBT Module— Package for High-Power Module “M404 Package”	249
Discrete SiC-SBD	252
Product Line-Up of More Compact “MiniSKiiP” Packages	254

1,200 V Withstand Voltage SiC Hybrid Module

KOBAYASHI, Kunio* KITAMURA, Shoji* ADACHI, Kazuya*

ABSTRACT

Fuji Electric is working on the development of a 1,200 V withstand voltage SiC hybrid module as a power device for inverters that contribute to energy conservation. This hybrid module uses a SiC-Schottky barrier diode (SiC-SBD) chip, which has been developed jointly with the National Institute of Advanced Industrial Science and Technology and has been mass-produced by Fuji Electric. As the insulated-gate bipolar transistor (IGBT), Fuji Electric's latest 6th-generation "V Series" IGBT chip was adopted. For its 300 A products, the generated loss has been reduced by approximately 25% compared with conventional Si modules.

1. Introduction

Faced with the need to prevent global warming, the urgent task of reducing emissions of greenhouse gases such as CO₂ is greater than ever. One of the means to achieve their reduction targets is to ensure energy saving in power electronics devices. An important aspect of this is to improve inverter efficiency by having technological innovation for components such as power devices, circuits and controls. An insulated gate bipolar transistor (IGBT), a major power device for which customers have a strong demand for low loss, has used a silicon (Si) IGBT chip and free-wheeling diode (FWD) chip so far. However, Si devices are hitting the theoretical limit in terms of performance based on their physical characteristics. For this reason, there are high expectations for silicon carbide (SiC) devices because of their heat resistance exceeding the limit of Si and high breakdown field tolerance, and it is hoped they will improve equipment efficiency and achieve miniaturization.

This paper describes a 1,200 V withstand voltage SiC hybrid module (2-in-1 package), of which a product line has recently been established.

2. Product Features

Table 1 shows the lineup of Fuji Electric's SiC hybrid modules. Hybrid modules that have been commercialized up to now include those in EP and PC packages that use 600 V withstand voltage SiC-Schottky barrier diode (SiC-SBD) for the 200 V series and 1,200 V withstand voltage SiC-SBD for the 400 V series⁽¹⁾, and those in 2-in-1 packages that use 1,700 V withstand voltage SiC-SBD for the 690 V se-

Table 1 SiC hybrid module lineup

Application	Composition	Package
200 V series	600 V withstand voltage SiC-SBD + V Series IGBT	EP package and PC package
400 V series	1,200 V withstand voltage SiC-SBD + V Series IGBT	
400 V series	1,200 V withstand voltage SiC-SBD + V Series IGBT	2-in-1 package
690 V series	1,700 V withstand voltage SiC-SBD + V Series IGBT	2-in-1 package

□: Newly developed product



Fig.1 SiC hybrid module (2-in-1 package)

ries. Equipment that uses these hybrid modules can achieve a generated loss reduction of approximately 25% from that with the conventional Si-IGBT modules.

For the package of the 1,200 V withstand voltage SiC hybrid modules that have been built into a product line, a 2-in-1 package, as with Si modules, has been adopted (see Fig. 1). Adoption of 2-in-1 packages, which are widespread, in addition to the conventional EP and PC packages makes it possible to easily replace the conventional Si modules. Fuji Electric developed

* Electronic Devices Business Group, Fuji Electric Co., Ltd.

an SiC-SBD chip jointly with the National Institute of Advanced Industrial Science and Technology, followed by the Company's launch of a mass-production line. This chip has been applied to FWD, while IGBT has been equipped with Fuji Electric's latest product, the sixth-generation "V Series" IGBT chip. With 300 A products, the generated loss has been confirmed to be lower by approximately 25% from the conventional Si modules.

3. Features

3.1 Forward characteristics of FWDs

Figure 2 illustrates the forward characteristics of the FWDs of the SiC hybrid module and Si module. With a junction temperature T_j of 25°C and rated current of 300 A, the forward voltage V_F is at the same level as the Si module V_F . While the V_F at 125°C is

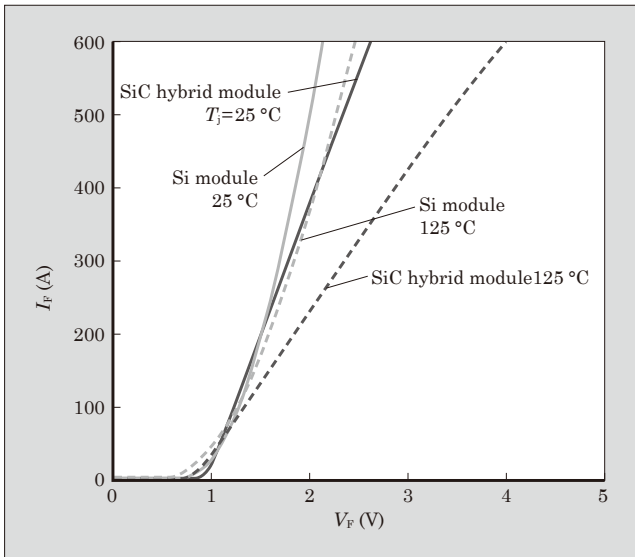


Fig.2 Forward characteristics of FWDs

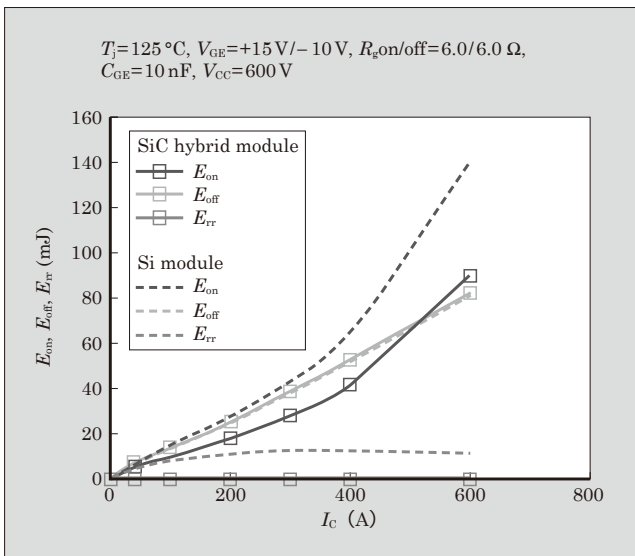


Fig.3 Switching loss

higher for the SiC hybrid module than for the Si module, the total loss is smaller for the SiC hybrid module as indicated in Section 3.2.

3.2 Switching loss

Figure 3 shows a comparison of the switching losses between the SiC hybrid module and Si module. Compared to the Si module, the turn-on loss E_{on} of the SiC hybrid module is smaller by approximately 35% and the reverse recovery loss E_{rr} is almost 0. Concerning the turn-off loss E_{off} , there is little difference between the SiC hybrid module and Si module.

(1) Turn-on waveforms

Figure 4 shows a comparison of turn-on waveforms. The peak reverse recovery current of the SiC-SBD has an effect on the IGBT turn-on current on the opposing arm side and the E_{on} of the SiC hybrid module is lower than that of the Si module by approximately 35%.

(2) Turn-off waveforms

Figure 5 shows a comparison of turn-off waveforms. The drift layer of SiC-SBD has an extremely low resistance compared to Si-FWD, and this lowers the transient on-voltage. Accordingly, the SiC hybrid module allows the surge voltage at turn-off to be held low.

(3) Reverse recovery waveforms

Figure 6 shows a comparison of reverse recovery waveforms. The SiC hybrid module scarcely has any peak reverse recovery current and the E_{rr} is almost 0. This is explained by the fact that SiC-SBD is a unipolar device, and so it causes no minority carrier injection.

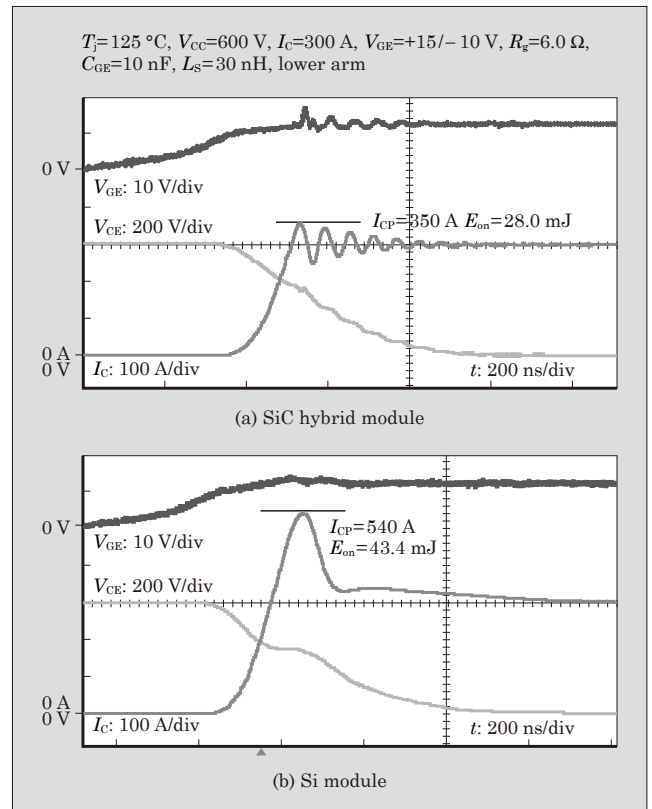


Fig.4 Turn-on waveforms

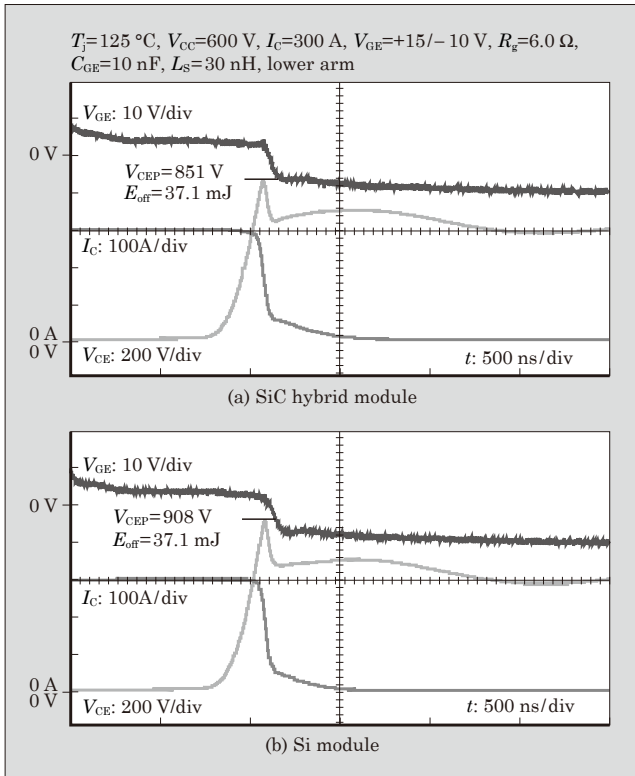


Fig.5 Turn-off waveforms

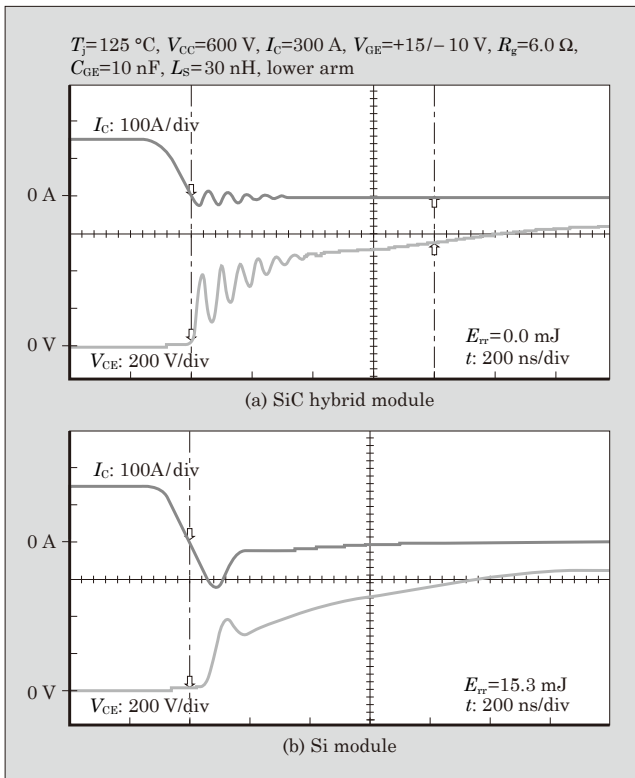


Fig.6 Reverse recovery waveforms

3.3 Load short circuit evaluation

Figure 7 shows load short circuit waveforms with the T_j of the SiC hybrid module varied from -40 to

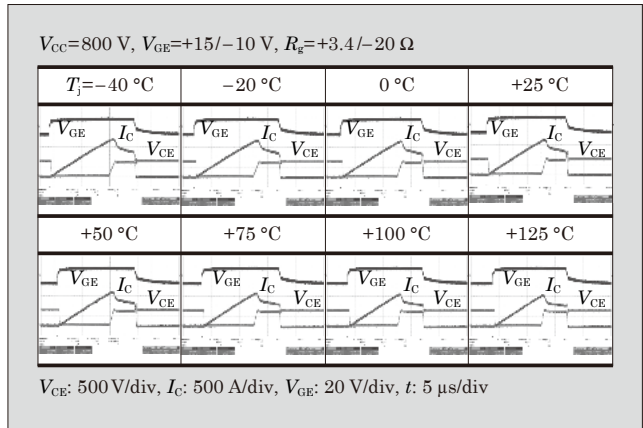


Fig.7 Load short circuit waveforms

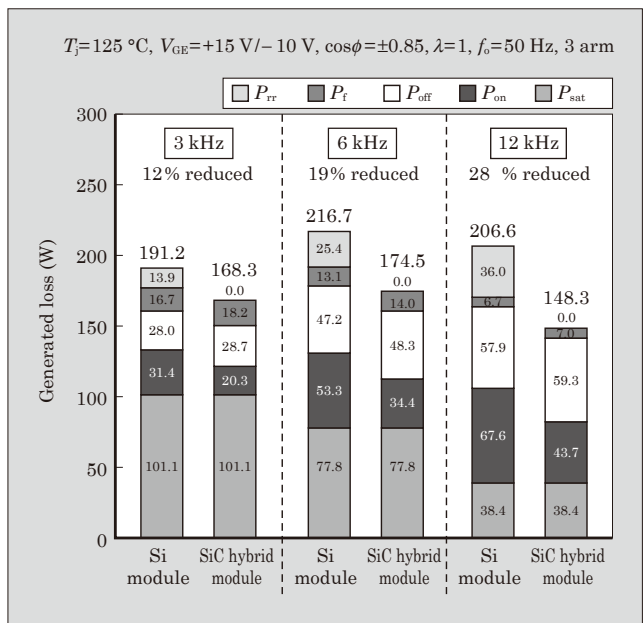


Fig.8 Inverter generated loss

$+125$ °C. It has been confirmed that no problem occurs in the range from low to high temperatures.

3.4 Inverter generated loss

As shown in Fig. 8, the generated loss of an inverter with the SiC hybrid module is lower than that with the Si module by 12 to 28% and the reduction rate is higher with a higher carrier frequency. This means that the SiC hybrid module is more advantageous in high-frequency operation.

4. Postscript

This paper has described the SiC hybrid module that deploys SiC-SBD, which was developed jointly with the National Institute of Advanced Industrial Science and Technology, and Fuji Electric's latest product, the sixth-generation "V Series" Si-IGBT. The SiC hybrid module has successfully attained a significant

loss-reduction within the device, probably enabling an efficiency enhancement for inverters to a great extent. In the future, we intend to continue applying SiC chip products and establishing various product lines to meet the withstand voltage, current capacity and package type demanded in the market. In this way, we aim to help prevent global warming by saving on the energy consumed by power electronics devices.

We would like to thank everyone at the Advanced

Power Electronics Research Center of the National Institute of Advanced Industrial Science and Technology who contributed to the development of the SiC-SBD chip.

References

- (1) Nakazawa, M. et al. Hybrid Si-IGBT and SiC-SBD Modules. FUJI ELECTRIC REVIEW. 2012, vol.58, no.2, p.70-74.



All-SiC Module for Mega-Solar Power Conditioner

NASHIDA, Norihiro* NAKAMURA, Hideyo* IWAMOTO, Susumu‡

ABSTRACT

An all-SiC module for mega-solar power conditioners has been developed. The structure developed for the all-SiC module has achieved a reduction in circuit inductance of approximately 80% from the existing structure that uses wire bonding. This allows for a significant reduction in loss, leading to an advantage in high-speed switching of SiC devices. In addition, it has shown a higher capability to thermal load in a power cycling test as compared with the conventional structure. We have developed an all-SiC chopper module for booster circuits by applying these technologies and integrated it in a mega-solar power conditioner, thereby achieving the world's highest level of efficiency of 98.8%.

1. Introduction

To realize a low carbon society, there has been a growing need to utilize renewable energy and save energy. Above all, power conversion technology is becoming increasingly important to efficiently use electric power, which is essential to our lives. In power conversion, power semiconductors play an important role. Recently, as next-generation semiconductors that replace silicon (Si) devices, which were the mainstream of power semiconductors, research and development efforts are actively in progress for power semiconductors that use wide-bandgap semiconductors of silicon carbide (SiC), gallium nitride (GaN), etc. Among them, SiC devices are increasingly being adopted for familiar power electronics products including consumer electronics as well as the industrial field and they are expected to be applied to an even wider range of products such as hybrid electric vehicles (HEVs) and electric vehicles (EVs).

This paper describes the technologies used for an all-SiC module equipped with SiC-metal-oxide-semiconductor field-effect transistor (SiC-MOSFET) and SiC-Schottky barrier diode (SiC-SBD) and application to a power conditioner (PCS) for mega-solar plants.

2. Characteristics of All-SiC Module

2.1 Module structure

Figure 1 shows cross-sectional views of modules with the developed and conventional structures. The structure developed for the all-SiC module greatly differs from that for conventional Si-insulated-gate bi-

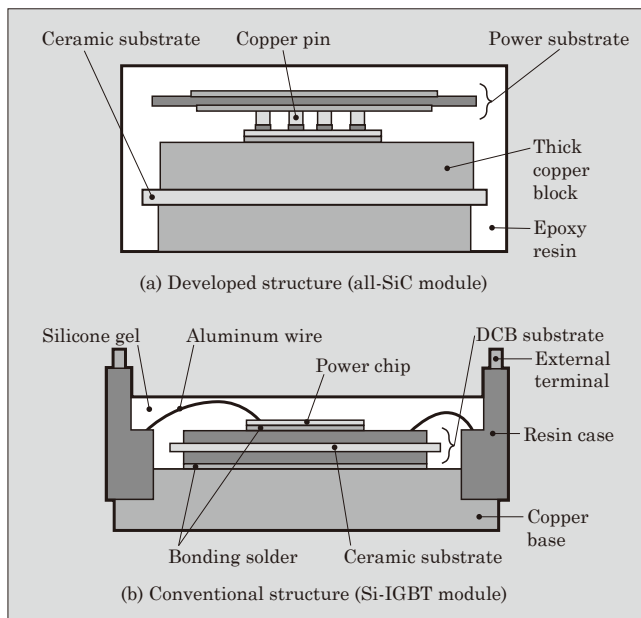


Fig.1 Cross-sectional views of modules

polar transistor (Si-IGBT) modules. In the developed structure, copper pins formed on the power substrate are used for interconnection instead of the conventional aluminum bonding wire. This allows a large current to be run and in turn high-density mounting of SiC devices. As the isolation substrate on which to mount the chip, in place of the conventional direct copper bonding (DCB) substrate, a Si_3N_4 (silicon nitride) ceramic substrate joined with a thick copper block is used for reducing thermal resistance. In addition, as the encapsulation material in the module, epoxy resin is used in place of the conventional silicone gel to ensure high reliability in high-temperature operation.

Figure 2 is a photo of the appearance of the all-SiC module in the new package and Si-IGBT module in the

* Corporate R&D Headquarters, Fuji Electric Co., Ltd.

‡ Electronic Devices Business Group, Fuji Electric Co., Ltd.

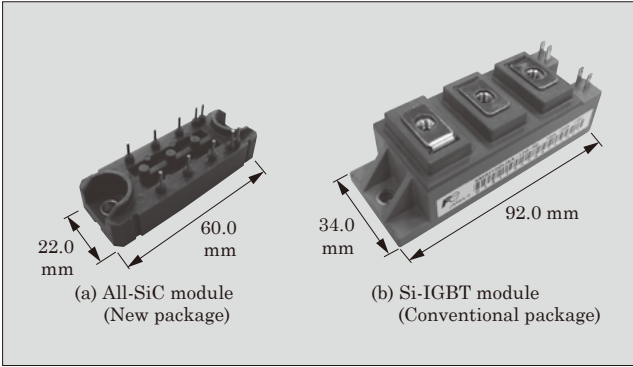


Fig.2 Appearance of modules

conventional package. Both modules have a rating of 1,200 V/100 A. The footprint of the new package has been reduced to approximately 40% of the conventional package.

2.2 Low-inductance design

(1) Inductance evaluation

As compared with Si-IGBT used for current power modules, SiC-MOSFET is capable of switching at a higher speed. However, because surge voltage generally increases in proportion to the switching speed, lowering the inductance of circuit in the module is important for reducing the impact of noise on gate signals.

Figure 3 shows a comparison of inductance between the gate circuit and main circuit. The comparison is based on the respective internal inductance of the gate circuit and main circuit determined by simulation with the conventional package, which is specified as 1. First, the inductance of the gate circuit has been confirmed to be reduced by approximately 80% from the conventional package. The same evaluation has also been conducted with the main circuit, which has verified that the new package achieves an approximately 80% reduction from the conventional package both in analysis and actual measurement.

These results show that, in the new package, the

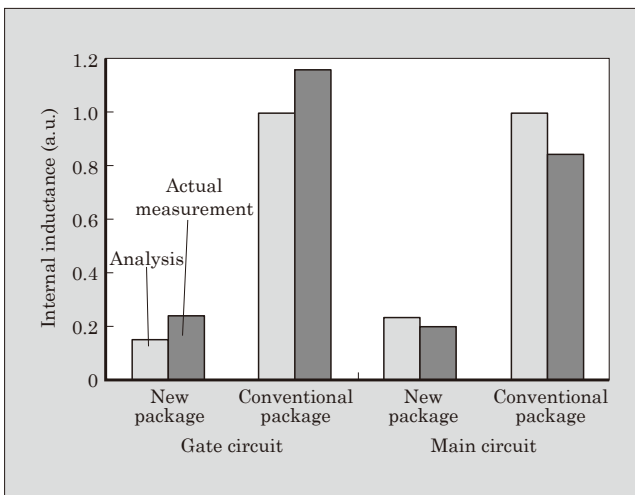


Fig.3 Inductance of gate circuit and main circuit

current pathways have been shortened by miniaturizing the module with the power substrate and a low-thermal-resistance isolation substrate, that significantly contributes to reducing the inductance. In addition, the power substrate and thick copper block are arranged in parallel and the magnetic field interactions between the current pathways reduces the inductance.

(2) Loss comparison

In order to verify the effect of the lower inductance of the all-SiC module, modules with the same SiC devices mounted in the new and conventional packages have been built to conduct a switching test. As shown in Fig. 4, the new package has achieved an approximately 50% reduction in the switching loss as compared with the conventional package. This is because of the surge voltage suppression effect of the new package with lower inductance.

Figure 5 shows a comparison of the total loss in the switching frequency range from 10 to 100 kHz. The total loss consists of the switching loss and on-state loss and the comparison is based on the total loss at 10 kHz with SiC-MOSFET mounted in the conventional package, which is specified as 1. With the conventional package, the switching loss increase becomes larger with a higher switching frequency and the total loss at 100 kHz is 2.2. Meanwhile, the loss increase is smaller

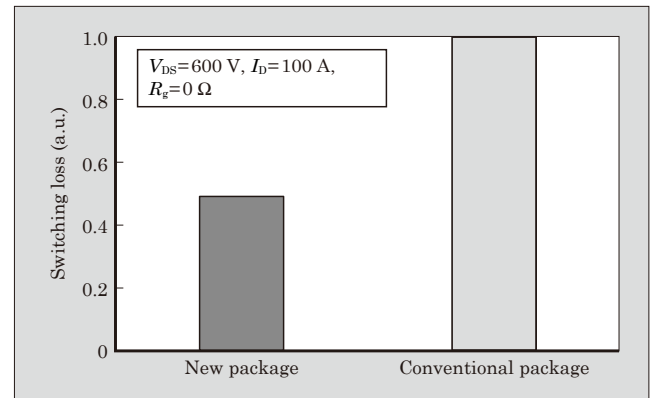


Fig.4 Switching loss of modules with SiC devices

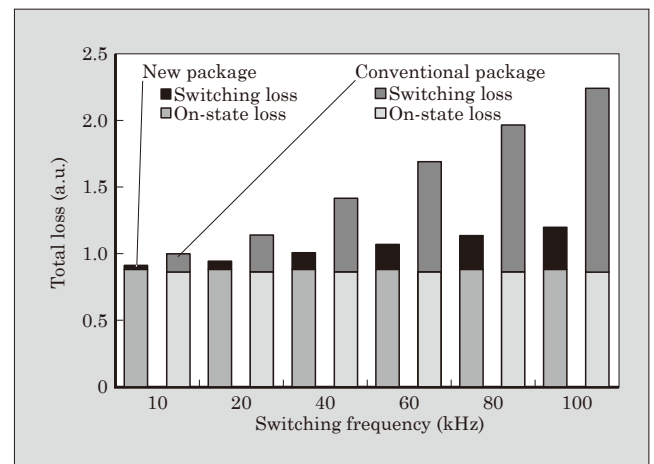


Fig.5 Total loss

with the new package and limited at 1.2. Focusing on the breakdown of the loss, the on-state loss is almost the same between the conventional and new packages and no frequency dependence is observed. In addition, the switching loss with the conventional package is more than 4 times higher than with the new package at any of the frequencies, which shows that it accounts for a larger proportion of the entire loss as the frequency increases. In this way, the new package, which has successfully reduced the internal inductance of the module, has been confirmed to be advantageous for high-speed switching of SiC devices.

2.3 High reliability

(1) ΔT_j power cycling test

In a power module, thermal stress is generated by temperature rise during device operation, which may cause breakage of a chip junction, etc. A ΔT_j power cycling test is a reliability test for evaluating the lifetime of a power module by repeating this device operation.

Figure 6 shows a comparison of ΔT_j power cycling test lifetime. With the test starting temperature at 25°C, the figure plots the temperature amplitude ΔT_j along the horizontal axis and the number of cycles with a cumulative failure rate of 1% [$F(t)=1\%$] along the vertical axis. The solid line shows the power cycling lifetime of the conventional package equipped with Si devices and the plot (O) is the lifetime verified with the new package equipped with Si devices. This result shows that, with the test condition $\Delta T_j=150^\circ\text{C}$, the new package is expected to offer a lifetime more than ten times longer than that of the conventional package.

Accordingly, implantation and epitaxial metal oxide semiconductor (IEMOS), which is the SiC-MOSFET jointly developed with the National Institute of Advanced Industrial Science and Technology, has been mounted in the new package to conduct a power cycling test with $\Delta T_j=150^\circ\text{C}$. The test result confirmed that 50,000 cycles with $F(t) = 1\%$, a lifetime improved by more than 20 times from the conventional package equipped with Si devices, has been achieved⁽¹⁾ (see plot

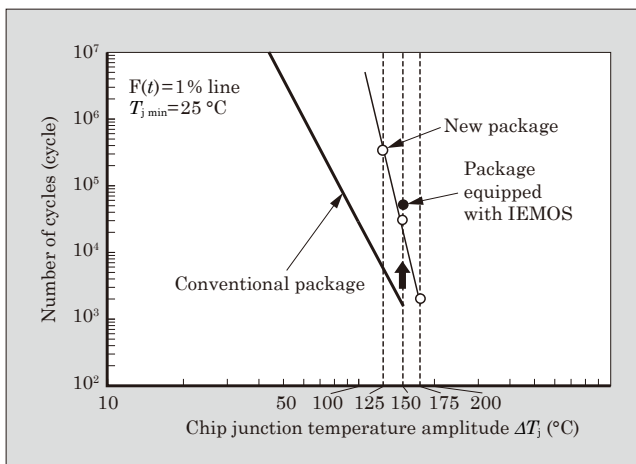


Fig.6 ΔT_j power cycling test lifetime

● in Fig. 6). With the conventional package, breakage such as separation of the chip electrode from wire bonding occurs as the operation temperature increases, and this reduces the lifetime⁽²⁾. Meanwhile, the new package is encapsulated in epoxy resin with high heat resistance and breakage of junction between the chip electrode and copper pin is restrained by mitigating the thermal stress generated during operation. In addition, an epoxy resin with a glass transition temperature T_g of 200°C or higher has been developed⁽³⁾, which limits variations in mechanical and physical properties such as linear expansion coefficient and elastic modulus to a certain extent within the range of operating temperature and achieves high reliability.

(2) ΔT_c power cycling test

For mounting in a PCS for photovoltaic power generation (solar PCS) of a mega-solar plant, etc., the operation modes must be grasped to conduct a reliability test. A solar PCS operates in continuous mode during power generation in the daytime and stops during the night-time. To verify the thermal load on the module in that process, it is also important to conduct a ΔT_c power cycling test with a varying module surface temperature T_c during operation.

Figure 7 shows a scanning acoustic tomograph image of a sample subjected to a ΔT_c power cycling test with the conventional package structure. After 20,000 cycles, breakage is generated in the solder bonding between the copper base and DCB substrate, which is not observed before the test, and the thermal resistance is estimated to have increased and caused the failure. With the new package, however, the structure does not include a copper base and the types of failure seen with the conventional package are unlikely but the durability of the junction between the isolation substrate and the chip has an impact on the lifetime in the ΔT_c power cycling test. Given this factor, with the test starting temperature of 25°C and the $\Delta T_c=80^\circ\text{C}$ condition, changes in the thermal resistance of the new package in the ΔT_c power cycling test have been verified (see Fig. 8). Thermal resistance along the vertical axis is based on the initial values of the respective samples to show variations. The result shows that, variations in the thermal resistance are confined within 7% of the initial values even after 25,000 cycles and no increasing tendency is observed.

Figure 9 shows a scanning acoustic tomograph image of the chip bottom junction of the package before

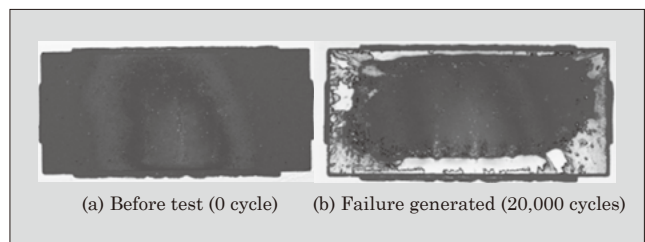


Fig.7 Scanning acoustic tomograph image of conventional package structure in ΔT_c power cycling test

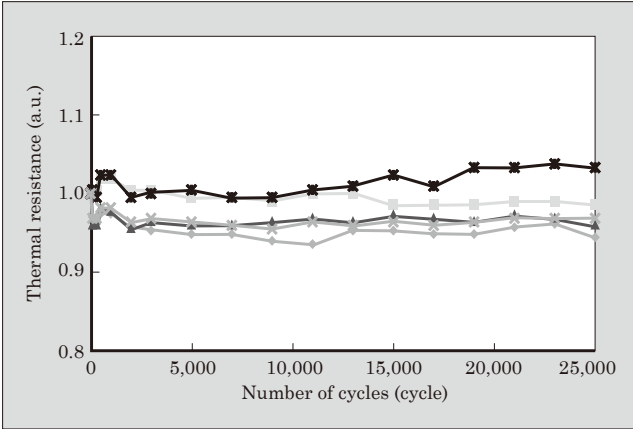


Fig.8 Changes in thermal resistance of new package structure in ΔT_c power cycling test

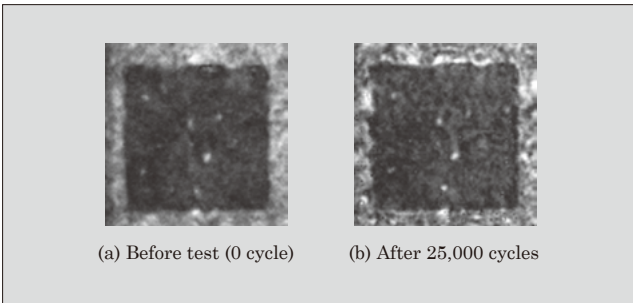


Fig.9 Scanning acoustic tomograph image of chip bottom solder bonding in ΔT_c power cycling test

and after the ΔT_c power cycling test. As compared with before the test, no change in the bonding condition has been observed even after 25,000 cycles. In addition, no crack in the ceramic substrate or separation of the thick copper block is observed, which confirms that the new package has sufficient durability for application to a PCS.

3. Application to Power Conditioner for Mega-Solar Plants

In mega-solar plants or other types of photovoltaic power generation, the DC voltage generated in photovoltaic cells is converted into AC voltage by PCS for transmission. Photovoltaic power generation has an issue of reduced conversion efficiency of the PCS due to a voltage reduction caused by a decrease in insolation or rise in temperature. One solution is to equip the PCS with a booster circuit (chopper circuit). This method makes it possible to raise the minimum input voltage to the inverter for conversion into AC voltage, which improves the AC voltage output along with the rise in the minimum input voltage. By applying the SiC devices to the booster circuit, generated loss of the boost converter can be suppressed, and this raises expectations for an improvement in the conversion efficiency of the entire PCS including the inverter. Furthermore, the boost converter, which requires a

volume equivalent to that of the inverter with the conventional Si devices, can be miniaturized by using SiC devices. Accordingly, we have applied the new package described up to now to develop an all-SiC chopper module for booster circuits that uses the features of SiC devices (see Fig. 10).

The SiC devices mounted in the all-SiC chopper module are IEMOS and SiC-SBD, jointly developed with the National Institute of Advanced Industrial Science and Technology, and they are mass-produced at our Matsumoto Factory (see Fig. 11). Figure 12 shows the appearance of the PCS for mega-solar plants equipped with this all-SiC chopper module. It measures $2,980 \times 900 \times 1,900$ (mm) and realizes an output apparent power of 1,000 kW, which is among the



Fig.10 All-SiC chopper module



Fig.11 6-inch SiC wafer



Fig.12 Power conditioner for mega-solar plants

world's highest as an indoor system. By applying the all-SiC chopper module that has been developed to the booster circuit, the loss has been successfully reduced and the world's highest-class PCS conversion efficiency of 98.8% has been achieved (98.5% with the conventional product)⁽⁴⁾. In addition, circuit miniaturization has also been realized to achieve a 20% size reduction from the conventional switchboard, which contributes to a reduction in installation costs including transportation cost.

4. Postscript

We have developed an all-SiC chopper module for PCS for mega-solar plants, achieved the world's highest-class conversion efficiency of 98.8%, which was difficult with Si devices, and realized miniaturization of equipment.

In the future, we intend to contribute to the real-

ization of a low carbon society by applying the all-SiC module to various power electronics devices to improve energy utilization efficiency.

References

- (1) Nashida, N. et al. "All-SiC Power Module for Photovoltaic Power Conditioner System". Proceedings of ISPSD 2014. p.342-345.
- (2) Momose, F. et al. New Assembly Technologies for T_j max =175°C Continuous Operation Guaranty of IGBT Module. FUJI ELECTRIC REVIEW. 2013, vol.59, no.4, p.226-229.
- (3) Horio, M. et al. "Ultra Compact and High Reliable SiC MOSFET Power Module with 200°C Operating Capability". Proceedings of ISPSD 2012. p.81-84.
- (4) Fujii, K. et al. "PVI1000": Outdoor High-Efficiency Power Conditioners for Mega Solar Projects. FUJI ELECTRIC REVIEW. 2012, vol.58, no.4, p.202-206.



RC-IGBT Module with New Compact Package for Industrial Use

TAKAHASHI, Misaki* YOSHIDA, Soichi* HORIO, Masafumi‡

ABSTRACT

Fuji Electric has developed an reverse conducting IGBT (RC-IGBT) for industrial use and it integrates an IGBT and freewheeling diode (FWD). We have combined it with a new package that achieves both low thermal resistance and high reliability to successfully realize a significant miniaturization of the IGBT module and power density improvement. The RC-IGBT has reduced power loss to a level equivalent to that of the conventional IGBT+FWD and achieved a reduction in thermal resistance of 30%. The new module, combining the RC-IGBT and new package, which has a footprint 42% that of the conventional module, realizes an almost equivalent inverter loss and a significant reduction in the IGBT junction temperature. A comparison based on the same IGBT junction temperature shows that it operates with a 58% larger output current.

1. Introduction

Recently, from the perspective of preventing exhaustion of fossil fuel and global warming, improvement of energy efficiency and reduction of CO₂ have been called for. As one important item for that purpose, demand for inverters is increasing. As power semiconductors for inverter use, insulated-gate bipolar transistor (IGBT) modules are widely applied in the industrial, consumer, automobile and renewable energy fields.

Ever since their commercialization in 1988, Fuji Electric's IGBT modules have achieved significant miniaturization by many technological innovations and contributed to miniaturization and cost reduction of inverters. However, while the size of IGBT module becomes smaller, the power density and operating temperature of IGBT module are increasing. These trends have negative effects on the reliability and lifetime of IGBT module. To realize a compact module with high reliability, technological innovations of IGBT chips and packages are necessary.

In order to enable compact IGBT module with high reliability, Fuji Electric has developed a reverse-conducting IGBT (RC-IGBT⁽¹⁾⁻⁽⁴⁾) for industrial use, which integrates IGBT and free wheeling diode (FWD), and combined it with a new package⁽⁵⁾⁻⁽⁸⁾ that has achieved both low thermal resistance and high reliability.

2. Characteristics of RC-IGBT and New Package

2.1 Characteristics of RC-IGBT

- (1) Parts count reduction and miniaturization of IGBT module

* Electronic Devices Business Group, Fuji Electric Co., Ltd.

‡ Corporate R&D Headquarters, Fuji Electric Co., Ltd.

Figure 1(a) shows a half-bridge inverter circuit, which is the main circuit of a pulse-width modulation (PWM)-controlled inverter. The conventional IGBT is a switching device that can conduct a current only in the direction from the collector to the emitter; therefore an FWD is required for conducting the reverse current. The RC-IGBT developed is an IGBT device

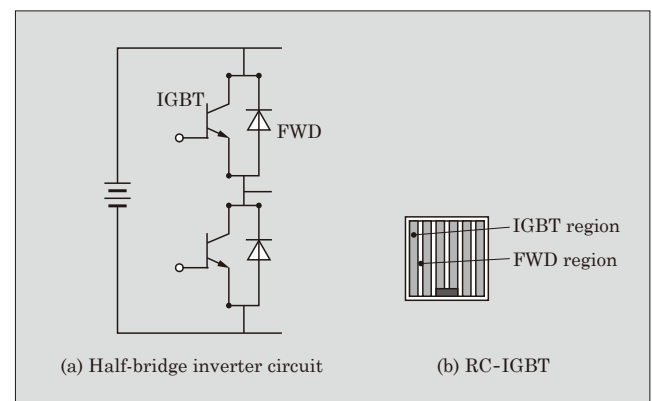


Fig.1 Half-bridge inverter circuit and RC-IGBT

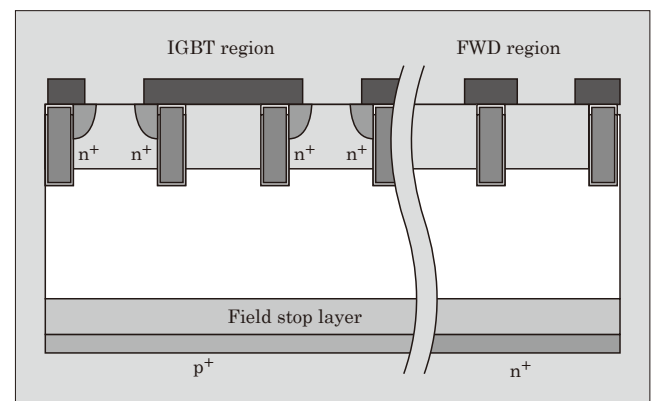


Fig.2 Cross-sectional view of RC-IGBT

capable of running the current in the reverse direction by integrating FWD as shown in Fig. 1(b) and allows reduction in the parts count of the applied circuit and miniaturization of the equipment.

As shown in Fig. 2, an RC-IGBT is a trench gate thin wafer IGBT based on the 6th-generation IGBT “V Series,” which is Fuji Electric’s latest product line. The manufacturing process is almost the same as that of the conventional IGBTs, and includes the process for forming the p-layer/n-layer on the back side and lifetime control process.

(2) Output characteristics and switching waveforms

Figure 3 shows output characteristics of the RC-IGBT. The RC-IGBT is capable of outputting current in the forward direction (IGBT) and reverse direction (FWD) with one chip. Three RC-IGBTs with different lifetime control amounts have been prepared as A, B and C to compare the output characteristics. A, with the smallest control amount, shows the smallest elec-

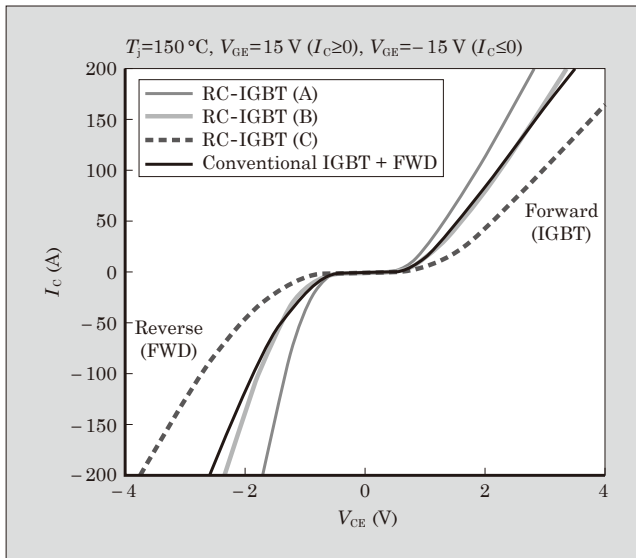


Fig.3 Output characteristics of RC-IGBT

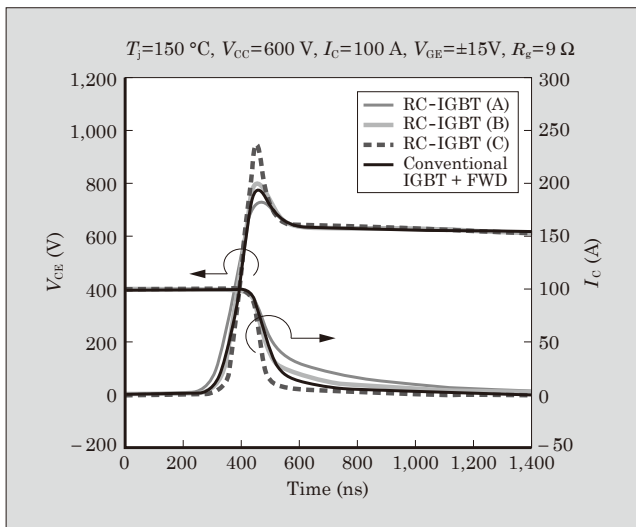


Fig.4 Turn-off waveforms of RC-IGBT

tric resistance for both the IGBT and FWD operation.

RC-IGBT turn-off waveforms are shown in Fig. 4, turn-on waveforms in Fig. 5 and reverse recovery waveforms in Fig. 6. While IGBT and FWD have conventionally been used as the switching element and reverse conducting element respectively, with an RC-IGBT, the RC-IGBT alone is responsible for switching for both the switching and reverse conducting elements. The switching waveforms of the RC-IGBT (B) are almost the same as those of the conventional IGBT + FWD and combination of RC-IGBTs allows switching operation similar to that of the conventional device. In addition, C with the largest lifetime control amount shows the smallest IGBT tail current at turn-off and FWD reverse recovery current at reverse recovery. The IGBT loss trade-off of RC-IGBT is shown in Fig. 7 and FWD loss trade-off in Fig. 8. RC-IGBT has similar loss trade-off characteristics to those of the conventional IGBT and FWD and the lifetime control amount can be used to adjust the trade-off from A with low con-

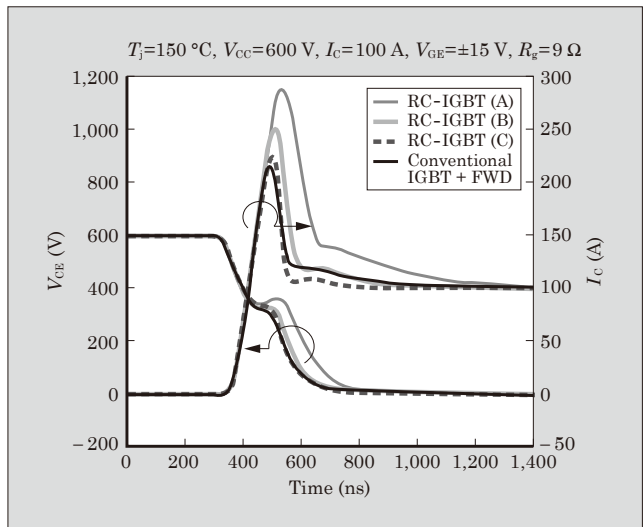


Fig.5 Turn-on waveforms of RC-IGBT

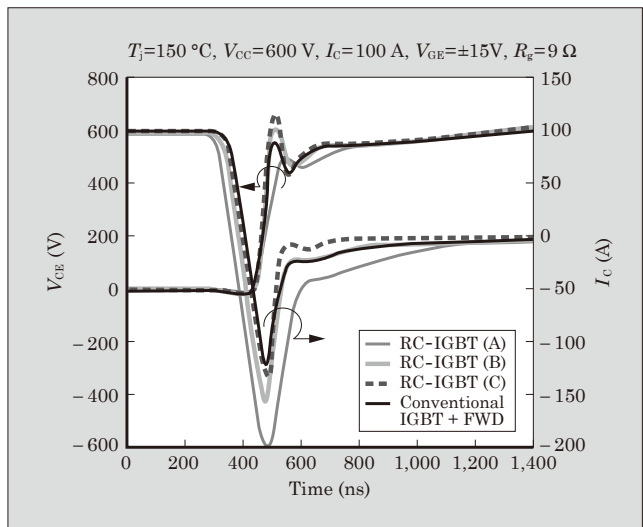


Fig.6 Reverse recovery waveforms of RC-IGBT

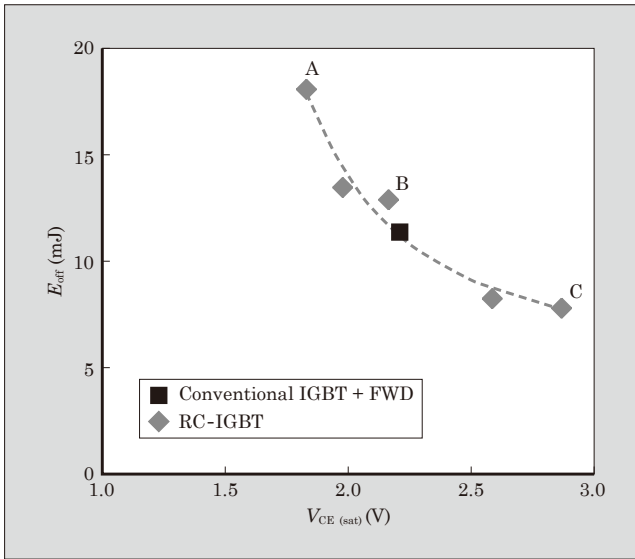


Fig.7 IGBT loss trade-off of RC-IGBT

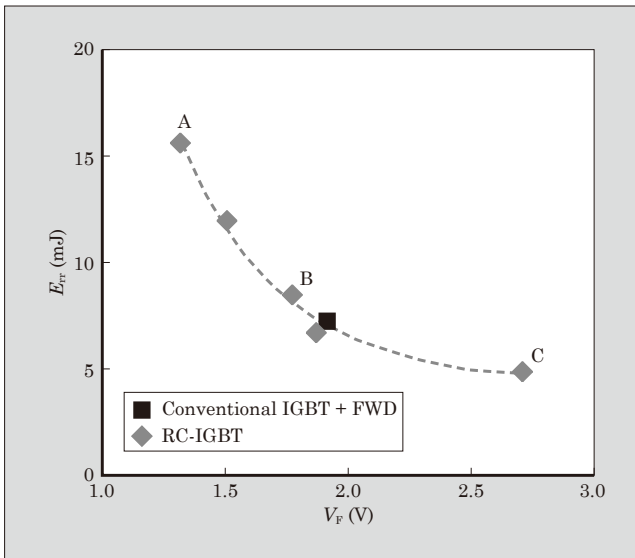


Fig.8 FWD loss trade-off of RC-IGBT

Table 1 Chip area and thermal resistance of RC-IGBT

Chip	Conventional IGBT + FWD	RC-IGBT
Rating	1,200 V 100 A	1,200 V
Active area (a.u.)	IGBT: 0.64, FWD: 0.36 (Total: 1.00)	1.00
Chip area (a.u.)	IGBT: 0.62, FWD: 0.38 (Total: 1.00)	0.91
Thermal resistance $R_{th(j-c)}$ (K/W)	IGBT: 0.24, FWD: 0.36	IGBT: 0.17, FWD: 0.18

ducting loss to C with low switching loss.

(3) Reduction of thermal resistance $R_{th(j-c)}$

Table 1 shows the chip area and thermal resistance $R_{th(j-c)}$ of the RC-IGBT. Even though the active area is the same, the chip size of the RC-IGBT is 9.4% smaller compared to the 6th-generation IGBT chip size and the 6th-generation FWD chip size. This is a result of the fact that the conventional IGBT and FWD need two

edge regions for IGBT and FWD, where the RC-IGBT needs only one edge region. In addition, as shown in Fig. 1, the RC-IGBT has the IGBT and FWD regions arranged in stripes, which have short intervals of approximately a few hundred μm , and heat is radiated from the entire chip including the FWD regions during IGBT operation. That is, the heat radiation area is larger than the conventional separate IGBT and FWD chips and $R_{th(j-c)}$ has been reduced by 30% during IGBT operation and 59% during FWD operation.

2.2 Characteristics of new package

(1) Footprint reduction

Figure 9 shows a cross-sectional view of the new package. Conventionally, wiring between the chip and respective terminals was achieved by wire bonding and copper pattern on the direct copper bonding (DCB) substrate (insulation substrate). With the new package, copper pins instead of wire bonding and the power substrate arranged above the chip instead of the copper pattern wiring on the DCB substrate provide wiring between the chip and respective terminals. This makes it possible to reduce the wire bonding area and copper pattern area, which has led to the realization of a footprint reduction of as much as 58%, as shown in Fig. 10.

(2) Reduction of thermal resistance $R_{th(j-c)}$

As the insulation of the DCB substrate, the new package uses Si_3N_4 , which has higher thermal conductivity than the conventional Al_2O_3 , and our new structure uses a thick copper block on both sides of the DCB substrate to diffuse heat in the lateral direction, thereby increasing the effective heat radiation area. This has successively reduced $R_{th(j-c)}$ by 55% in a comparison on the same chip area.

(3) Improvement of power cycling lifetime

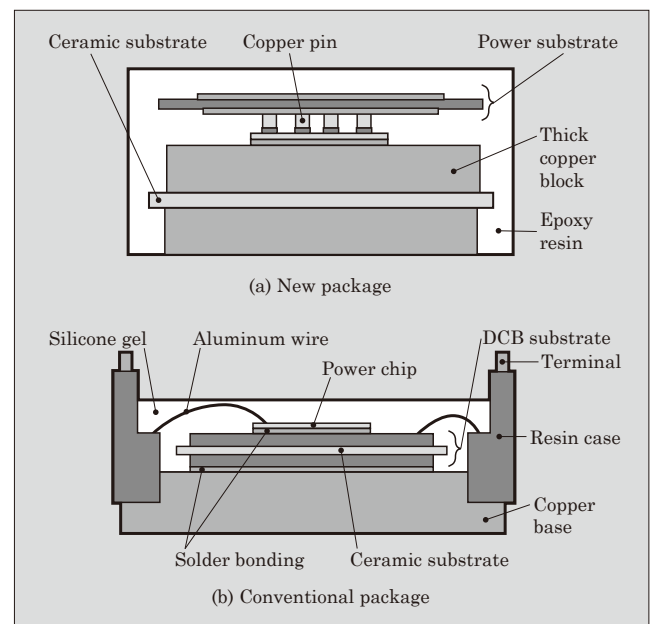


Fig.9 Cross-sectional view of new package

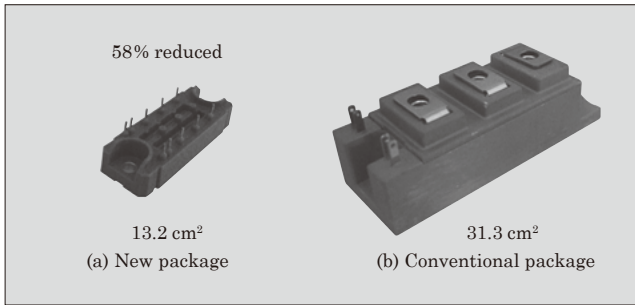


Fig.10 Footprint of new package (1,200 V/100 A)

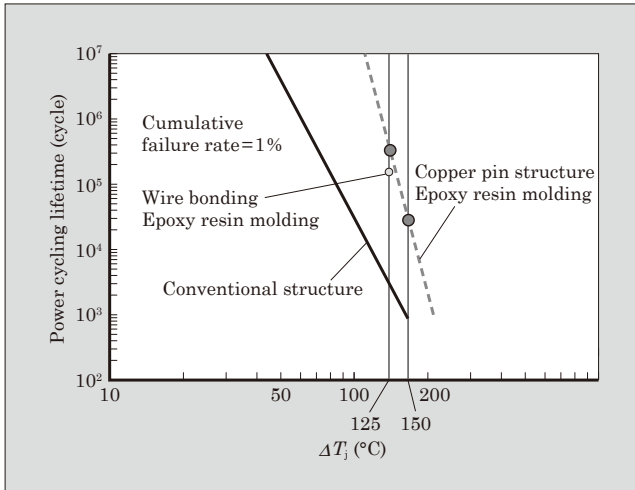


Fig.11 Power cycling lifetime of new package

Power cycling lifetime is restricted by breakage of the bonding contacts and the solder layer between the chip and DCB substrate due to thermal stress, which is caused by heat cycling. With the new package, the drawback of bonding contacts has been eliminated by replacing wire bonding, which was used for conventional packages, with a copper pin structure. In addition, epoxy resin molding has been used in place of the conventional gel molding to firmly secure the copper pins, chip and DCB substrate as a whole. This mitigates the heat stress (strain) on the solder layer and, as shown in Fig. 11, the power cycling lifetime has been improved by more than 20 times in a comparison at $\Delta T_j = 150^\circ\text{C}$.

3. Inverter Loss and IGBT Junction Temperature

To compare the performance between the conventional IGBT + FWD and RC-IGBT and between the conventional and new packages, we have made a comparison of the inverter loss and IGBT junction temperature T_j (see Fig. 12).

With a combination of the RC-IGBT and conventional package, the inverter loss of the RC-IGBT is lower by 3% from the conventional module and T_j is reduced by 5°C . The RC-IGBT features heat radiation from the entire chip including the FWD regions, which offers a larger heat radiation area, and $R_{th(j-c)}$ is 30%

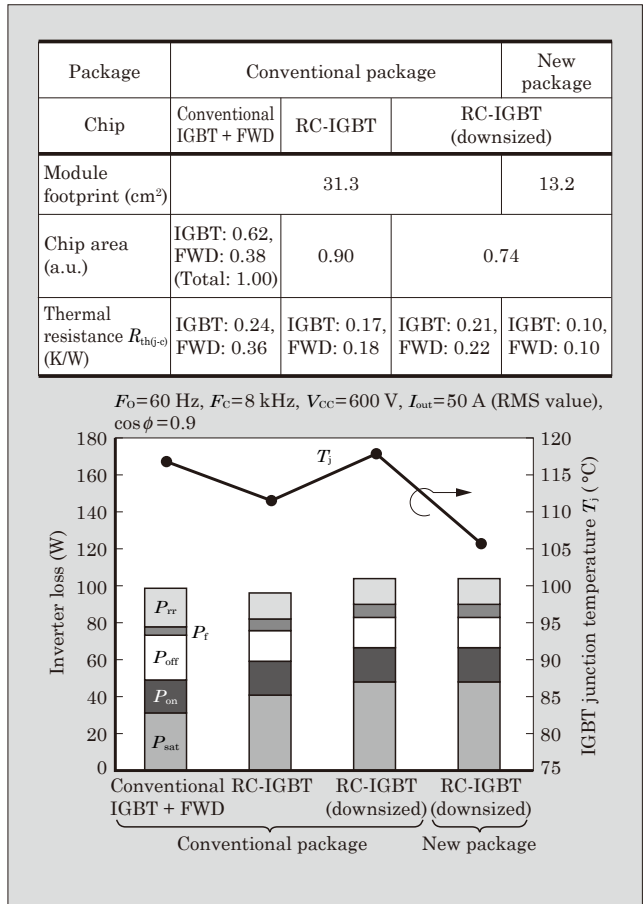


Fig.12 RC-IGBT inverter loss and IGBT junction temperature calculation results

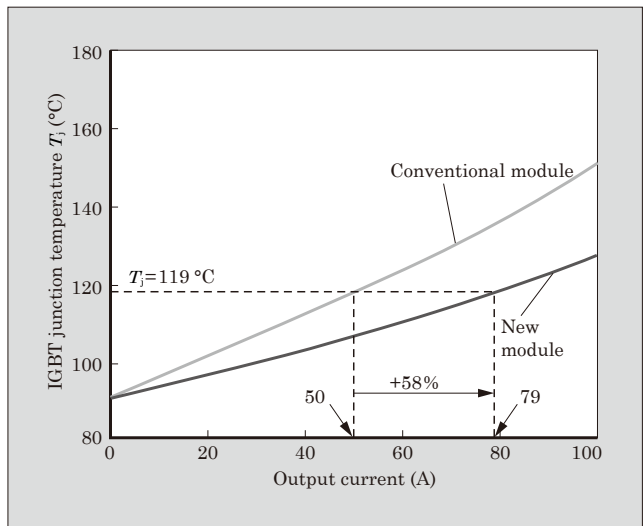


Fig.13 T_j of new module

lower than the conventional IGBT, allowing T_j to be reduced. In the same active area, the RC-IGBT offers lower T_j than that of the conventional module and the chip area can be made smaller by that much.

The RC-IGBT with the chip area reduced by 26% achieves an inverter loss and T_j equivalent to those of the conventional module. That is, as compared with

the conventional IGBT + FWD, the RC-IGBT allows a 26% chip area reduction in the same package and IGBT module miniaturization contributes to the miniaturization of the entire inverter device.

Lastly, we have discussed a new module combining the new RC-IGBT and the new package. The combination of the new RC-IGBT and the new package has successfully reduced $R_{th(j-c)}$ of the IGBT by 62%. In this way, the IGBT junction temperature of the new module has been lowered by 11 °C while the inverter loss remains equivalent to that of the conventional module. The relationship between the output current and IGBT junction temperature of the new and conventional modules is shown in Fig. 13. In the case of $T_j=119^\circ\text{C}$, as compared with $I_{out}=50\text{ A}$ (RMS value) of the conventional module, the new module can conduct $I_{out}=79\text{ A}$ (RMS value), a 58% increase in the output current.

4. Postscript

In this paper, we have described a newly developed RC-IGBT integrating diode functions and a newly developed compact package with low thermal resistance and high reliability. These innovations make significant contributions to miniaturization and cost reduction of inverters. In the future, we will continue to work on technological innovations of IGBT chips

and packages in order to help realization of an energy-saving society.

References

- (1) Takahashi, H. et al. "1200 V Reverse Conducting IGBT". Proceeding of ISPSD 2004. p.133-136.
- (2) "Satoh, K. et al. "A New 3 A/600 V Transfer Mold IPM with RC (Reverse Conducting) -IGBT". Proceeding of PCIM Europe 2006."
- (3) H. R thing. et al. " 600 V Reverse Conducting (RC-) IGBT for Drives Application in Ultra-Thin Wafer Technology". Proceeding of ISPSD 2007. p.89-92.
- (4) S. Voss. "Anode Design Variation in 1200-V Trench Field-stop Reverse-conducting IGBTs". Proceeding of ISPSD 2008. p.169-172.
- (5) Horio, M. et al. " New Power Module Structure with Low Thermal Impedance and High Reliability for SiC Devices". Proceeding of PCIM Europe 2011.
- (6) Iizuka, Y. et al. "A Novel SiC Power Module with High Reliability". Proceeding of PCIM Europe 2012.
- (7) Ikeda, Y. et al. "Investigation on Wirebond-less Power Module Structure with High-Density Packaging and High Reliability". Proceeding of ISPSD 2011. p.272-275.
- (8) Ikeda, Y. et al. "Ultra Compact and High Reliable SiC MOSFET Power Module with 200°C Operating Capability", Proceeding of ISPSD 2012. p.81-84.



RC-IGBT for Mild Hybrid Electric Vehicles

NOGUCHI, Seiji* ADACHI, Shinichiro* YOSHIDA, Soichi*

ABSTRACT

Hybrid electric vehicles and electric vehicles are attracting attention as people's environmental awareness is growing. Above all, mild hybrid electric vehicles, in which one motor is responsible for both driving and power generation, is expected to account for a higher proportion of vehicles. To reduce the loss and size of Insulated-gate bipolar transistor (IGBT) modules for mild hybrid electric vehicles, Fuji Electric has developed a reverse-conducting IGBT (RC-IGBT) that has a withstand voltage of 650 V, which integrates an IGBT and freewheeling diode (FWD) into one chip. The RC-IGBT has realized a lower loss and reduced package size that surpass the conventional IGBTs and FWDs.

1. Introduction

As awareness of the need for environmental protection including prevention of global warming is growing around the world, hybrid electric vehicles (HEVs), which use both an engine and a motor for reducing CO₂ emissions, and electric vehicles (EVs), which are totally motor-driven, are becoming popular.

Among HEVs, mild HEVs are attracting particular attention. Mild HEVs use 1 motor for both driving and power generation. As compared with full HEVs, which use 2 separate motors for driving and power generation, mild HEVs have a simpler structure and offer less price differences from gasoline-fueled vehicles and are expected to account for a higher proportion of vehicles worldwide in the future.

Fuji Electric is working on the development of an insulated-gate bipolar transistor (IGBT) module to be mounted in inverters for mild HEVs. In order to meet the need for miniaturization as well as loss reduction of the in-vehicle module for improving fuel efficiency, we have developed a reverse-conducting IGBT (RC-IGBT) with a withstand voltage of 650 V that integrates an IGBT and freewheeling diode (FWD) into one chip. RC-IGBTs have already been commercialized as small-capacity chips for consumer electronics. However, as large-capacity chips required for in-vehicle use, technological hurdles for reducing loss have been too difficult to overcome up to now⁽¹⁾. This paper describes the RC-IGBT for mild HEVs and the effect of its application to the module.

2. RC-IGBT Design

The 650 V withstand voltage RC-IGBT for mild HEVs has been developed based on the field stop (FS) IGBT⁽²⁾ mass-produced by Fuji Electric, which has alternating IGBT and FWD regions arranged in stripes. Figure 1 shows a schematic structure of the RC-IGBT.

While the current carrying capacity of the IGBT module for mild HEVs depends on the motor capacity, it generally operates in the ranges of 300 to 400 V as the power supply voltage V_{CC} and 5 to 10 kHz as the carrier frequency f_{sw} . Figure 2 shows the loss generated in inverter operation as the RC-IGBT for mild HEVs is applied to the module.

It indicates that, even in an operating condition with a high switching frequency (10 kHz), where the

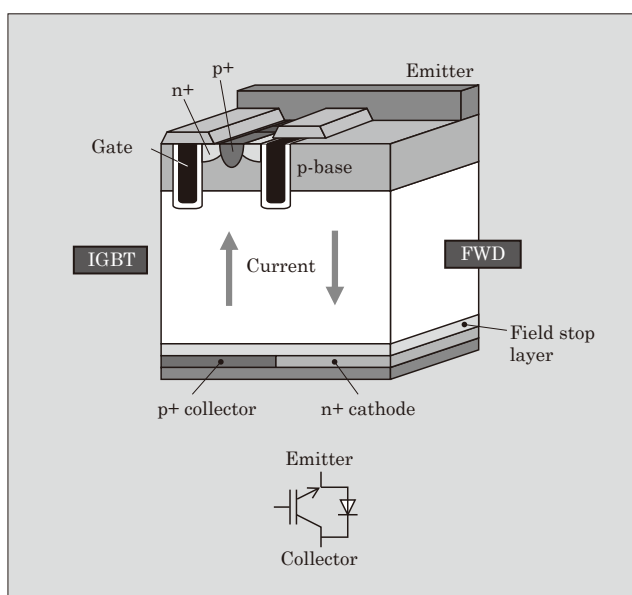


Fig.1 RC-IGBT schematic structure

* Electronic Devices Business Group, Fuji Electric Co., Ltd.

* Power Electronics Business Group, Fuji Electric Co., Ltd.

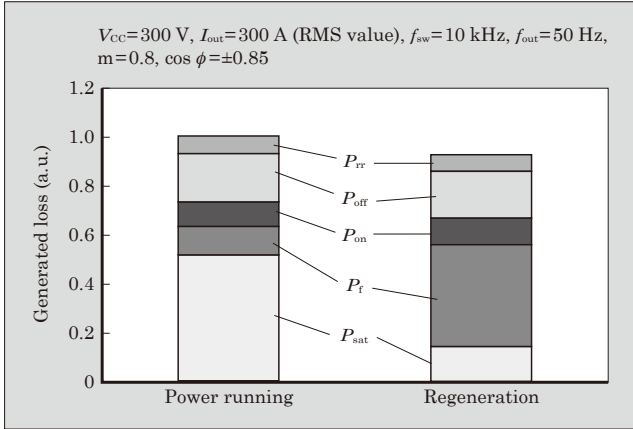


Fig.2 IGBT module generated loss during inverter operation

switching losses (P_{on} , P_{off} , P_{rr}) are high, the steady-state losses of the IGBT and FWD (P_{sat} , P_f) are dominant. By using ingenuity in the design of the device surface, such as the trench pitch of the IGBT regions, for reducing the steady-state losses, the collector-emitter saturation voltage, which is a parameter that determines the steady-state losses, has been minimized⁽³⁾. With a thicker chip, the withstand voltage can be ensured more easily and manufacturing is easier but the saturation voltage and forward voltage increase, which worsen the steady-state losses, and a thinner chip is more desirable. Accordingly, Fuji Electric has been actively working on technology for fabricating thinner wafers since the early period.

We have now developed cutting-edge thin wafer processing technology, which has enabled us to make wafers thinner and achieve the thickness necessary and sufficient for a withstand voltage of 650 V, which was conventionally impossible, to realize reduced loss. In addition, we have also developed patterning technology suited for the back side of thin wafers and impurity layer formation technology to successfully form the IGBT collector p-type layer and FWD cathode n-type layer on the back side of one chip. The switching losses of IGBT and FWD have a trade-off relationship with steady-state losses. For that reason, we have performed carrier lifetime control for optimizing the trade-off.

3. Loss Characteristics

3.1 Electrical characteristics

This section presents the electrical characteristics of an RC-IGBT with the same active area as the conventional IGBT and FWD.

(1) IGBT characteristics

Figure 3 shows the saturation voltage output characteristics of the RC-IGBT and the conventional IGBT. The RC-IGBT has achieved a lower saturation voltage than that of the conventional IGBT by wafer thinning and surface structure optimization. In addition, electrons flow into the n-type layer, which is the back

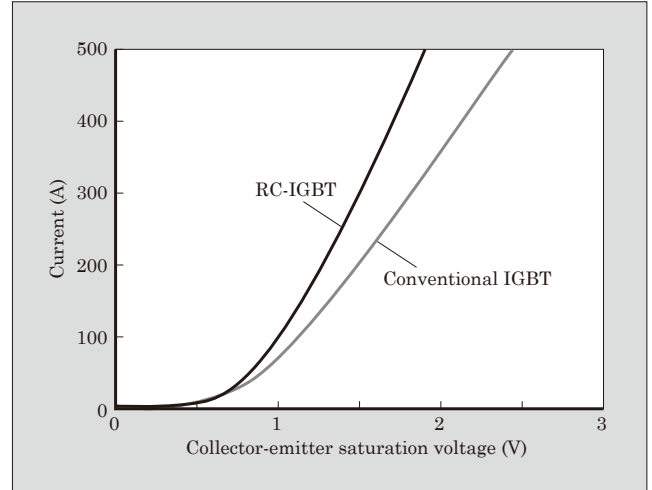


Fig.3 IGBT saturation voltage output characteristics

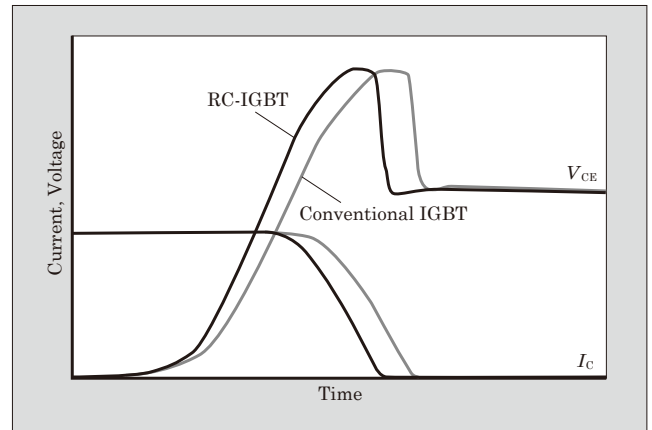


Fig.4 IGBT turn-off characteristics

side cathode of an FWD region adjacent to an IGBT region, and hole injection from the p-type layer, or the IGBT collector, is suppressed to hinder conductivity modulation. For that reason, in the low saturation voltage region, snapback* has been reported to occur in the current-saturation voltage curve⁽⁴⁾. Occurrence of snapback causes the saturation voltage to increase, which may worsen the losses. To prevent this, we have optimized the structures of the IGBT and FWD regions respectively to facilitate conductivity modulation for suppressing snapback.

Figure 4 shows the turn-off characteristics of the RC-IGBT and the conventional IGBT. It indicates that the RC-IGBT offers larger dv/dt at turn-off than the conventional IGBT and a higher carrier emission rate. This is because the RC-IGBT has the collector p-type layer and cathode n-type layer short-circuited on the back side, which causes electrons to be emitted not only from collector p-type layer but also from the cathode n-type layer on the back side of the adjacent

* Snapback: Refers to a phenomenon in which current and saturation voltage increase following a decrease in the process.

FWD region. This results in a benefit of reduced turn-off loss with the RC-IGBT than the conventional IGBT. With the RC-IGBT, adjustment to the direction that improves steady-state losses (lower saturation voltage) allows reduced turn-off loss compared with that of the conventional IGBT, and this has made a significant improvement in the trade-off characteristics (see Fig. 5).

(2) FWD characteristics

Figure 6 shows the forward output characteristics

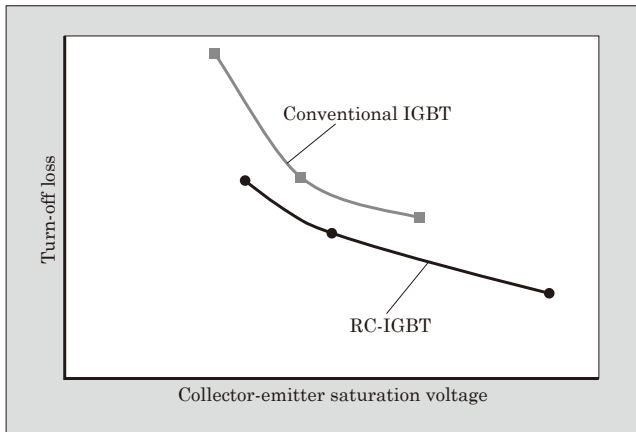


Fig.5 IGBT trade-off characteristics

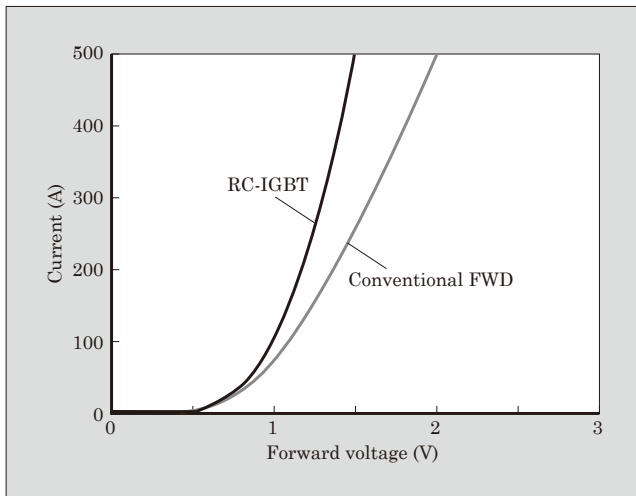


Fig.6 Forward output characteristics

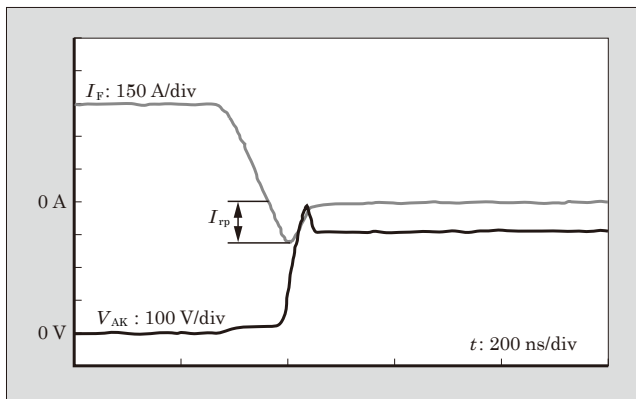


Fig.7 Switching waveforms during RC-IGBT reverse recovery operation

of the RC-IGBT and conventional FWD. As with the steady-state loss of IGBT, the RC-IGBT has achieved less forward voltage reduction as compared with the conventional FWD by the effect of wafer thinning and surface structure optimization.

Figure 7 shows switching waveforms during RC-IGBT reverse recovery operation. With the RC-IGBT, there was an issue of electrons diffusing into IGBT as well as the FWD regions during FWD steady-state operation and the reverse recovery current I_{rp} becoming larger than the conventional FWD during reverse recovery operation, which made the reverse loss Err larger, but the lifetime control technology has been used to successfully reduce I_{rp} .

3.2 Heat radiation characteristics

The RC-IGBT has achieved a reduction in the chip area and module area by integrating the IGBT and FWD. In addition, the RC-IGBT radiates heat from the FWD regions also via the IGBT regions, which makes the thermal resistance significantly lower than that of the conventional FWD. A module with a direct liquid cooling structure has been assumed to compare the thermal resistance between the RC-IGBT and the conventional IGBT and FWD with the same active

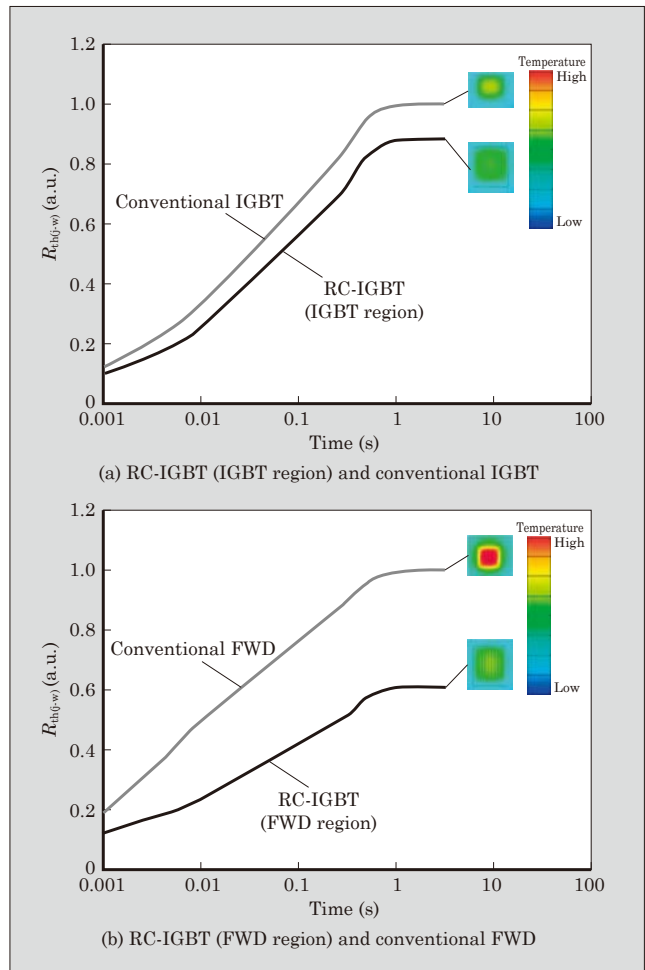


Fig.8 Thermal resistance based on same active area

area (see Fig. 8). The thermal resistance of the IGBT regions of the RC-IGBT is 12% lower than that of the conventional IGBT and the thermal resistance of the FWD regions is 40% lower than the conventional FWD.

4. Effect of Application to Module

This section describes the miniaturization effect of the RC-IGBT as it is applied to the IGBT module for mild HEVs.

Figure 9 shows the results of calculating loss and temperature during inverter operation with the RC-IGBT having the same active area as that of the conventional IGBT and FWD and miniaturized RC-IGBT. Table 1 shows a comparison of the chip active area and module area. As compared with the conventional IGBT, the RC-IGBT is capable of reducing power loss

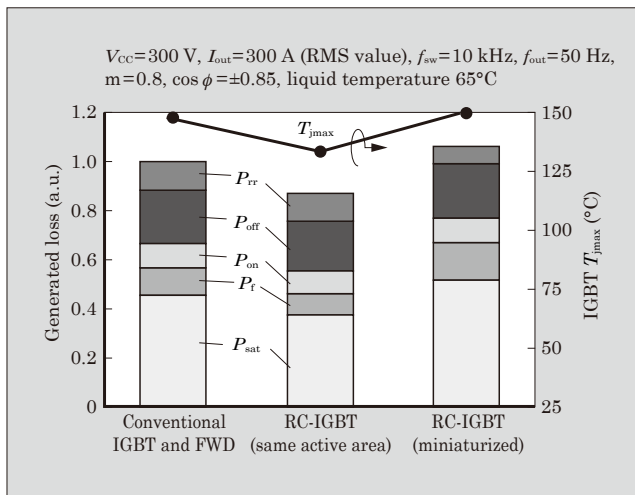


Fig.9 Generated loss of RC-IGBT and conventional IGBT and FWD

Table 1 Chip active area and module area

	Conventional IGBT and FWD	RC-IGBT (miniaturized)
Chip active area (a.u.)	1.00	0.75
Module area (a.u.)	1.00	0.80

during inverter operation by 10% or more by reducing the saturation voltage, forward voltage and turn-off loss. In addition to reduced loss, the advantage of heat radiation described in Section 3.2 allows the chip's maximum temperature to be lowered by about 14°C. The chip size of a module depends on the maximum temperature in operation and this result indicates that the RC-IGBT with smaller chip size can operate an inverter of the same rating. The RC-IGBT with the size reduced by 25% shows a temperature equivalent to the conventional IGBT and FWD, which means that the module area can be reduced by 20%.

5. Postscript

This paper has described the RC-IGBT for mild HEVs and the effect of its application to the module.

From the perspective of responding to environmental issues, HEVs and EVs are expected to continue to significantly evolve in the future. In that process, the importance of miniaturization of in-vehicle devices is estimated to further increase, and RC-IGBT that can realize miniaturization seems to be a very effective means to that end. In the future, we intend to make further contributions to this field by improving devices, developing devices using new materials, etc.

References

- (1) Takahashi, K. et al. "New Reverse-Conducting IGBT (1200 V) with Revolutionary Compact Package". Proceedings of ISPSD 2014. p.131-134.
- (2) Laska, T. et al. "The Field Stop IGBT (FS IGBT) – A New Power Device Concept with a Great Improvement Potential". Proceedings of ISPSD 2000. p.355-358.
- (3) Momota, S. et al. Plated Chip for Hybrid Vehicles. FUJI ELECTRIC REVIEW. 2008, vol.54, no.2, p.49-51.
- (4) M. Rahimo. et al. "The Bi-mode Insulated Gate Transistor (BIGT) A Potential Technology for Higher power Applications". Proceedings of ISPSD 2009. p.283-286.

Packaging Technology of 2nd-Generation Aluminum Direct Liquid Cooling Module for Hybrid Vehicles

GOHARA, Hiromichi* SAITO, Takashi* YAMADA, Takafumi*

ABSTRACT

As activities for preventing global warming and allowing for effective use of resources, further improvements in the fuel efficiency of eco-friendly vehicles such as hybrid electric vehicles is called for. To that end, size and weight reduction of intelligent power modules (IPMs) for hybrid electric vehicles is required. To meet this need, Fuji Electric has developed three new packaging technologies: technology for designing a radiator with a structure capable of direct liquid cooling using aluminum, ultrasonic bonding technology and thermal resistance improvement technology that allows continuous operation at 175 °C. The 2nd-generation direct liquid cooling IPM using aluminum, which applies these technologies, has achieved a volume reduction of 30% and mass reduction of 60% from the 1st-generation model.

1. Introduction

Prevention of global warming and effective use of resources are gaining importance as shared activities by all the countries of the world. In the automotive industry, the development and dissemination of hybrid electric vehicles (HEVs) and electric vehicles (EVs) are accelerating. Inverter units, which are used for power control of these vehicles, are mounted in a limited space. They need to have a compact size and high degree of freedom for mounting, together with weight reduction and efficiency improvement in view of low fuel consumption. Power modules mounted in inverters also require size and weight reduction and efficiency improvement, and a size and weight reduction of 20% or more is desired for each generation. With in-vehicle power modules, in particular, efforts are underway to increase heat radiation using a direct liquid cooling structure and reduce weight with aluminum cooler.

Fuji Electric has developed an in-vehicle intelligent power module (IPM) with an aluminum direct liquid cooling structure that integrates inverters to

control 2 motors and an buck-boost converter⁽¹⁾ to realize the high output required for HEVs. Figure 1 shows in-vehicle IPMs with an aluminum direct liquid cooling structure. The 2nd-generation IPM has achieved a volume reduction by 30% and mass reduction by 60% from the 1st-generation model⁽²⁾.

This paper describes 3 packaging technologies applied to the 2nd-generation IPM: technology for designing a radiator with direct liquid cooling using aluminum, ultrasonic welding technology, and thermal resistance improvement technology that allows continuous operation at 175 °C.

2. Technological Issue with Cooling Structure

Figure 2 shows a cross-sectional structure of the 1st-generation IPM with aluminum direct liquid cooling. In this structure, the module and heat sink are bonded together directly by soldering.

The water jacket is designed independently by the user, which means that the heat sink and the water jacket are separate parts, and this requires a design process considering water-tightness and tolerance in

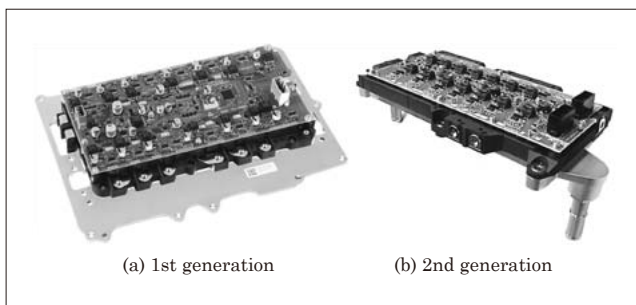


Fig.1 IPM with aluminum direct liquid cooling for automotive devices

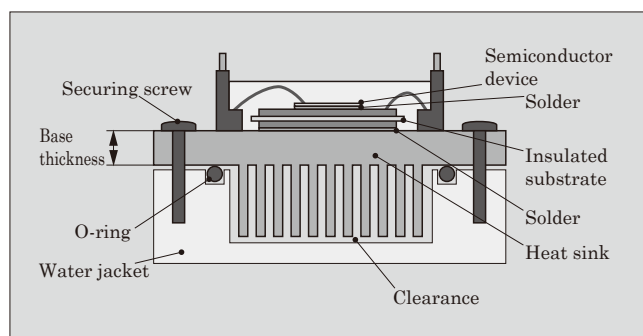


Fig.2 Cross-sectional structure of 1st-generation IPM with aluminum direct liquid cooling

* Corporate R&D Headquarters, Fuji Electric Co., Ltd.

addition to the flow channel design. For that reason, it is necessary to select materials and choose a base thickness in consideration of buckling and deformation, and this was a factor leading to an increase in thermal resistance.

In order to solve this issue and ensure improved heat radiation capacity and high reliability in the aluminum direct liquid cooling structure, we have developed an aluminum cooler integrating a heat sink and water jacket.

3. Cooler Designing Technology

3.1 Design of heat radiation performance

The heat radiation performance of a power module can be represented by 2 values: thermal resistance and thermal conductivity coefficient. Thermal resistance (R_{th}) is a value dividing the temperature difference between the chip junction and that of the point for comparison by the generated loss. Thermal conductivity coefficient (h) indicates the heat exchange performance of the coolant and fins. These relationships are represented by formula (1). It can be replaced by formula (2).

$$h = \frac{1}{R_{th}A} \dots\dots\dots(1)$$

h : Thermal conductivity coefficient [W/(m²·K)]
 R_{th} : Thermal resistance (K/W)
 A : Fin surface area (m²)

$$h = \frac{Nu\lambda}{L} \dots\dots\dots(2)$$

h : Thermal conductivity coefficient [W/(m²·K)]
 Nu : Nusselt number
 λ : Thermal conductivity of component [W/(m·K)]
 L : Fin representative length (m)

Nusselt number (Nu) can be calculated by formula (3) using geometry parameters. Here, Reynolds number (Re) can be represented by formula (4) and Prandtl number (Pr) by formula (5).

$$Nu = 0.664Re^{1/2}Pr^{1/3} \dots\dots\dots(3)$$

Nu : Nusselt number
 Re : Reynolds number
 Pr : Prandtl number

$$Re = \frac{\rho v L}{\eta} \dots\dots\dots(4)$$

Re : Reynolds number
 ρ : Density of coolant (kg/m³)
 v : Flow rate of coolant (m/s)
 L : Fin representative length (m)
 η : Viscosity of coolant (Pa·s)

$$Pr = \frac{\eta Cp}{\lambda} \dots\dots\dots(5)$$

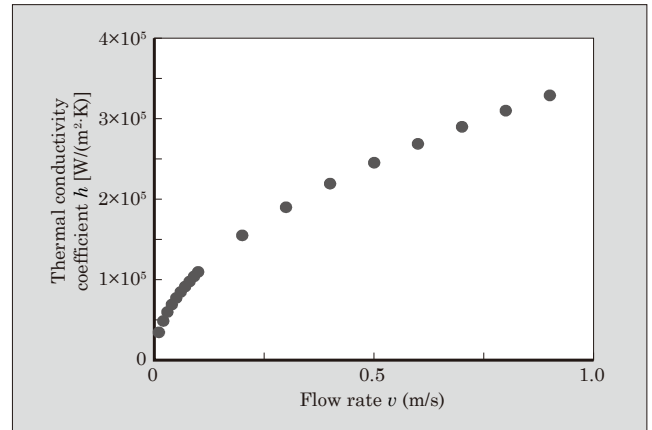


Fig.3 Relationship between thermal conductivity coefficient and coolant flow rate

Pr : Prandtl number
 η : Viscosity of coolant (Pa·s)
 Cp : Specific heat [J/(kg·K)]
 λ : Thermal conductivity [W/(m·K)]

These formulas show that the thermal conductivity coefficient can be calculated from the density, viscosity, specific heat, thermal conductivity and flow rate of the coolant to be used. Figure 3 shows the thermal conductivity coefficient as functions of the flow rate calculated from the length per unit.

A higher fin surface flow rate provides a larger thermal conductivity coefficient that indicates the heat exchange performance. The heat generated in the chip is transmitted to the fins and radiated through the coolant, and the flow rate of the coolant on the fin surface has a significant impact on the heat radiation performance. Accordingly, improving the flow rate on the fin surface is the key point in heat radiation design⁽³⁾.

3.2 Flow rate and heat radiation performance

With the conventional cooling structure that uses a sealing material, the water jacket is designed and prepared by the user; therefore, there is a need for tolerance design. This means that a clearance is required between the fin tips and the water jacket. We tentatively calculated the impact of this clearance on the heat radiation performance using a simplified model. The fins were shaped to have a thickness of 1 mm and height of 10 mm and arranged at intervals of 1 mm and the coolant was set to flow evenly into the coolant inlet at 1 L/min. Figure 4 shows the simplified model and simulation results.

It shows that a larger clearance caused the thermal resistance to increase and worsen. Because the coolant flows where the pressure resistance is low, it flows out in a wide clearance cross-sectional area, and the flow rate between the fins is reduced. In addition, parallel connection of modules is estimated to cause a significant reduction in the coolant flow rate.

It indicates that integrating the heat sink and water jacket to eliminate the clearance is effective in

increasing the coolant flow rate between fins and decreasing the thermal resistance.

Figure 5 shows a cross-sectional view of the new structure, which has been adopted as the 2nd-generation aluminum direct liquid cooling structure. In the new structure, the water jacket and fin tips have been bonded to eliminate the clearance. This has created a cooling structure that makes the most of the coolant. The portion that corresponds to the base has been

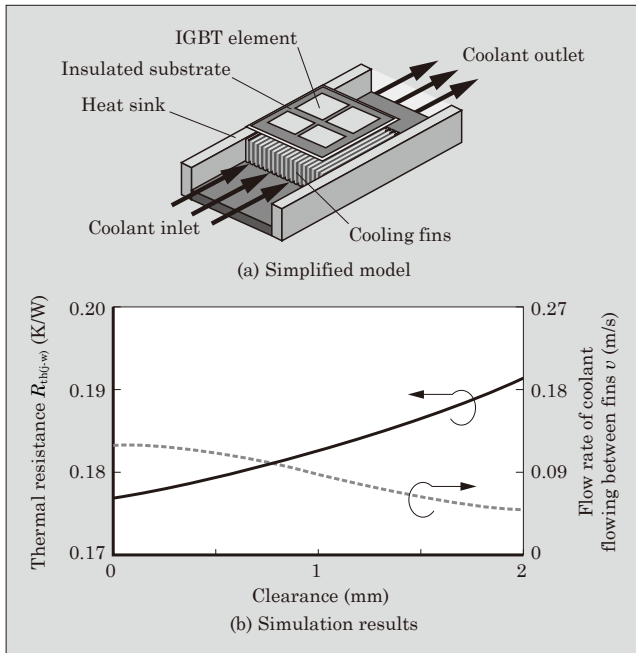


Fig.4 Simplified model and simulation results

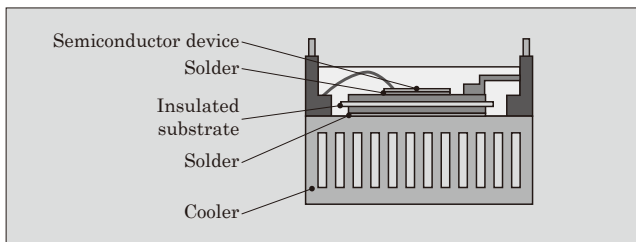


Fig.5 Cross-sectional structure of 2nd-generation IPM with aluminum direct liquid cooling

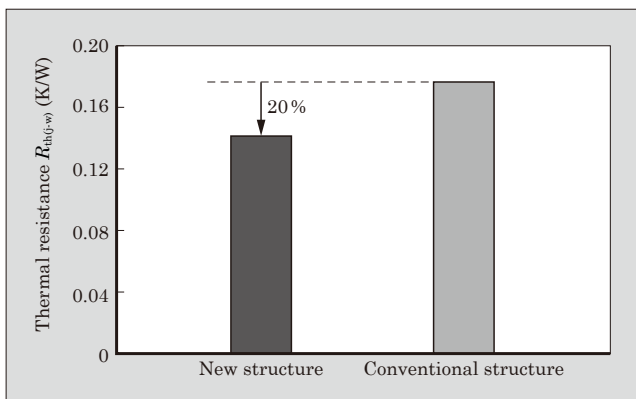


Fig.6 Thermal resistance

made thinner and a high heat conductivity material has been used.

Figure 6 shows the result of comparing thermal resistances. The new structure takes into account the utilization of the coolant and thermal conductivity and is capable of reducing the thermal resistance by 20% from the conventional structure.

4. Ultrasonic Welding Technology

In the 1st-generation aluminum direct liquid cooling IPM, aluminum wire was used for connecting between the main terminals and internal circuit board. It required an area that allowed for the bonding of the number of wires required for ensuring the current density, and a large footprint according to the output was necessary for the wiring portion. To achieve size and weight reduction, the 2nd-generation IPM used ultrasonic welding for connection between the copper terminals, which are main terminals, and the internal circuit board. Figure 7 shows a photo of the appearance of the ultrasonic-welded copper terminals. Ultrasonic welding, in which copper terminals and a copper circuit of the board are directly bonded by solid-phase diffusion, offers secure bonding. Figure 8 shows a comparison between footprints of copper terminal ultrasonic welding and aluminum wire welding with the same current carrying capacity. By using direct welding of copper terminals, which have a higher conductivity

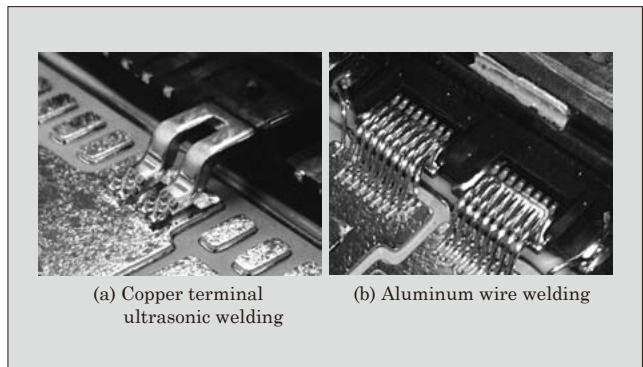


Fig.7 Appearance of welding

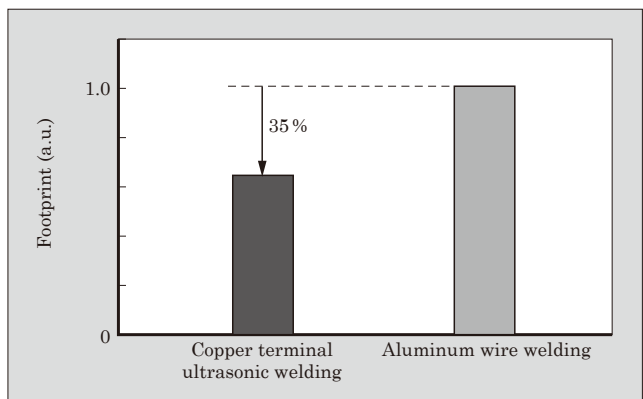


Fig.8 Footprint

than aluminum wire, the ultrasonic welding structure has achieved a footprint reduction by 35% from the aluminum wire welding structure.

The application of the ultrasonic welding technology, in addition to the improvement of heat radiation performance in the direct liquid cooling structure, has enabled the 2nd-generation aluminum direct liquid cooling IPM to realize a 30% volume reduction and 60% mass reduction from the 1st generation model.

5. Thermal Resistance Improvement Technology Allowing Continuous Operation at 175°C

The heat generated in the chip during IPM operation is radiated from the cooling fins through the baseplate. The upper limit of element temperature (T_j) is generally 150°C. The maximized output in the range of ΔT_j , which is the difference between the water temperature and the element upper limit temperature, is determined. We aimed to achieve higher output by increasing the element guarantee upper limit T_{jmax} to 175°C, in addition to reducing the thermal resistance.

To raise T_{jmax} from 150°C to 175°C, the impact of the element peripheral components on reliability must be improved⁽⁴⁾. We used the conventional module structure to conduct a power cycling test with T_{jmax} fixed. Figure 9 shows the test results. A temperature rise of 25°C caused the lifetime to decrease by 40% with $\Delta T_j=75^\circ\text{C}$.

Here, we focus on the lifetime decrease of the solder bond under the element. With the conventional Sn-Ag-based solder, strength degradation due to thermal deterioration is a possible factor causing the lifetime decrease. Next, we analyzed fracture modes and developed a new solder incorporating strengthening mechanisms to realize high thermal resistance and high strength.

5.1 Fracture modes of Sn-Ag-based solder

Figure 10 shows the result of observation of a cross section after the power cycling test. Cracks were observed along the grain boundaries of Sn. Sn-Ag-based

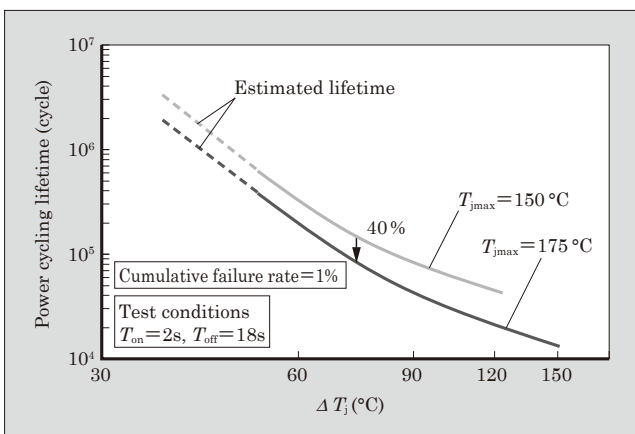


Fig.9 Power cycling lifetime decrease due to rise in T_{jmax}

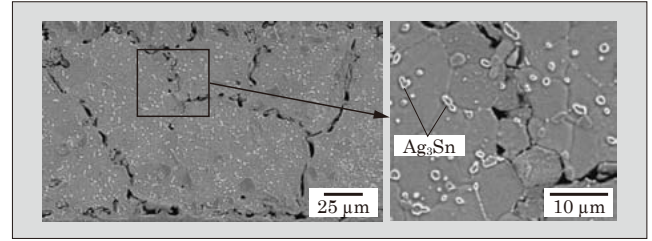


Fig.10 Power cycling lifetime decrease due to rise in T_{jmax}

solder has a structure that suppresses crack growth by strengthening grain boundaries with Ag_3Sn precipitating in Sn grain boundaries. However, heat generation in the soldered part and repeated stress due to the power cycling test brought about Ag_3Sn aggregation and Sn grain coarsening. This eliminated the grain boundary strengthening structure, which is a possible cause of the reduced lifetime. In particular, continuous operation at 175°C causes the temperature of the solder bond directly under the chip to rise by approximately 25°C as compared with operation at 150°C. This accelerated the crack growth due to a change of the metallographic structure and thermal fatigue, apparently causing a lifetime decrease.

5.2 Strengthening mechanism of solder

To develop a solder that does not change in the metallographic structure even in continuous operation at 175°C and maintains the strength, we have focused on the strengthening mechanisms of metal materials. Typical strengthening mechanisms of solder include precipitation strengthening represented by Sn-Ag-based solder and solid solution strengthening with the addition of In or Sb⁽⁵⁾. Conventionally, either of the strengthening mechanisms was used for composition. However, in order to ensure reliability in continuous operation at 175°C, we have added the third element with Sn-Sb-based solder used as the base. In this way, we have developed a new composite strengthening-type solder that combines the two strengthening mechanisms: precipitation strengthening and solid solution strengthening.

5.3 Mechanical characteristics of solder

Concerning the mechanical characteristics of the solder having both the precipitation and solid solution strengthening mechanisms, in order to examine the impact of strength degradation due to structural change under high temperature, we measured the tensile strength of samples subjected to aging* at room temperature and the high temperature of 175°C for 1,000 h. Figure 11 shows the results of measurement with an Sn-Ag-based solder, an Sn-Sb-based solder and the new solder.

The Sn-Ag-based solder showed a strength deg-

* Aging: A phenomenon in which metallic properties (for example hardness) change over time

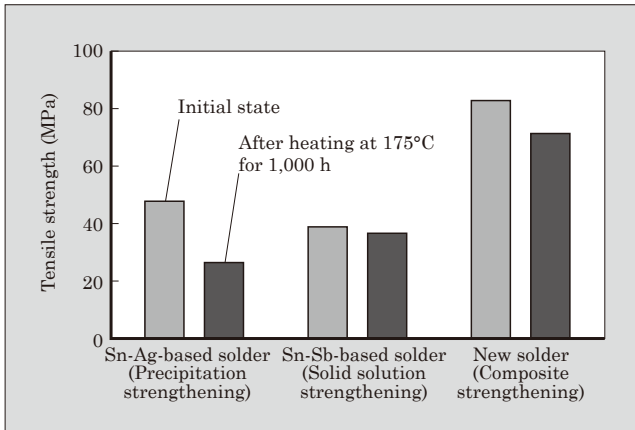


Fig.11 Tensile strength

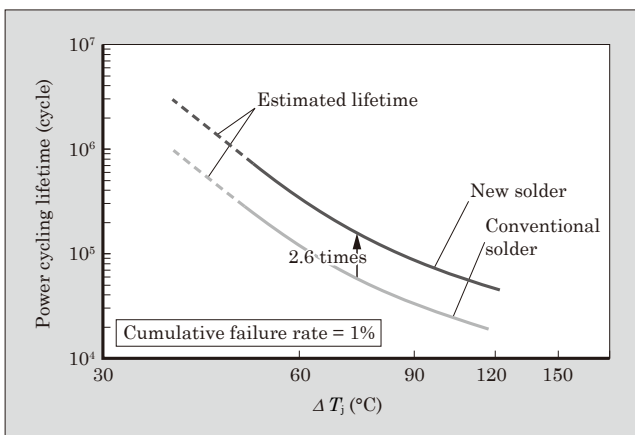


Fig.12 Results of power cycling test on new solder

radation of approximately 44% after heating at 175°C for 1,000 h and the Sn-Sb-based solder, which has the solid solution strengthening mechanism, showed a strength degradation of approximately 5%. Meanwhile, the new solder with the composite strengthening mechanism showed a strength degradation of 13%. While the rate of strength degradation was somewhat high, the composite strengthening type features high strength in itself and raises expectations for improving the lifetime⁽⁶⁾.

5.4 Results of power cycling test

To evaluate the reliability of the developed new

solder at high temperature, we have conducted a power cycling test under the test condition of $T_{jmax}=175^{\circ}\text{C}$. Figure 12 shows the results of the power cycling test. As compared with the Sn-Ag-based solder, the new solder has been shown to have a power cycling lifetime that is 2.6 times longer at $\Delta T_j=75^{\circ}\text{C}$.

6. Postscript

This paper has described packaging technologies for realizing size and weight reduction of IPMs for hybrid electric vehicles: technology for designing a radiator with a structure capable of direct liquid cooling using aluminum, ultrasonic welding technology and thermal resistance improvement technology that allows continuous operation at 175°C.

Packaging technologies support customers with inverter development and design. We intend to use these technologies as the basis for working on further technological innovation to offer products that contribute to high efficiency and energy conservation.

References

- (1) Gohara, H. et al. Packing Technology of IPMs for Hybrid Vehicles. FUJI ELECTRIC REVIEW. 2013, vol.59, no.4, p.235-240.
- (2) Gohara, H. et al. "Next-gen IGBT module structure for hybrid vehicle with high cooling performance and high temperature operation". Proceedings of PCIM Europe 2014, May 20-22, Nuremberg, p.1187-1194.
- (3) Morozumi, A. et al. "Next-gen IGBT module structure for hybrid vehicle with high cooling performance and high temperature operation". Proceedings of the 2014 IEEJ, Hiroshima, p.671-676.
- (4) K, Vogel. et al. "IGBT with higher operation temperature- Power density, lifetime and impact on inverter design". Proceedings of PCIM Europe, 2011, p.679-684.
- (5) Saito, T. et al. "New assembly technologies for $T_{jmax}=175^{\circ}\text{C}$ continuous operation guaranty of IGBT module". Proceedings of PCIM Europe 2013, Nuremberg, p.455-461.
- (6) Saito, T. et al. "Novel IGBT Module Design, Material and Reliability Technology for 175°C Continuous Operation". Proceedings of IEEE 2014, Sep 14-18, Pittsburgh, p.4367- 4372.

3rd-Gen. Critical Mode PFC Control IC “FA1A00 Series”

SUGAWARA, Takato* YAGUCHI, Yukihiro* MATSUMOTO, Kazunori*

ABSTRACT

Switching power supplies, which are widely used for electronic devices, are required to have a power factor correction (PFC) circuit to reduce harmonic current. In order to meet the market demand for less power consumption and lower cost of power supplies, Fuji Electric has developed the third-generation critical mode PFC control IC “FA1A00 Series” intended for PFC circuits. The bottom-skip function has successfully improved the efficiency under low load and the power good signal function has reduced the number of power circuit parts. Safety has also been improved by having an overshoot suppression function and improved reference voltage accuracy.

1. Introduction

Switching power supplies are widely in use to achieve size and weight reduction of electronic devices. Switching power supplies use a capacitor-input rectifier and smoothing circuits and a large harmonic current is generated. An increase in harmonic current causes problems such as device operation failure and an increase of reactive power due to a power factor reduction. In order to restrain the harmonic current to a certain value, international standard IEC 61000-3-2 classifies electrical and electronic equipment into classes A to D as shown in Table 1, and they are respectively assigned regulation values.

To solve these harmonic current and power factor problems, a power factor correction (PFC) circuit is necessary and an active filter PFC circuit, which provides an especially high power factor, is widely used. Meanwhile, Fuji Electric has commercialized many ICs for controlling PFC circuits⁽¹⁾.

In order to curb the deterioration in the global environment, saving the energy consumed by electrical products in general is gaining importance. Standards that limit the energy consumption of electronic equipment, such as the ENERGY STAR program of the

U.S. and the Energy-using Products (EuP) Directive of Europe, have been established and the regulations are increasingly becoming stricter year after year.

For example, there are regulations on standby power consumption and the minimum and average efficiency in a wide load range including low load. Accordingly, ICs for controlling PFC circuits are required to reduce standby power consumption and improve the efficiency under low load.

In addition, following the recent demand for lower prices of electronic equipment and growing consumer awareness about safety, power supplies are also strongly required to achieve both reduced cost and improved safety.

To meet these demands, Fuji Electric has developed the 3rd-generation critical control IC “FA1A00 Series” following the 2nd-generation critical control IC “FA5590 Series⁽¹⁾”. The products in the new series is capable of reducing power supply cost and lowering standby power consumption and they have achieved an enhanced protective function as well as improved efficiency under low load.

2. Overview and Features of Product

The appearance of FA1A00 is shown in Fig. 1 and a performance comparison between FA1A00 and FA5590 in Table 2. FA1A00, which meets demands such as improved efficiency under low load, reduced power supply cost and improved stability and safety of PFC circuits, has the following features.

- (1) Improvement of efficiency under low load
 - Bottom-skip function
The efficiency has been improved by 14% with 240 V AC and 10% load.
- (2) Reduction of power supply cost
 - Power good signal function

Table 1 Classification of harmonic current regulation (IEC 61000-3-2)

Classification	Typical equipment
Class A	Major household appliances, audio equipment
Class B	Handheld power tools, arc welders
Class C	Lighting equipment
Class D	TVs, PCs

* Electronic Devices Business Group, Fuji Electric Co., Ltd.

* Sales Group, Fuji Electric Co., Ltd.

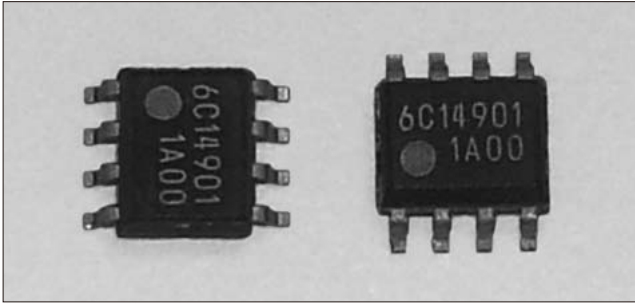


Fig.1 “FA1A00”

Table 2 Critical PFC control IC performance comparison

Item		FA1A00	FA5590
High efficiency	Switching frequency under low load	200 kHz (Efficiency improved by 14 points with 240 V AC and 10% load)	600 kHz
	Power good signal function	Provided	Not provided
Stability	Stabilization under low-load function	Provided	Not provided
	Zero current detection voltage	-4 mV ±3 mV	-10 mV ±5 mV
Safety	Overshoot suppression function	Provided (Overshoot voltage reduced by 10 V)	Not provided
	Reference voltage	2.5 V ±1.0%	2.5 V ±1.4%
	Overcurrent detection voltage	-0.6 V ± 2.0%	-0.6 V ±3.3%

One n-metal oxide semiconductor field-effect transistor (n-MOSFET) has been added and 1 shunt regulator, 2 resistors and 1 capacitor have been eliminated.

- (3) Improvement of operation stability
 - Low-load stabilization function
- (4) Improvement of safety
 - Overshoot suppression function
 - The overshoot voltage has been reduced by 10 V.
 - Improvement of reference voltage tolerance
 - Improvement of overcurrent detection tolerance

2.1 Bottom-skip function

A critical mode PFC circuit, which turns on the MOSFET after the inductor current has dropped to zero, has a problem that the switching frequency increases under low load to increase the switching loss of the MOSFET, and this degrades efficiency.

Fuji Electric has addressed this problem by improving the function to reduce the switching frequency under low load for each new generation of critical mode PFC control IC.

Table 3 lists the frequency reduction functions and switching frequencies of the respective generations

under low load. The switching frequency has been reduced from 800 kHz of the 1st generation FA5500 through 600 kHz of the 2nd generation FA5590 to 200 kHz of the 3rd generation FA1A00, thereby improving efficiency.

Figure 2 shows operation waveforms of the bottom-skip function. In critical operation, the MOSFET is turned on when the first bottom of VDS of the MOSFET is detected. With FA1A00, the MOSFET is turned on at the first bottom under high load as with ordinary critical operation, but the turn-on timing is delayed from the first bottom through the second to the third bottom as the load decreases. This operation prolongs the period of MOSFET turn-off, decreasing the switching frequency.

Figure 3 shows the efficiency of FA5590 and FA1A00 under low load with the rated 200 W power supply. The efficiency of FA1A00 has achieved an improvement of 3 points with 20% load and 14 points

Table 3 Frequency reduction functions and switching frequencies under low load

Generation	Model	Frequency reduction function	Switching frequency under low load
1st generation	FA5500	Not provided	800 kHz
2nd generation	FA5590	Maximum switching frequency limiting function	600 kHz
3rd generation	FA1A00	Bottom-skip function	200 kHz

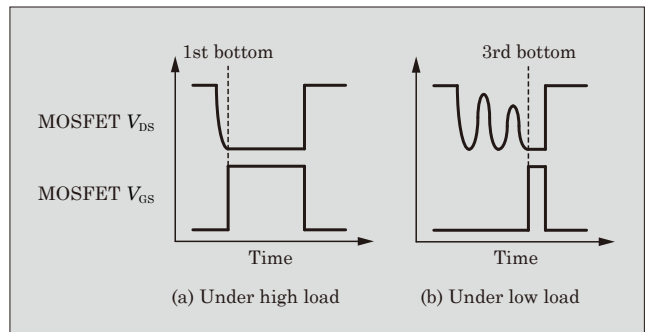


Fig.2 Operation waveforms of bottom-skip function

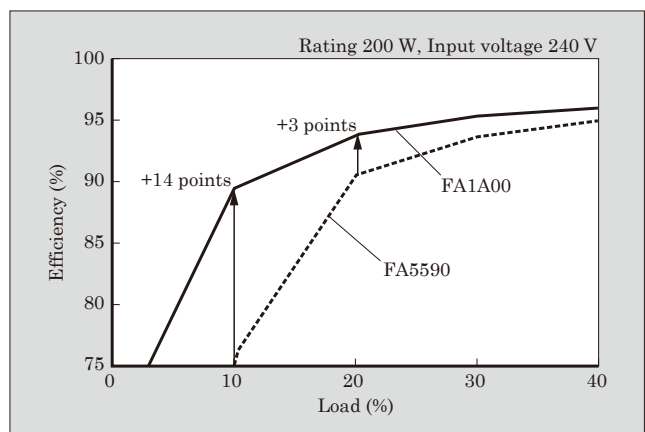


Fig.3 Efficiency under low load

with 10% load from FA5590 due to the bottom-skip function.

Use of FA1A00 provides conformance to standards such as the ENERGY STAR program. In addition, reduction of MOSFET loss decreases heat generation. It allows the heat sink for heat radiation to be made smaller, leading to a reduction in the power supply cost.

2.2 Power good signal function

With general power supplies, the PFC circuit is used to boost the 90 to 264 V AC input voltage to around 400 V, and this is further converted with the DC/DC converter in the later stage for supplying to the load. The DC/DC converter is designed to operate at the voltage boosted by the PFC circuit and may malfunction if the PFC circuit output voltage decreases to a certain voltage level. For that reason, the power supply uses a circuit that monitors the output voltage of the PFC circuit and, if it drops to a certain level, stops the DC/DC converter.

FA1A00 incorporates the function of this circuit. Figure 4 shows operation waveforms of the power good signal function. The power good signal is turned from L to H when the PFC output voltage has increased to a certain voltage or higher and from H to L when it has decreased to a certain voltage or lower. Transmitting this signal to the DC/DC converter in the later stage makes it possible to reduce the output voltage monitoring circuit in a power supply, thus realizing a reduction in power supply cost. A certain hysteresis is provided to the voltage for switching the power good signal, which prevents chattering and allows stable operation.

FA1A00 is provided with a terminal for monitoring the PFC output voltage. In addition, sharing the power good signal output with the existing oscillating frequency setting terminal has achieved the above function without increasing the number of terminals.

2.3 Low-load stabilization function

As described in Section 2.2, a wide-ranging input voltage from 90 to 264 V may be applied on the PFC circuit. Setting a high gain for the pulse width control, so that power can be supplied with a low input voltage

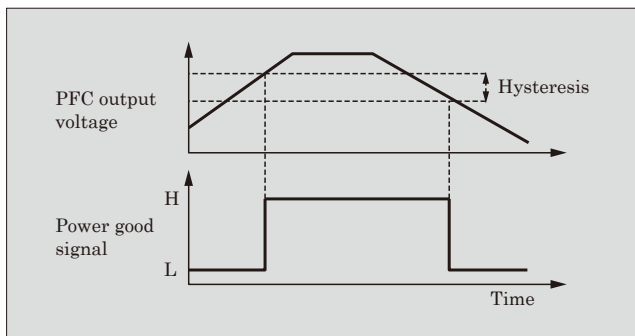


Fig.4 Operation waveforms of power good signal function

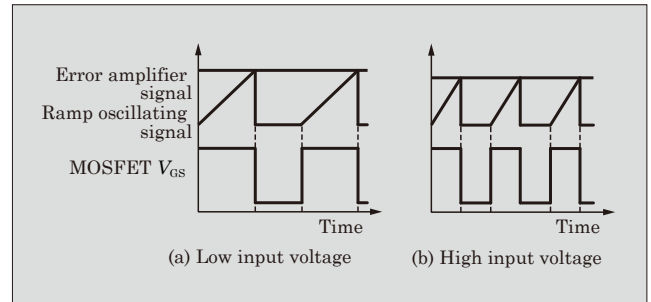


Fig.5 Operation waveforms of low-load stabilization function

and high load, may cause unstable operation with a high input voltage and low load because the gain is too high, and this possibly will increase the output voltage ripples. In this case, problems may occur such as a malfunction of the DC/DC converter connected in the later stage of the PFC circuit and increase of the switching noise.

FA1A00 integrates a function that allows stable supply of power by increasing the gain only when the input voltage is low and load is high and decreasing the gain when the input voltage is high and load is low.

Figure 5 shows operation waveforms of the stabilization under low-load function. The output power of the PFC circuit is controlled by the MOSFET “on” width. The MOSFET “on” width is determined by a turn-on and turn-off of the ramp oscillating signal: its level increases steadily after a turn-on to reach the error amplifier signal level between the output voltage and the reference voltage in the IC, then it turns off. Accordingly, the control gain depends on the gradient of the ramp oscillating signal.

Because a smaller gradient of the ramp oscillating signal provides a higher gain and a larger gradient provides a lower gain, FA1A00 has incorporated a function that increases the gradient of the ramp oscillating signal under high input voltage and low load. With this function, operation can be stabilized by reducing the control gain under high input voltage and low load.

2.4 Overshoot suppression function

In the PFC circuit, response of the output voltage control is set to be slow in order to decrease the output voltage ripples generated at the input power supply frequency. With slow response, however, an overshoot occurs in the output voltage at start-up. In addition, there are more cases recently to connect an electrolyte capacitor with a withstand voltage that does not have a sufficient margin from the actual use condition, to the output of a PFC circuit to reduce the power supply cost. It causes temporary overvoltage due to an overshoot at start-up, which reduces the lifespan of the electrolyte capacitor.

With FA1A00, if the output voltage reaches the setting voltage at start-up, the response is temporarily quickened to reduce the overshoot of the output volt-

age. Figure 6 shows operation waveforms of the overshoot suppression function.

PFC control IC supplies larger power to the output with a higher error amplifier signal. At start-up, large power is required to raise the output voltage to the setting voltage and the error amplifier signal level is raised to the maximum value. As described above, the output voltage control response is set to be slow, which causes a delay in the decrease of the error amplifier signal level when the output voltage reaches the setting, and excessive power is supplied, resulting in overshoot of the output voltage.

FA1A00 reduces the response delay by forcing to lower the error amplifier signal level when the output voltage reaches the setting, thereby reducing the overshoot at start-up. This makes it possible to safely use electrolyte capacitors with a low withstand voltage.

In addition to the protective function described

above, FA1A00 has improved the safety of power supply by improving the reference voltage tolerance of the output voltage control and tolerance of the overload

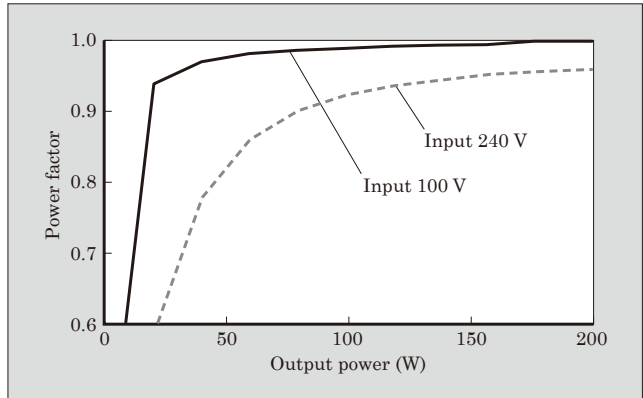


Fig.8 Power factor characteristics

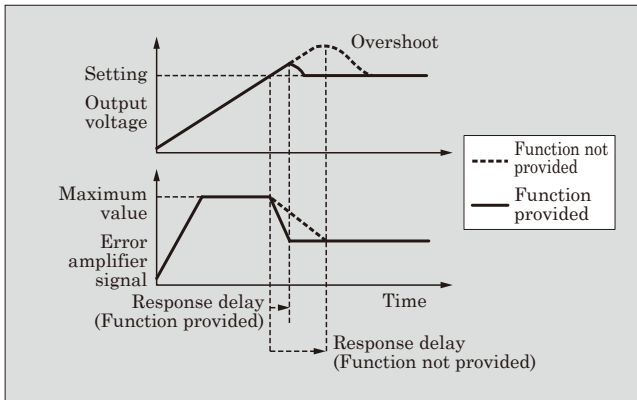


Fig.6 Operation waveforms of overshoot suppression function

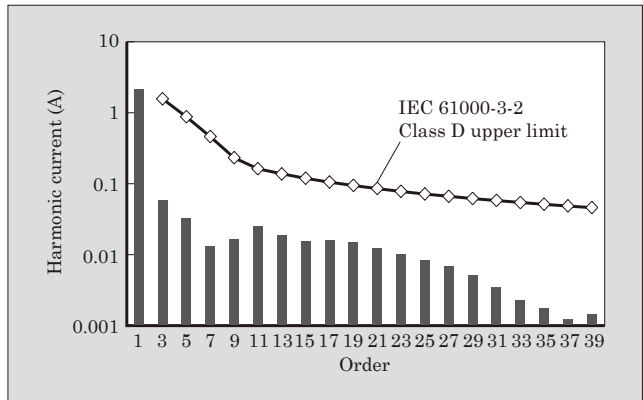


Fig.9 Harmonic current characteristics

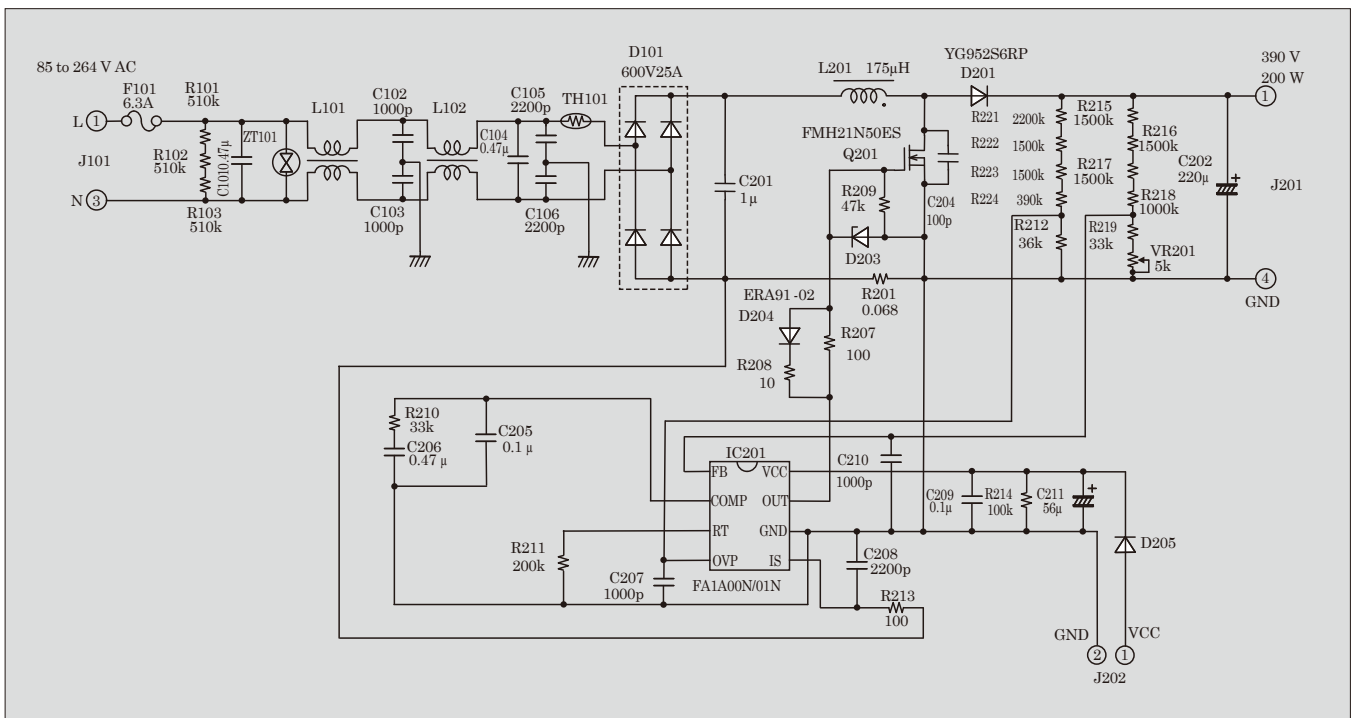


Fig.7 Sample application circuit

protection detection voltage.

3. Sample Application Circuit

Figure 7 shows a sample application circuit (input 90 to 264 V, output 390 V and 200 W) and Fig. 8 and Fig. 9 respectively show the power factor and harmonic current characteristics measured with the circuit.

Regarding the power factor characteristic, a minimum power factor of 0.95, which is required of general electronic equipment, is ensured with the standard input voltage (100 V and 240 V) and rated load. The harmonic current characteristic satisfies the requirement of IEC 61000-3-2 Class D, which is necessary for TVs, PCs and other electronic equipment.

4. Postscript

This paper has described the 3rd-generation critical mode PFC control IC “FA1A00 Series” capable of realizing reduced standby power consumption, improved efficiency under low load, cost reduction and improved safety of switching power supplies. In the future, we intend to continue to incorporate functions that meet the demands of the market. We will strive to establish a product line and work on development to comply with the standards and regulations that are becoming increasingly stricter year after year.

References

- (1) Kashima, M.; Shiroyama, H. CMOS Power Factor Control IC. FUJI ELECTRIC REVIEW. 2002, vol.48, no.1, p.6-8.



Circuit Technology of LLC Current Resonant Power Supply

KAWAMURA, Kazuhiro* YAMAMOTO, Tsuyoshi* HOJO, Kota*

ABSTRACT

For relatively large capacity power supplies, such as ones for large screen TVs and server devices, LLC current resonant power supplies are commonly used to meet the requirements for high efficiency, reduced size and lower noise. An LLC current resonant power supply uses leakage inductance of a transformer for resonance and the voltage gain varies along with the switching frequency, which makes the design of a transformer more difficult than other control methods. Fuji Electric is working on the development and mass production of control ICs of LLC current resonant power supplies and provides technical support for customers in the area of power supply development. This paper describes the principle of operation of an LLC current resonant power supply and the design method and characteristics of transformers.

1. Introduction

As power supplies for electrical and electronic equipment, switching power supplies, which have realized compact sizes, low prices and high efficiency have come to be commonly used in recent years, thanks to the evolution of ICs and other electronic components. With relatively large-capacity power supplies, in particular, demand is growing for higher efficiency, lower noise and reduced size along with the growth in screen size of flat-screen TVs and the capacity increase of server equipment led by evolution of telecommunications.

In this field of switching power supplies, Fuji Electric has commercialized a control IC for LLC current resonant power supplies, which can configure compact and thin power supplies ranging from the 100 W class to relatively large capacity 500 W class, and offer high efficiency and low noise. This control IC features the integration of a function for preventing shoot-through current caused by short-circuiting of the upper arm metal oxide semiconductor field-effect transistor (MOSFET) and lower arm MOSFET, which has become an issue with the LLC current resonant converter, and operation in the low standby power mode under light load such as during equipment standby. This makes it possible to configure a power supply that provides higher safety and does not require a power supply exclusively for standby, which was conventionally necessary for lowering the standby power⁽¹⁾.

At the same time, in order to facilitate smooth power supply development when customers adopt Fuji Electric's control ICs for power supplies, we provide demo boards, application materials and proposal of constants for IC peripheral circuits. In addition, we

provide support with regards to design of transformers, which are especially difficult to design and crucial to power supply operation..

This paper describes the operating principle of an LLC current resonant power supply, transformer design method and example and typical characteristics of a prototype power supply using the transformer.

2. LLC Current Resonant Converter

Figure 1 shows the circuit diagram of an LLC current resonant converter.

This circuit is composed of a half-bridge circuit that connects 2 MOSFETs (Q_1 and Q_2) in series, a capacitor for resonance (C_r), a transformer (T), output rectifier diodes (D_1 and D_2) and an output electrolyte capacitor (C_o). N_p is the number of turns of the primary winding of the transformer and N_s is the number of turns of the secondary winding.

A transformer used in an LLC current resonant converter has a small coupling coefficient to provide large leakage inductance, which is used as the inductor for resonance. An equivalent circuit diagram indicating the leakage inductance is shown in Fig. 2. L_{r1} and

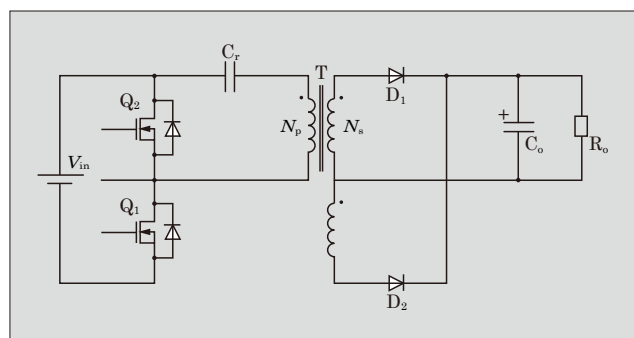


Fig.1 LLC current resonant converter circuit

* Sales Group, Fuji Electric Co., Ltd.

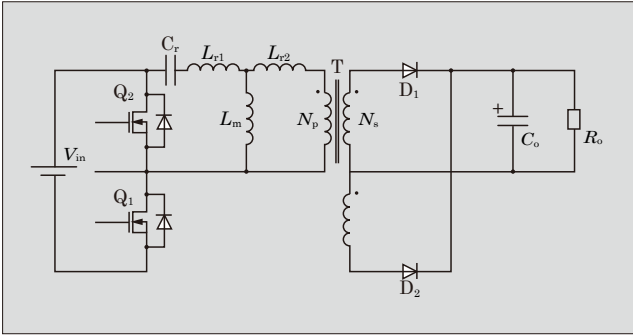


Fig.2 Equivalent circuit diagram indicating leakage inductance

L_{r2} represent the leakage inductance and L_m the magnetizing inductance.

3. Basic Operation of LLC Current Resonant Converter

Figure 3 shows operation waveforms of the LLC current resonant converter. The basic operation can be divided into 4 states from A to D and repetition of

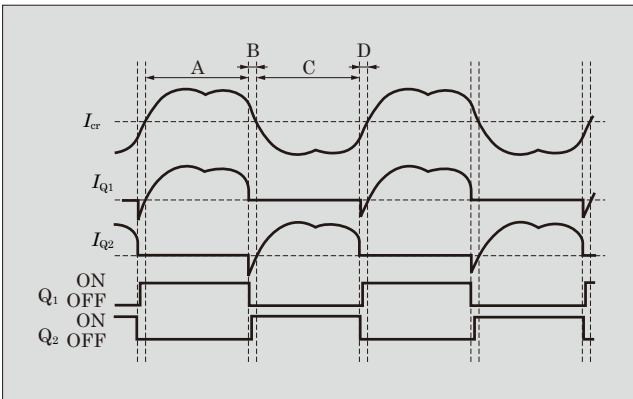


Fig.3 Operation waveforms of LLC current resonant converter

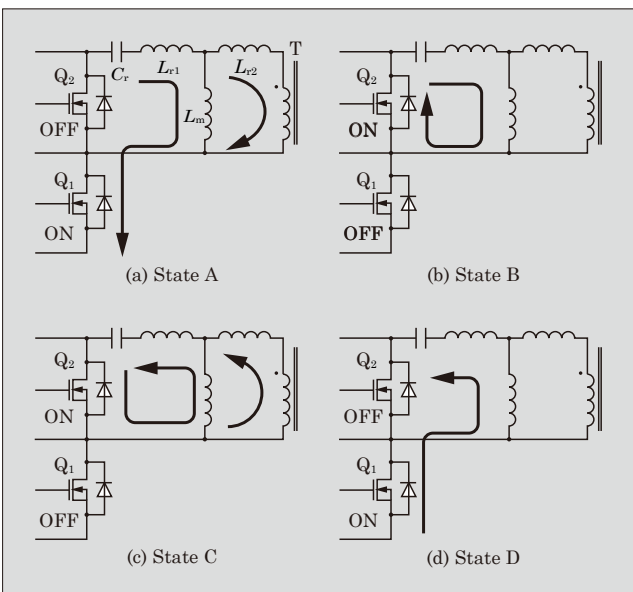


Fig.4 Current pathways

the operation controls the resonance current. Figure 4 shows the current pathways of the respective states.

- (a) State A: Q_1 is on and a current in the positive direction I_{Q1} flows through Q_1 .
- (b) State B: Q_1 is turned off with I_{Q1} in the positive direction, which, in the period immediately after the turn-off, causes current in the negative direction to flow to Q_2 through the body diode of Q_2 and the resonance current I_{cr} changes continuously. While the current flows through the diode, Q_2 is then turned on.
- (c) State C: When I_{cr} turns from the positive to the negative direction, a current in the positive direction I_{Q2} flows through Q_2 .
- (d) State D: Q_2 is turned off with I_{Q2} in the positive direction, which, in the period immediately after the turn-off, causes current in the negative direction to flow to Q_1 through the body diode of Q_1 and the resonance current I_{cr} changes continuously. While the current flows through the diode, Q_1 is then turned on.

In State B, zero voltage switching takes place, in which the body diode of Q_2 turns on first and, with the voltage of Q_2 almost 0, Q_2 is turned on. In State D, the same applies to Q_1 .

4. Operation Modes of LLC Current Resonant Converter

The LLC current resonant converter uses a circuit system that controls the output voltage by frequency modulation and, to determine the I/O characteristics, an equivalent circuit as shown in Fig. 5 is generally used.

The output voltage is shown by the voltage V_{po} , converted to the primary side. The AC equivalent resistance R_{ac} is represented by formula (1).

$$R_{ac} = \frac{8}{\pi} n^2 \frac{V_o}{I_o} = \frac{8n^2}{\pi^2} R_o \dots\dots\dots (1)$$

- R_{ac} : AC equivalent resistance (Ω)
- n : Transformer turns ratio
- V_o : Output voltage (V)
- I_o : Output current (A)
- R_o : Load resistance (Ω)

where n is represented by formula (2).

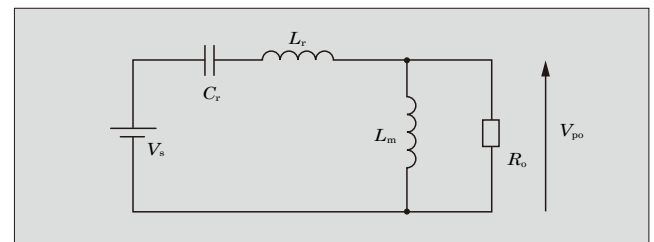


Fig.5 Equivalent circuit of LLC current resonant converter

$$n = \frac{N_p}{N_s} \dots\dots\dots (2)$$

N_p : Number of turns of transformer primary winding
 N_s : Number of turns of transformer secondary winding

In this equivalent circuit, the input-to-output voltage gain is as shown by formula (3).

$$\frac{V_{po}}{V_s} = \frac{1}{1 + \frac{L_r}{L_m} \left(1 - \frac{\omega_0^2}{\omega^2}\right) + jQ \left(\frac{\omega}{\omega_0} - \frac{\omega_0}{\omega}\right)} \dots\dots (3)$$

V_{po} : Output voltage converted to primary side (V)
 V_s : Equivalent input voltage (V)
 L_r : Leakage inductance (H)
 L_m : Magnetizing inductance (H)
 ω, ω_0 : Angular frequency (rad/s)

where ω, ω_0 and Q are shown by formulae(4) to (6).

$$\omega = 2\pi f_s \dots\dots\dots (4)$$

ω : Angular frequency (rad/s)
 f_s : Switching frequency (Hz)

$$\omega_0 = \frac{1}{\sqrt{L_r C_r}} \dots\dots\dots (5)$$

ω_0 : Angular frequency (rad/s)
 L_r : Leakage inductance (H)
 C_r : Capacitance of resonant capacitor (F)

$$Q = \sqrt{\frac{L_r}{C_r}} \frac{1}{R_{ac}} \dots\dots\dots (6)$$

L_r : Leakage inductance (H)
 C_r : Capacitance of resonant capacitor (F)
 R_{ac} : AC equivalent resistance (Ω)

The LLC current resonant converter shown in Fig. 1 is a half-bridge converter, the input voltage in the equivalent circuit is therefore equal to half the input voltage.

$$V_s = \frac{V_{in}}{2} \dots\dots\dots (7)$$

V_s : Equivalent input voltage (V)
 V_{in} : Input voltage (V)

Formulae (1) to (3) have been used to find the input-to-output voltage gain for switching frequency f_s (see Fig. 6). With the LLC current resonant converter, the operation mode changes at the maximum value of the input-to-output voltage gain. Of the regions corresponding to the different modes, the region in which the frequency is lower than the maximum voltage gain frequency is referred to as the capacitive operation region. Operation in this region causes a shoot-through

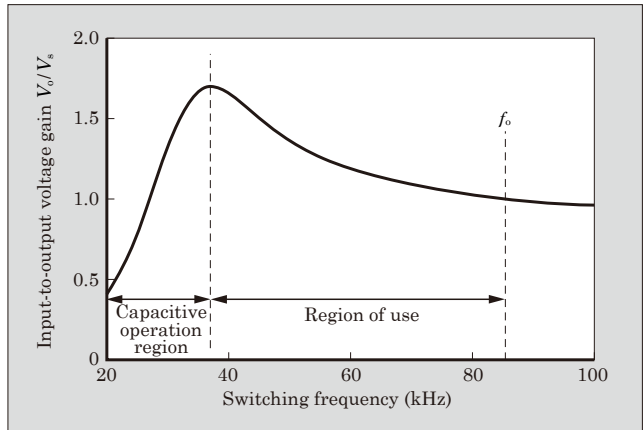


Fig.6 Input-to-output voltage gain against switching frequency

between the upper and lower arm. If this occurs, the MOSFET may be broken. Therefore, in order to avoid this condition, the converter is generally used in the frequency region in which the frequency is higher than the maximum voltage gain frequency. In addition, the region in which f_s is higher than the resonance frequency ($f_o = \omega_0 / 2\pi$) is generally not used for reasons including that the output voltage change is too small for the change of f_s to provide high controllability. For that reason, it is used in the region for the voltage boost mode, in which the input-to-output gain is larger than 1.

5. Transformer Design of LLC Current Resonant Converter

This chapter describes the procedure for designing a transformer that actually uses the LLC current resonant control IC, followed by the result of design of the transformer with specific specifications and verification with an actual power supply.

5.1 Design procedure

As described in Chapter 4, the LLC current resonant converter operates in the voltage boost mode and the input-to-output voltage gain should be determined so that it operates in the voltage boost mode even at the maximum input voltage. First, determine the number of turns of the transformer secondary winding, followed by the number of turns of the primary winding. Resonance frequency f_o is the maximum switching frequency, and it should be determined in advance in a range that does not exceed the maximum frequency of the IC.

- (1) Determine the number of turns of the transformer secondary winding N_s by using formula (8).

$$N_s = \frac{(V_o + V_F) T_{ON}}{2A_e B_m} \dots\dots\dots (8)$$

N_s : Number of turns of secondary winding
 V_o : Output voltage (V)
 V_F : Forward voltage drop of rectifier diode (V)

T_{ON} : Maximum on time of switching element (s)
 (Equal to 1/2 of minimum switching period)
 A_e : Effective cross-sectional area of transformer core (m²)
 B_m : Magnetic flux density of core (T)
 (B_m shall be a value that does not cause core saturation)

- (2) To ensure operation in the voltage boost mode even at the maximum input voltage, determine the transformer primary-to-secondary turns ratio n by using formula (9). Note that V_s is the value at the maximum input voltage.

$$n = \frac{N_p}{N_s} \geq \frac{V_s}{(V_o + V_F)} \quad \dots\dots\dots (9)$$

n : Turns ratio
 N_p : Number of turns of transformer primary winding
 N_s : Number of turns of transformer secondary winding
 V_s : Equivalent input voltage (V)
 V_o : Output voltage (V)
 V_F : Forward voltage drop of rectifier diode (V)

- (3) Determine the number of turns of the transformer primary winding by using formula (10).

$$N_p = nN_s \quad \dots\dots\dots (10)$$

N_p : Number of turns of transformer primary winding
 n : Turns ratio
 N_s : Number of turns of transformer secondary winding

- (4) Find the leakage inductance L_r .

In this converter, the leakage inductance of the transformer is used as the inductor for resonance. The number of turns of the primary winding N_p determines L_r measured from the transformer primary winding.

- (5) Determine the capacitance of the resonance capacitor C_r .

From the resonance frequency f_o and L_r , calculate C_r by using formula (5).

- (6) Determine the magnetizing inductance L_m .

Find the input-to-output voltage gain in which the rated value is obtained at the output voltage when the input voltage is the lowest, and determine L_m . The switching frequency here is at the minimum and determined in view of the voltage gain and core gap. The core gap of the transformer l_g is calculated by using formula (11).

$$l_g = \frac{\mu_0 A_e N_p^2}{L_m} - \frac{l_e}{\mu_c} \quad \dots\dots\dots (11)$$

l_g : Transformer core gap (m)
 μ_0 : Space permeability (= $4\pi \times 10^{-7}$ H/m)
 A_e : Effective cross-sectional area of transformer

core (m²)
 N_p : Number of turns of transformer primary winding
 L_m : Magnetizing inductance (H)
 l_e : Effective magnetic path length of core (m)
 μ_c : Amplitude permeability of core (=3,000 H/m)

5.2 Design example

The following shows an example of transformer design. Figure 7 is the transformer peripheral circuit actually designed.

- Input voltage V_{in} 390 V (350 to 400 V)
- Output voltage V_o 12 V
- Output current I_o 12 A ($R_o=1 \Omega$)
- Transformer used EE4717
 $A_e=90 \text{ mm}^2$
 $l_e=70 \text{ mm}$
 $B_m=0.20 \text{ T}$
- Resonance frequency Around 125 kHz
- Minimum switching frequency 85 kHz ($T_{ON}=5.88 \mu\text{s}$)
- Forward voltage drop of rectifier diode V_F 0.6 V

- (1) Transformer secondary winding N_s (from formula (8))

$$N_s = \frac{(V_o + V_F) T_{ON}}{2 A_e B_m} = \frac{(12 + 0.6) \times 5.88}{2 \times 90 \times 0.20} \doteq 2.1$$

Accordingly, set N_s to the minimum of 3 turns.

- (2) Transformer turns ratio n (from formula (9))

$$n = \frac{N_p}{N_s} \geq \frac{V_s}{(V_o + V_F)} = \frac{200}{(12 + 0.6)} \doteq 15.9$$

- (3) Number of turns of transformer primary winding N_p (from formula (10))

$$N_p = nN_s = 15.9 \times 3 = 47.7$$

Accordingly, set N_p to the minimum of 48 turns.
 From (1) to (3), the transformer turns ratio $n=16$.

- (4) Calculation of transformer leakage inductance L_r

With the EE4717 transformer, the leakage inductance per turn is 38 nH and the leakage inductance with the number of turns of the primary winding- $N_p=48$ is $87.6 \mu\text{H}$ [= $48^2 \times 38$ (nH)].

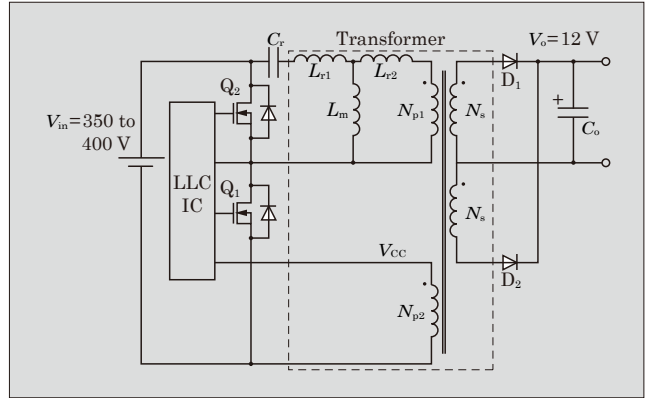


Fig.7 Diagram of peripheral circuit of designed transformer

(5) Determination of resonance capacitor C_r

Substituting $f_o=125$ kHz and $L_r=87.6$ μ H in formula (5) provides C_r of 0.019 μ F, so the capacitor of 0.022 μ F is selected.

(6) Determination of magnetizing inductance L_m

Find L_m in which the rated value is obtained at the output voltage when the input voltage is at the lowest. The minimum value of the input voltage is 350 V and the input-to-output voltage gain here should be determined from the number of turns of the transformer.

$$\frac{V_{po}}{V_s} = \frac{V_o + V_F}{\frac{N_s}{N_p} \frac{V_{in}}{2}} = \frac{12+0.6}{\frac{3}{48} \times \frac{350}{2}} \doteq 1.2$$

Accordingly, using formula (3), find L_m that provides an input-to-output voltage gain of 1.2 or larger when the switching frequency is at the lowest (here, $f_s=85$ kHz).

As a result, L_m should be 490 μ H or lower. Then, $L_m=450$ μ H is selected and the transformer core gap l_g is determined by using formula (11), which results in approximately 0.6 mm.

$$l_g = \frac{\mu_0 A_e N_p^2}{L_m} - \frac{l_e}{\mu_c}$$

$$= \frac{4\pi \times 10^{-7} \times 90 \times 10^{-6} \times 48^2}{450 \times 10^{-6}} - \frac{70 \times 10^{-3}}{3,000} \doteq 0.6 \times 10^{-3}$$

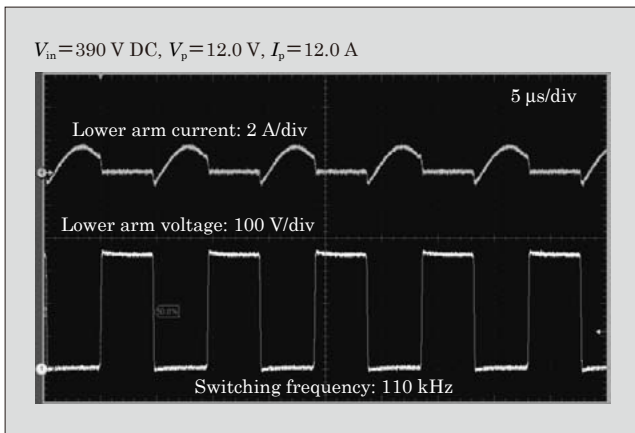


Fig.8 Operation waveforms

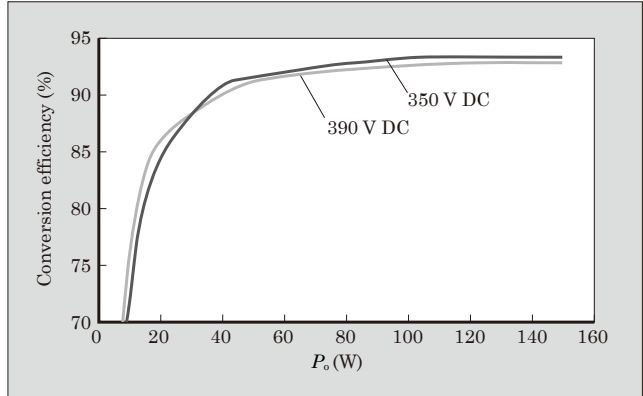


Fig.9 Conversion efficiency characteristics of prototyped transformer

5.3 Characteristics of prototyped transformer

Operation waveforms with a power supply using the prototyped transformer are shown in Fig. 8. The switching frequency at the rating is 110 kHz, which is almost equal to the value targeted in the design.

In addition, the conversion efficiency of the power supply using the prototyped transformer has proved to be high at 93 to 94% (see Fig. 9).

6. Postscript

This paper has described an example of transformer design and the typical characteristics of a power supply that uses the prototype transformer. The aim is to allow customers to smoothly adopt and use Fuji Electric's LLC current resonant control ICs.

In the future, we intend to continue to develop in a timely manner products that meet the demands of the market and strive to support customers with even smoother power supply development.

References

- (1) Yamadaya, M. et al. 2nd Generation LLC Current Resonant Control IC, "FA6 A00N Series". FUJI ELECTRIC REVIEW. 2013, vol.59, no.4, p.245-250.

High Current IPS for Vehicle

IWAMIZU, Morio* TAKEUCHI, Shigeyuki* NISHIMURA, Takeyoshi*

ABSTRACT

Fuji Electric has developed a high current intelligent power switch (IPS) for controlling high output motors of vehicles. The power MOSFET using a trench structure and the control IC are built into a chip-on-chip structure, thereby realizing low on-state resistance (maximum of 5 mΩ) with a compact package. To achieve high reliability, protective functions such as overcurrent/overheat detection and low voltage detection have been provided. In addition, a package with good heat dissipation properties has been adopted, and a configuration that offers well-balanced energy distribution in parallel connections is provided. This package can thereby cope with temperature rises caused by an increased current due to a low on-state resistance.

1. Introduction

In the field of automotive electrical components, reduction of exhaust gas, safe vehicle control and advanced combustion technology are used as means to improve fuel efficiency under the keywords of “environment,” “safety” and “energy saving.” This has accompanied increasing complexity of electronic systems, which is causing electronic control units (ECUs) to grow in size. An ECU is installed near the engine or other location in order to create space for mounting and the temperature of the installation environment is becoming higher every year. For that reason, a size reduction of ECUs and an improvement of their reliability in a high-temperature environment have been strongly desired and hence there are increasing applications of smart power devices, which integrate power semiconductors and their peripheral protective circuits, state detection and output circuits, drive circuits, etc.

To meet these demands, Fuji Electric has developed a high-current intelligent power switch (IPS) for vehicles.

2. Features and Functions

2.1 Features

Figure 1 shows a full view of the high-current IPS for vehicles. This product is designed especially for use in applications including control of inductive loads such as motors and replacement of mechanical relays with semiconductors. The main features are as follows.

- (1) Low on-resistance
- (2) Compact package with high-heat-dissipation
- (3) Various protective functions

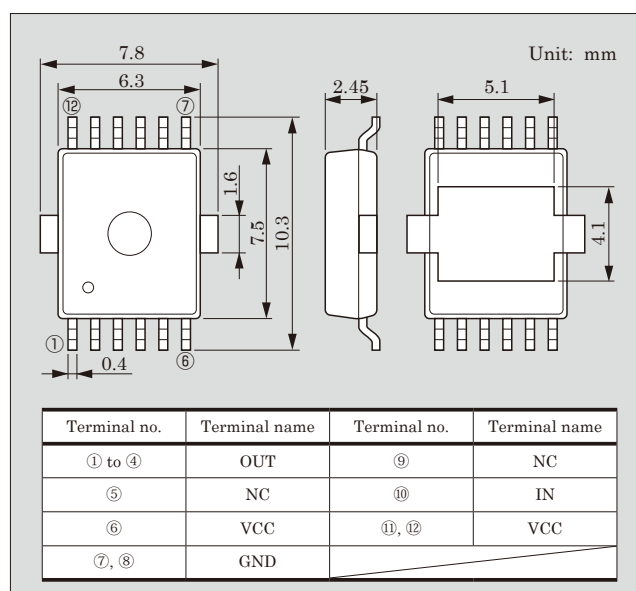


Fig.1 Full view of high-current IPS for vehicles

The functions are provided to suppress temperature rise in battery reverse connection.

- (4) High inductive load energy withstand capability

This prevents any breakage caused by motor stalling and allows energy to be distributed in parallel connections.

2.2 Basic performances

In order to achieve the low on-resistance of 5 mΩ ($T_c=25^\circ\text{C}$, $I_{out}=40\text{ A}$) and the small package (see Fig. 1) as development target, we used the 3rd-generation trench gate metal oxide semiconductor field-effect transistor (MOSFET) technology, which has a proven track record in devices for automotive electrical components, to develop a low- R_{on} A power MOSFET chip. The 4th-

* Electronic Devices Business Group, Fuji Electric Co., Ltd.

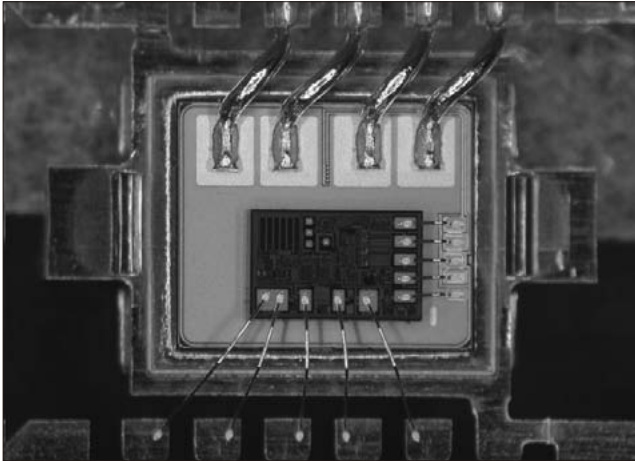


Fig.2 Chip of high-current IPS for vehicles

Table 1 Specifications of high-current IPS for vehicles

Item		Rating		
Rating	Operating power voltage	6.0 to 16.0 V		
	Output current	80 A		
	Allowable power loss	114 W (at 25 °C)		
	Junction temperature	150 °C		
Item		Condition	Standard	
Characteristic	Static power supply current	$I_{cc(off)}$ $V_{cc}=16\text{ V}$, OUT-GND short circuit, 110 °C	50 μA (max.)	
	On-resistance	R_{on}	25 °C, 40 A, 16 V	5.0 m Ω (max.)
			150 °C, 40 A, 16 V	9.0 m Ω (max.)
			25 °C, 40 A, 6 V	7.5 m Ω (max.)
			150 °C, 40 A, 6 V	14.5 m Ω (max.)
	Switching time	$t_{d(on)}$ t_r $t_{d(off)}$ t_f	$V_{cc}=16\text{ V}$, $R=0.25\ \Omega$	0.2 ms (max.)
				0.8 ms (max.)
				0.8 ms (max.)
				0.7 ms (max.)
	Steady-state thermal resistance	$R_{th(j-c)}$	—	1.1 °C/W
Protective function	Inductive load clamping capacity	$I_{out} \leq 80\text{ A}$, $V_{cc}=16\text{ V}$, $T_j=150\text{ °C}$	800 mJ (min.)	
	Overcurrent detection function (load short-circuit protection)	$V_{cc}=16\text{ V}$, load short circuit	100 A (min.)	
	Overheat detection function	Detection 155 °C (min.), Recovery 150 °C (min.)		
	Low voltage detection function	Detection 4.0 V (min.), Recovery 6.0 V (max.)		
Item		Condition	Result	
Reliability	Temperature cycle test	-55 °C to +150 °C	> 1,000 cycles	
	Pressure cooker test	130 °C, 85 %	> 300 hours	
	High temperature high humidity bias test	85 °C, 85 %, 16 V	> 1,000 hours	
	Power cycle test	$\Delta T_j=100\text{ °C}$	> 20,000 cycles	

generation IPS device and process technology has been applied to the circuit portion to realize a circuit chip size reduction with the protective functions described in Section 2.3 added. The chip-on-chip (COC) assembly

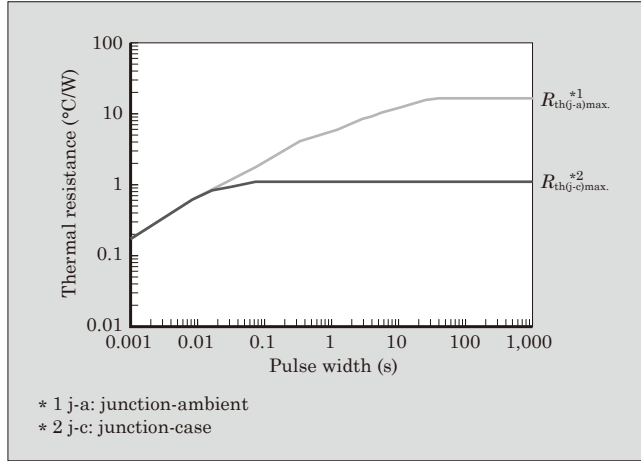


Fig.3 Example of thermal resistance characteristics in board-mounted condition

technology (see Fig. 2) has been used to arrange the circuit chips on top of the power MOSFET chip, allowing to energize a high current with a compact package⁽¹⁾. The specifications of this product are shown in Table 1, and the thermal resistance R_{th} characteristics observed as it is mounted on board are shown in Fig. 3.

2.3 Protective functions

This product has been made to be suitable for applications including control of inductive loads such as motors and replacement of mechanical relays with semiconductors. In order to realize high reliability and minimize redundant design in the ECU, the following protective functions are provided.

- (1) Load short-circuit protection function (overcurrent and overheat detection functions)

This product has been designed to realize a high response to power MOSFET temperature rises and prevent power MOSFET breakage even in a load short-circuit condition. This is achieved by mounting the current and temperature sensors on the power MOSFET chip to detect load short-circuit conditions. The load short-circuit protection provides dual protection against overcurrent and overheat; and for overcurrent protection, 2 types, namely limiting and latch types, have been made available to allow the user to select according to the application.

- (2) Low voltage detection function

This product takes into account direct connection of VCC terminals to the battery. Sufficient energizing capability is ensured even if the battery voltage drops to a certain level in midwinter. In addition, a low voltage detection function has been provided, which turns off the output completely when the voltage has dropped below that level.

- (3) Battery reverse polarity protection function

Reverse connection of the battery with low load impedance causes a high current to flow in the body diode of the power MOSFET. The heat generated in this condition raises the temperature of the chip, which

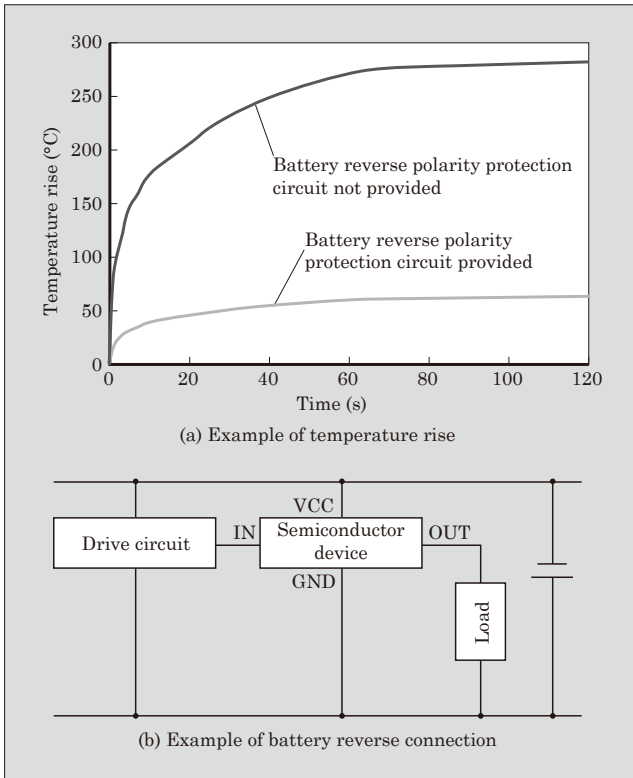


Fig.4 Example of circuit and temperature variation in battery reverse connection

may create a risk of melting the solder on the terminals (see Fig. 4).

This product has adopted a battery reverse polarity protection circuit, which actively turns on the power MOSFET when the battery has been connected in reverse. Energization of the power MOSFET leads to a significantly lower loss than running current in the body diode, thus preventing breakage of the power MOSFET due to the loss generated by battery reverse connection.

(4) Inductive load clamping capacity

One issue with power MOSFETs that drive inductive loads such as motors is to process the excessive inductive load energy generated when a high current is cut off due to motor stalling. To that end, a design is required that does not cause element breakage even if high inductive load energy is applied when the motor is stalled.

With this product, the inductive load clamping capacity per element has been increased. In addition, as a redundant design for driving inductive loads in parallel connections, the inductive load energy is distributed among all elements connected in parallel for improving avalanche capability.

2.4 Power package

This product has adopted a power package with good heat dissipation properties (PSOP-12) to deal with the current increase caused by the lowered on-resistance. In addition, the COC assembly technology

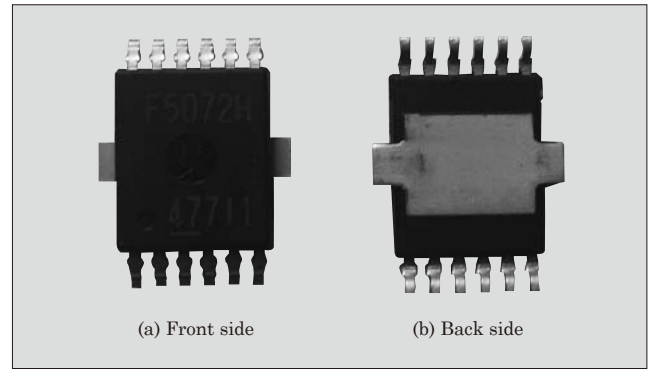


Fig.5 Structure of power package (PSOP-12)

has been used to place the power MOSFET that runs a high current at the center of the chip mounting area to achieve a good heat dissipation balance. Furthermore, in order to confirm the spread of solder in the cooling part on the back side from the front side at the time of mounting, the package has a structure with the frame projecting from both sides (see Fig. 5).

3. Applied Technology

3.1 3rd-generation trench gate MOSFET technology

To realize the on-resistance of 5 mΩ ($T_c=25^\circ\text{C}$, $I_{out}=40\text{ A}$) as development target, the 3rd-generation trench gate MOSFET technology has been applied to the power MOSFET. Of this technology, the micro-fabrication technology has been incorporated to improve the cell density by 40% or more, and the process and wafer specifications have also been optimized to achieve a significant reduction of the on-resistance and a higher current (see Fig. 6). In addition, to ensure reliability of the thinned trench gate, the shape, process and screening conditions have been optimized.

3.2 IC circuit miniaturization and function enhancement technology

In order to realize miniaturization and function enhancement of IC circuits, this product applies the 4th-generation IPS device and process technology⁽²⁾. This

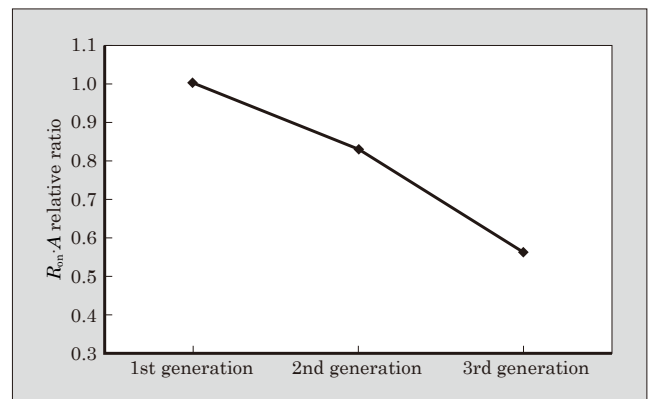


Fig.6 $R_{on}\cdot A$ of trench MOSFETs of respective generations

technology has not only achieved smaller design rules of the element devices themselves but also successfully reduced the area of wiring for connection between element devices by applying multi-metal layer technology.

As devices for IC circuits, 60 V CMOS devices are provided in addition to 5 V CMOS devices for circuits. The 60 V devices are of the high side type and have the back side of the chip directly connected to power supply terminals, which satisfies the requirements for resistance to various surges such as a load dump surge that may be generated in 12 V batteries for vehicles.

As the gate oxide film, 2 types are available, namely thin film and thick film. A MOSFET with a thin gate oxide film has a low threshold voltage and can be used for a circuit that requires driving when the battery voltage has dropped. Meanwhile, a MOSFET with a thick gate oxide film has a high threshold voltage, and the breakdown voltage of the gate can be made high. This, for example, makes it suitable for a circuit that requires gate driving at a high voltage such as the one directly driven by the external power supply voltage VCC.

Polysilicon-applied devices, which eliminate the possibility of parasitic operation, and trimming devices

have also been made available.

By combining these element devices, higher integration and accuracy than those of the conventional products can be achieved to meet market demands.

4. Postscript

This paper has described the features and functions of the high-current IPS for vehicles and technologies applied to the product. Fuji Electric will start supplying the high-current IPS to vehicles by the end of FY2014. Concerning semiconductors for high-current applications, we intend to continue working on miniaturization and function enhancement by further reducing the on-resistance using power MOSFETs and evolving smaller design rules of ICs to serve the market needs in the future.

References

- (1) Imai, M. et al. "Development of Power Chip-On-Chip (COC) Package Technology". Mate 2008. p.323-326.
- (2) Toyoda, Y. et al. "60 V-Class Power IC Technology for an Intelligent Power Switch with an Integrated Trench MOSFET" ISPSD 2013. p.147-150.



1,700 V Withstand Voltage SiC Hybrid Module

USHIJIMA, Taro*

Recently, reduction in greenhouse gases such as CO₂ is being required, more than ever before, as preventative measures against global warming. As a method for reducing greenhouse gases, power electronic devices are becoming more energy efficient. Among these devices are high efficiency inverters which, in particular, are strongly required to be equipped with low power-loss power devices as the major elements of the inverters.

Insulated gate bipolar transistor (IGBT) modules, which are representative of power devices, traditionally used Si (silicon) IGBT chips and free wheeling diode (FWD) chips. As an alternative to Si devices, SiC (silicon carbide) devices that are heat resistant and have high breakdown electric field intensity are expected to help achieve the development of equipment that is highly efficient and compact.

Fuji Electric has completed the development of 600 V withstand voltage SiC-Schottky barrier diodes (SiC-SBDs) and 1,200 V withstand voltage SiC-SBDs and is commercially manufacturing SiC hybrid modules mounted with a combination of a SiC-SBD and a Si-IGBT. We have recently developed and released 1,700 V withstand voltage SiC hybrid modules for 690 V input inverters.

In this paper, we will describe the features and switching characteristics of the 1,700 V withstand voltage SiC hybrid modules mounted in the “M277 Package.”

1. Features

Figure 1 shows the external appearance and outline drawing of the M277 Package. The product utilizes the M277 Package, which is the same as Si modules, to replace the conventional Si modules easily. It comes equipped with a sixth-generation “V Series” IGBT chip and a 1,700 V withstand voltage SiC-SBD chip mass-produced by Fuji Electric. SiC-SBD has superior switching characteristics and low resistance compared with conventionally used Si diodes. In addition, there are very few thermally excited carriers due to a wide band gap, it is therefore scarcely unaffected by a temperature increase. Figure 2 shows the simulation results of the total generated loss. When the carrier frequency f_c is 2 kHz, the total loss of a SiC hybrid module is

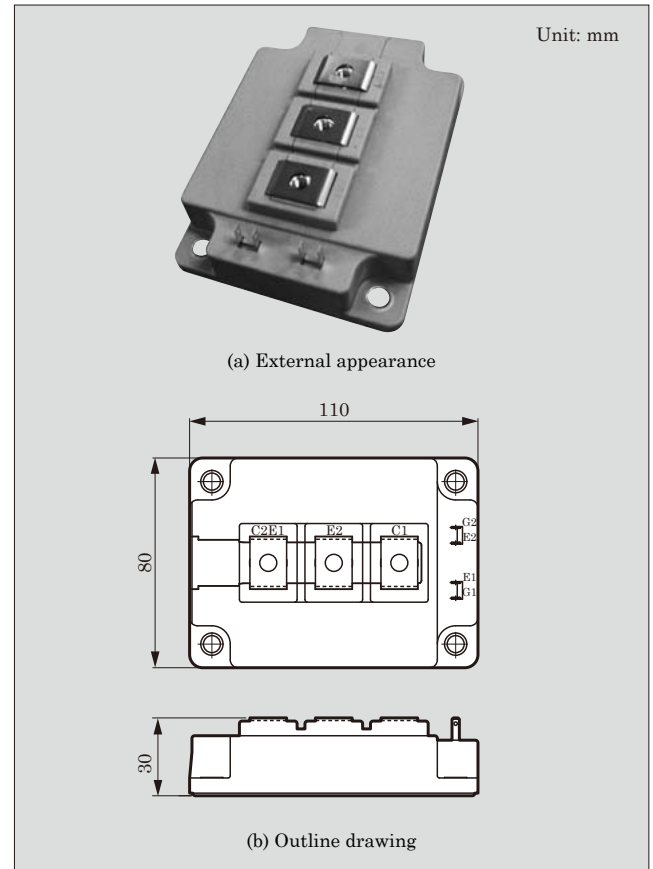


Fig.1 “M277 Package”

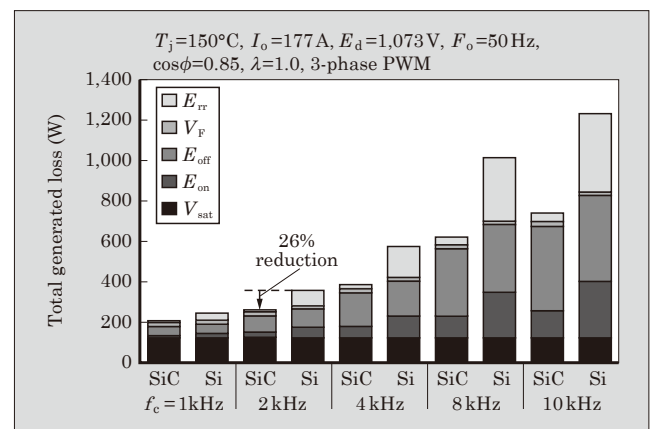


Fig.2 Simulation results of total generated loss

approximately 26% lower than that of a Si module. Furthermore, the product has the advantage of high frequency operation because loss in high regions of f_c

* Electronic Devices Business Group, Fuji Electric Co., Ltd.

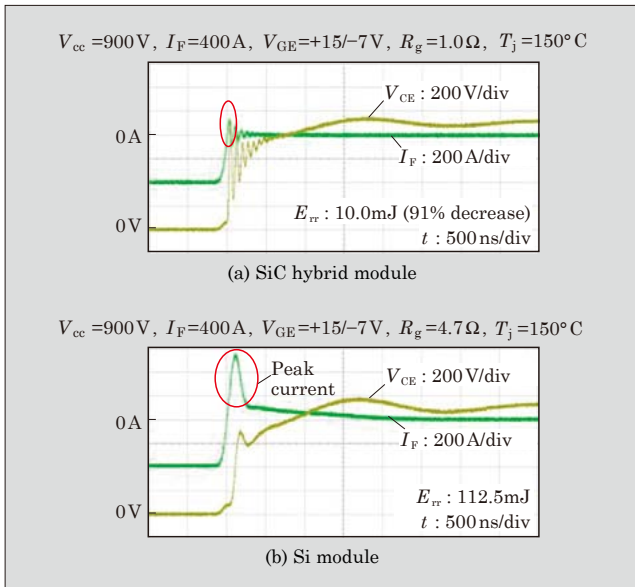


Fig.3 Reverse recovery waveform

of SiC hybrid modules is lower than that of Si modules.

2. Switching Characteristics

(1) Reverse recovery loss characteristics

Figure 3 shows the reverse recovery waveform of SiC hybrid modules and Si modules in 400 A products. The SiC hybrid module has almost no reverse recovery peak current because SiC-SBD is a unipolar device, in which minority carrier injection does not occur. The reverse recovery loss of 400 A products is approximately 91% lower than that of Si modules.

(2) Turn-on loss characteristics

Figure 4 shows the turn-on waveform of SiC hybrid modules and Si modules in 400 A products. The turn-on loss of the SiC hybrid module is reduced be-

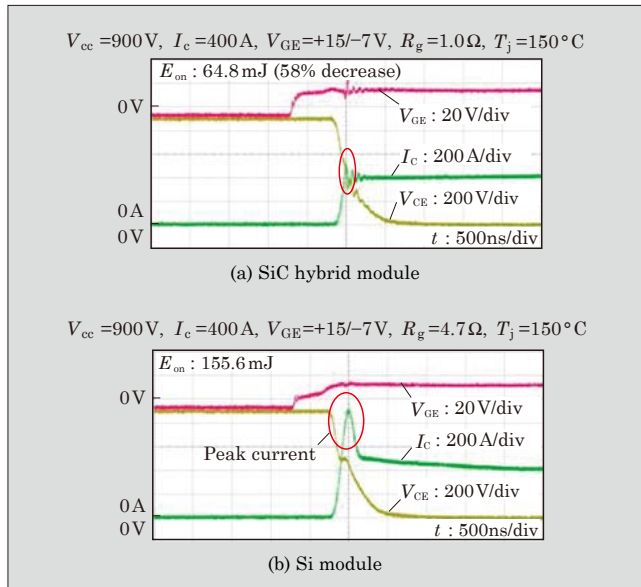


Fig.4 Turn-on waveform

cause SiC-SBD reverse recovery peak currents influence IGBT turn-on currents of the opposite arm-side. Similar to the reverse recovery waveform, there is almost no turn-on peak current, and the turn-on loss of 400 A products is approximately 58% lower than that of Si modules.

Launch time

October 2014

Product Inquiries

Module Technology Department, Business Planning Division, Electronic Devices Business Group, Fuji Electric Co., Ltd.
Phone: +81-263-27-7457

AT-NPC 3-Level High-Power IGBT Module— Package for High-Power Module “M404 Package”

YAMAMOTO, Sayaka*

In recent years, renewable energies have been gathering attention, and the markets for photovoltaic and wind power generation, in particular, have been growing. In order to improve the power conversion efficiency in these fields, developments are continuously being made to create high-voltage, high-power and high-efficiency equipment.

Fuji Electric has already manufactured 1,200 V/400 A rated insulated gate bipolar transistor (IGBT) modules that have a 3-level power conversion circuit in one package. Furthermore, in order to correspond to higher power needs, we have enhanced the part of the PrimePACK*¹ and have developed the “M404 Package,” a highly versatile 3-level high-power IGBT module package capable of meeting the demands of power conditioners (PCSs) for photovoltaic power generation, wind power generation and uninterruptible power supplies (UPSs). We have offered a line-up that contains three types: rated voltage of 1,200 V and a rated current of 450 A, 650 A and 900 A. The M404 Package can be easily interconnected in parallel, allowing them to be used in larger capacity equipment.

In this paper, we will describe the features and electrical characteristics of the M404 Package.

1. Features

The M404 Package is the package for high-power IGBT modules that integrates a thermistor and a 3-level conversion circuit in the existing high-power package PrimePack. Figure 1 shows the external appearance and outline drawing of the M404 Package. Table 1 lists the line-up and main features of the M404 Package.

- (a) Parallel connection is possible for increased power capacity.
- (b) Internal inductance is small due to the laminate structure of the main terminal bus bar inside the module.
- (c) Reduced module footprint can reduce the cooling fin area, enabling equipment to be downsized.
- (d) A built-in thermistor for temperature detection is installed.

*1: PrimePACK is a trademark or registered trademark of Infineon Technologies AG.

* Electronic Devices Business Group, Fuji Electric Co., Ltd.

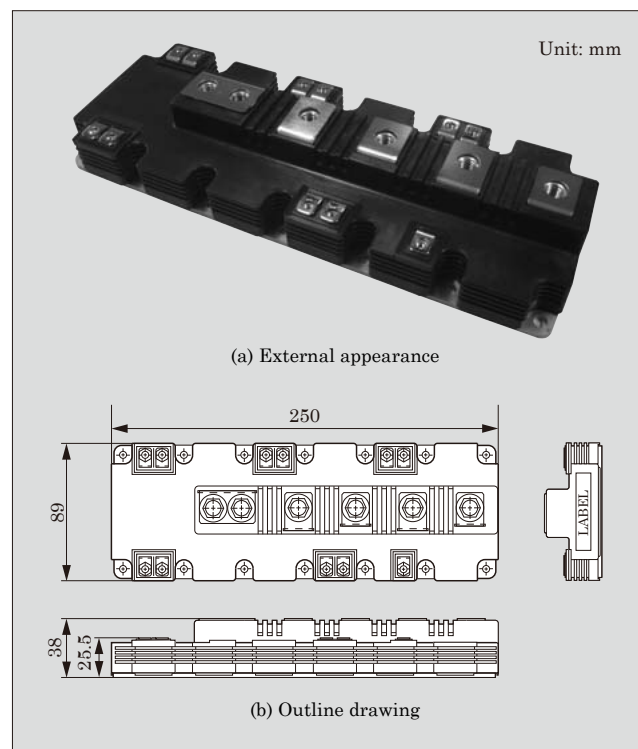


Fig.1 “M404 Package”

2. Electrical Characteristics

Using a reverse-blocking IGBT (RB-IGBT) reduces the number of elements, decreases an on-resistance, and improves conversion efficiency.

(1) Reduced conduction loss

The 3-level power conversion system has higher conversion efficiency than the 2-level power conversion system. There are two types of 3-level power conversion systems, namely, the advanced T-type neutral-point-clamped (AT-NPC) system that utilizes neutral-point bi-directional switching (AC switch) and the NPC system that connects switching elements in series. Figure 2 shows the equivalent circuit.

The AT-NPC system has fewer elements that conduct an electrical current than the NPC system, and this helps to reduce conduction loss. In addition, by employing Fuji Electric’s uniquely developed RB-IGBT for the AC switch, the number of elements will be decreased and conduction loss will be further reduced. Figure 3 shows the total generated loss and total efficiency in each conversion system. The AT-NPC sys-

Table 1 “M404 Package” line-up and main features

Item		Specification		
System		AT-NPC		
Type		4MBI450VB-120R1-50	4MBI650VB-120R1-50	4MBI900VB-120R1-50
Package dimensions		L250×W89×H38 (mm)		
Inverter	V_{CES}	1,200 V		
	I_C (IGBT)	450 A	650 A	900 A
	$-I_C$ (FWD)	450 A	650 A	900 A
	V_{GES}	±20 V		
	T_j	175 °C		
	T_{jop}	150 °C		
	$V_{GE(th)}$ (chip) $V_{GE}=20$ V	6.0 to 7.0 V ($I_C=450$ mA)	6.0 to 7.0 V ($I_C=650$ mA)	6.0 to 7.0 V ($I_C=900$ mA)
	$V_{CE(sat)}$ (chip) $V_{GE}=15$ V, $T_j=25$ °C	typ.1.85 V ($I_C=450$ A)	typ.1.8 V ($I_C=650$ A)	typ.1.85 V ($I_C=900$ A)
	V_F (chip) $T_j=25$ °C	typ.1.70 V ($I_C=450$ A)	typ.1.75 V ($I_C=650$ A)	typ.1.70 V ($I_C=900$ A)
	$R_{th(j-c)}$ (IGBT)	max. 0.068 °C/W	max. 0.049 °C/W	max. 0.038 °C/W
$R_{th(j-c)}$ (FWD)	max. 0.098 °C/W	max. 0.077 °C/W	max. 0.054 °C/W	
AC switch	V_{CES}	900 V		
	I_C (RB-IGBT)	450 A	650 A	900 A
	V_{GES}	±20 V		
	T_j	150 °C		
	T_{jop}	125 °C		
	$V_{GE(th)}$ (chip) $V_{GE}=20$ V	5.3 to 7.3 V ($I_C=450$ mA)	5.3 to 7.3 V ($I_C=650$ mA)	5.3 to 7.3 V ($I_C=900$ mA)
	$V_{CE(sat)}$ (chip) $V_{GE}=15$ V, $T_j=25$ °C	typ.2.30 V ($I_C=450$ A)	typ.2.25 V ($I_C=650$ A)	typ.2.30 V ($I_C=900$ A)
	$R_{th(j-c)}$ (RB-IGBT)	max. 0.063 °C/W	max. 0.047 °C/W	max. 0.034 °C/W
Common	V_{iso}	4,000 V AC (AC: 1 min)		

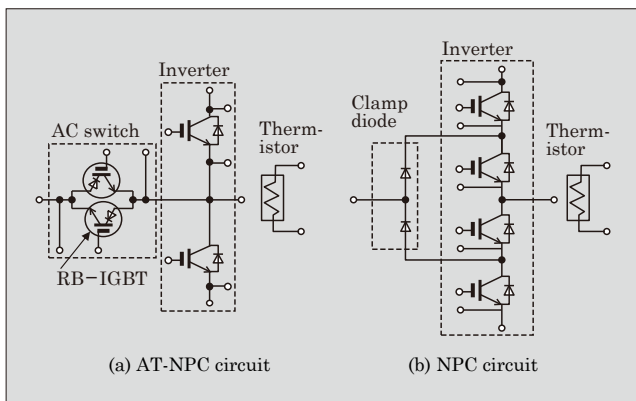


Fig.2 Equivalent circuit of 3-level IGBT module

tem that uses the RB-IGBT improves efficiency by 0.1 points when compared to a system that does not use the RB-IGBT. Compared to 2-level power conversion systems, efficiency has improved by 0.6 points.

(2) Optimized withstand voltage

As for existing 3-level products, the AC switch was composed of a RB-IGBT with a 600 V withstand voltage. In contrast, a bus voltage of 1,000 V DC is currently becoming increasingly mainstream in the field of photovoltaic power generation, and the AC switch

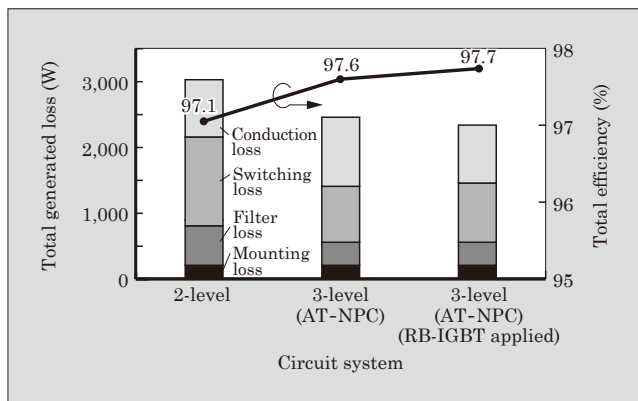


Fig.3 Total generated loss and total efficiency in each conversion system

part in this field switches at 500 V DC. As a result, existing elements with a withstand voltage of 600 V may be damaged due to overvoltage. On the other hand, for an existing RB-IGBT with a withstand voltage of 1,200 V, the increased on-voltage affects the amount of loss while a chip occupancy area increases and integration becomes problematic. Therefore, we have developed and optimized an RB-IGBT with a withstand voltage of 900 V, which has sufficient overvoltage tolerance against applied voltages.

Launch time

January 2015

Product Inquiries

Module Technology Department, Business Planning
Division, Electronic Devices Business Group, Fuji
Electric Co., Ltd.
Phone: +81-263-27-2943



Discrete SiC-SBD

ICHINOSE, Masaki*

Power semiconductors are used in large numbers for power electronics devices including power conditioners for photovoltaic power generation, DC/AC converters for wind power generation, and high-efficiency inverters for hybrid electric vehicles (HEVs), electric vehicles (EVs) and air conditioners. To reduce the power loss of power electronics devices, it is essential to improve the efficiency of power semiconductors. To that end, as next-generation semiconductors that break down the performance limits of conventional Si semiconductors, wide-bandgap semiconductors like SiC (silicon carbide) and GaN (gallium nitride) are being put to practical use. SiC features good physical properties as compared with Si such as a bandgap that is more than 3 times wider, an electric breakdown field that is 5 times higher, an electron saturation velocity that is 2 times higher and a thermal conductivity that is about 3 times as high, and it can be used at higher temperatures than Si. Replacing Si semiconductors with SiC semiconductors makes it possible to significantly reduce the power loss of power conversion circuits by decreasing the on-resistance of power semiconductors, and this realizes a substantial improvement in energy utilization efficiency and power saving of devices.

Fuji Electric has so far commercialized power semiconductor modules equipped with SiC-Schottky barrier diodes (SiC-SBDs) and has recently developed SiC-SBDs of 650 V/10 to 50 A and 1,200 V/18 to 36 A in discrete packages. This paper uses the 650 V/10 A product as a representative example to describe the features and application examples.

1. Features

1.1 Forward characteristics

Figure 1 shows the forward characteristics of an SiC-SBD. The forward voltage V_F of an SiC-SBD is lower than that of an Si-fast recovery diode (Si-FRD). Unlike an Si-FRD, it has a positive temperature coefficient and V_F increases as the temperature rises. When diodes are used in parallel, Si-FRDs show a decrease in V_F due to a temperature rise and the current flows more easily, which results in the current concentrating on some diodes. With SiC-SBDs, however, the currents of diodes at high temperatures are reduced due to increased V_F and the currents are shared among

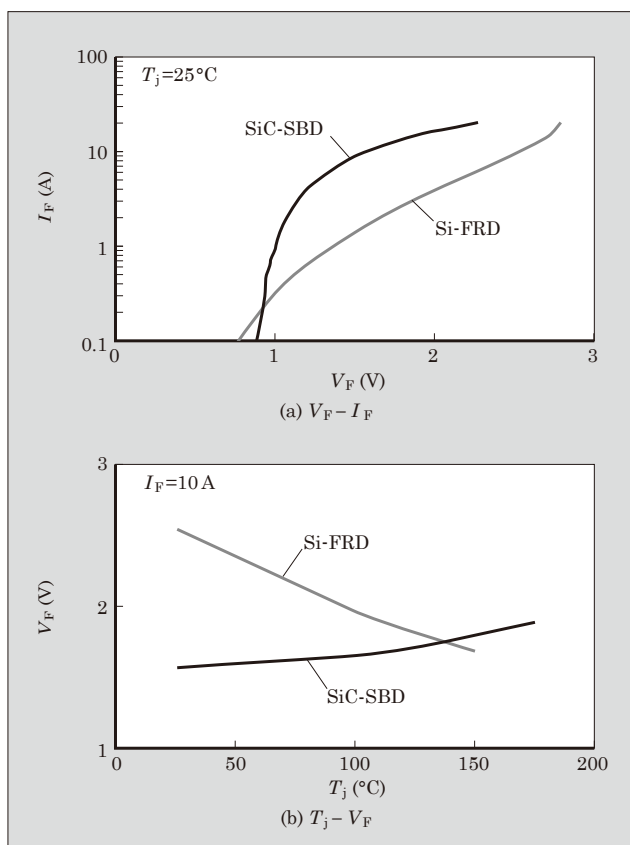


Fig.1 Forward characteristics

parallel diodes, facilitating parallel use. In addition, SiC-SBDs have less temperature dependency, which makes them suitable for high-temperature use.

1.2 Reverse characteristics

Figure 2 shows the reverse characteristics of an SiC-SBD. An SiC-SBD features a smaller reverse leakage current I_R than that of an Si-FRD. The current I_R is small even at a high temperature, which makes SiC-SBDs less prone to thermal runaway in high-temperature operation.

1.3 Switching characteristics

Figure 3 shows a comparison of switching waveforms between SiC-SBDs and Si-FRDs. An Si-FRD, which is characterized by bipolar operation, has an accumulation of minority carriers that take time to disappear and the switching speed depends on the temperature. Meanwhile, with an SiC-SBD, which

* Electronic Devices Business Group, Fuji Electric Co., Ltd.

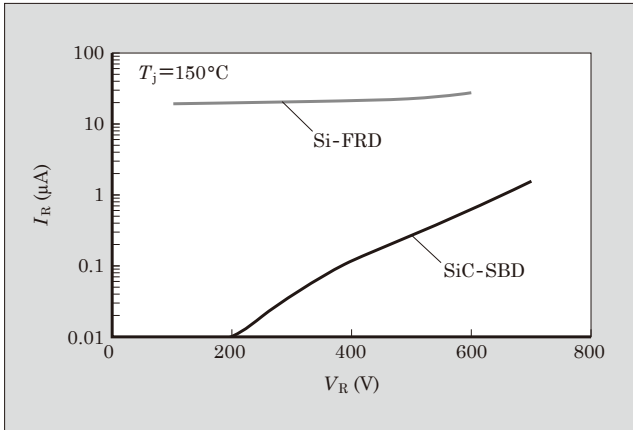


Fig.2 Reverse characteristics $V_R - I_R$

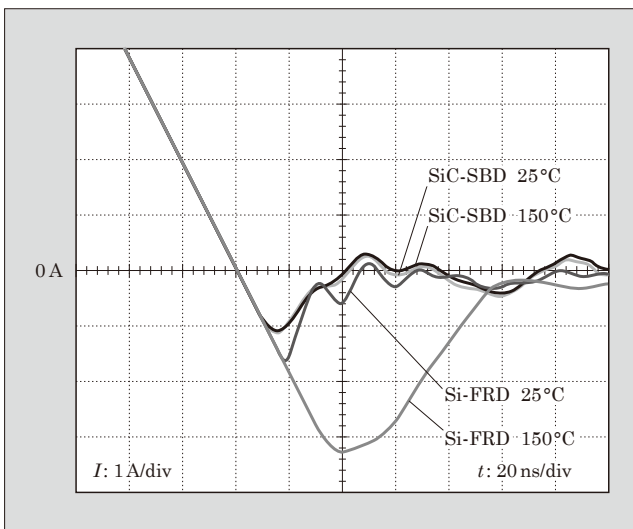


Fig.3 Switching waveforms

is a unipolar device, the contributor to conduction is majority carriers that do not have the accumulation effect and only current charging and discharging based on parasitic capacitance occur, which allows high-speed switching and causes little temperature dependency. In addition, a decreased switching current also decreases noise. These features make SiC-SBDs extremely advantageous for high-temperature, high-frequency operation.

2. Application Examples

Application examples of discrete SiC-SBDs include the chopper circuit of power conditioners for photovoltaic power generation (see Fig. 4) and DC/DC converters and inverters of quick chargers for electric vehicles (EVs). Reducing the switching loss makes a significant contribution to efficiency improvement, noise reduction and high-frequency driving. With power conditioners

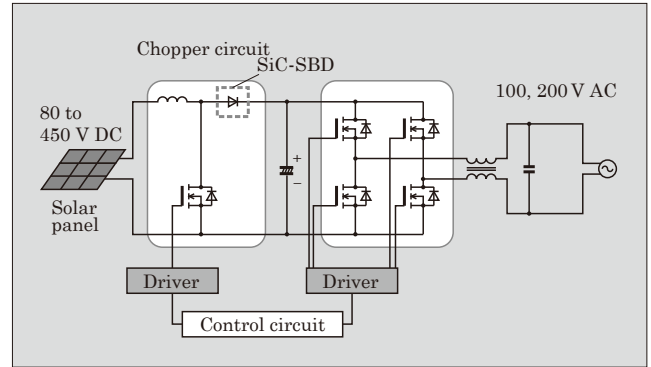


Fig.4 Photovoltaic power generation power conditioner

Table 1 Discrete SiC-SBD product lineup

Voltage (V)	Current (A)	Package			
		TO-220	TO-220F	T-Pack(s)	TO-247
650	10	FDCP10S65	FDCA10S65	FDCC10S65	FDCY10S65
	20	FDCP20C65	FDCA20C65	FDCC20C65	FDCY20C65
	25	FDCP25S65	FDCA25S65	FDCC25S65	FDCY25S65
	50	—	—	—	FDCY50C65
1,200	18	—	FDCA18S120	—	FDCY18S120
	36	—	—	—	FDCY36C120

for photovoltaic power generation, an improvement of efficiency in the current continuous mode, which requires high-speed switching, can be expected. For quick chargers for EVs, an ability to charge a high-output, large-capacity secondary battery in a short time is required and there are higher expectations for a significant improvement in power conversion efficiency.

Efficiency improvement and noise reduction decrease power loss and heat generation, which makes it possible to miniaturize or eliminate cooling mechanisms, noise suppression parts and peripheral parts. This realizes high-density mounting, which makes it possible to provide high-efficiency, high-reliability power supplies in small and lightweight units.

3. Product Lineup

Table 1 shows the discrete SiC-SBD product lineup.

Launch time

January 2015

Product Inquiries

Discrete & IC Technology Department, Business Planning Division, Electronic Devices Business Group, Fuji Electric Co., Ltd.
Phone: +81-263-25-2942

Product Line-Up of More Compact “MiniSKiiP” Packages

SEKINO, Yusuke* ISOZAKI, Makoto* KOMATSU, Kosuke*

As power integrated modules (PIMs) consisting of a converter circuit, an inverter circuit, a brake circuit and temperature sensor, Fuji Electric has developed new products with its latest “V Series” insulated gate bipolar transistor (IGBT) chip integrated in the very compact package “MiniSKiiP*1” and established a product line.

The demand of customers and market is to reduce the size of inverters while the efficiency should be increased. This trend leads to the necessity to reduce the size and the losses of IGBT Modules.

Fuji Electric has already developed a lineup of PIM-type “ECONOPIM*2” products that contribute to improved efficiency and inverter size reduction. By applying spring contact technologies and a base-plate less structure, the newly released MiniSKiiP products achieve a footprint reduction of 36% compared to con-

ventional ECONOPIM.

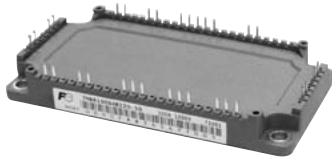
1. Features

1.1 Product lineup

Table 1 shows the MiniSKiiP product line up in comparison to the conventional ECONOPIM product lineup. While the rated current of conventional products reach from 25 A to 150 A, the new MiniSKiiP products cover a current range from 8 A to 100 A, which expands the existing lineup below 25 A rated current.

The MiniSKiiP module package type 1 are rated with 8 A and 15 A, while the next bigger MiniSKiiP module package type 2 can realize 25 A and 35 A rated current and type 3 rated currents are 75 A and 100 A. Figure 1 shows the MiniSKiiP 1 internal circuit config-

Table 1 Lineups of MiniSKiiP and ECONOPIM products

Rated current		8 A	15 A	25 A	35 A	50 A	75 A	100 A	150 A
MiniSKiiP (New product)	Package type	MiniSKiiP 1		MiniSKiiP 2		MiniSKiiP 3			————
	Appearance								————
	Footprint	MiniSKiiP 1 1,680 mm ²		MiniSKiiP 2 3,068 mm ² (36% reduced)		MiniSKiiP 3 4,838 mm ² (36% reduced)			————
	Weight	35 g		58 g (68% reduced)		91 g (70% reduced)			————
ECONOPIM (Conventional product)	Package type	————	ECONOPIM 2			ECONOPIM 3			————
	Appearance	————							————
	Footprint	————	ECONOPIM 2 4,837 mm ²			ECONOPIM 3 7,564 mm ²			————
	Weight	————	180 g			300 g			————

*1 MiniSKiiP: Trademark or registered trademark of SEMIKRON Elektronik GmbH & Co. KG

*2 ECONOPIM: Trademark or registered trademark of Infineon Technologies AG

* Electronic Devices Business Group, Fuji Electric Co., Ltd.

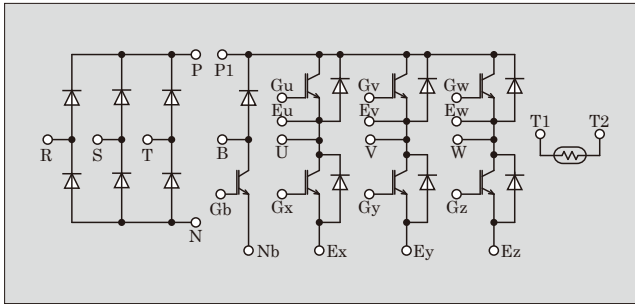


Fig.1 MiniSKiiP 1 internal circuit configuration

uration. Since a 3-phase converter circuit, a 3-phase inverter circuit, a brake circuit and temperature sensor are integrated into one package, it enables 3-phase AC inverter designs with only one unit. This contributes to the downsizing of inverter system and improves the design efficiency.

1.2 Package downsizing

As shown in Table 1, a comparison at the same rated current shows that MiniSKiiP 2 achieves a footprint reduction of 36% and weight reduction of 68% compared to ECONOPIM 2. MiniSKiiP 3 realizes a footprint reduction of 36% and weight reduction of 70% compared to ECONOPIM 3.

1.3 Reduction of mounting worktime

Figure 2 shows the cross-section of MiniSKiiP and ECONOPIM mounted on an inverter.

MiniSKiiP products adopt a spring contact structure without solder. This allows simultaneous mounting of the module and the printed circuit board (PCB) on the heat sink with only one screwing process.

On the other hand, with ECONOPIMs products, the PCB mounting has to be done separately, before

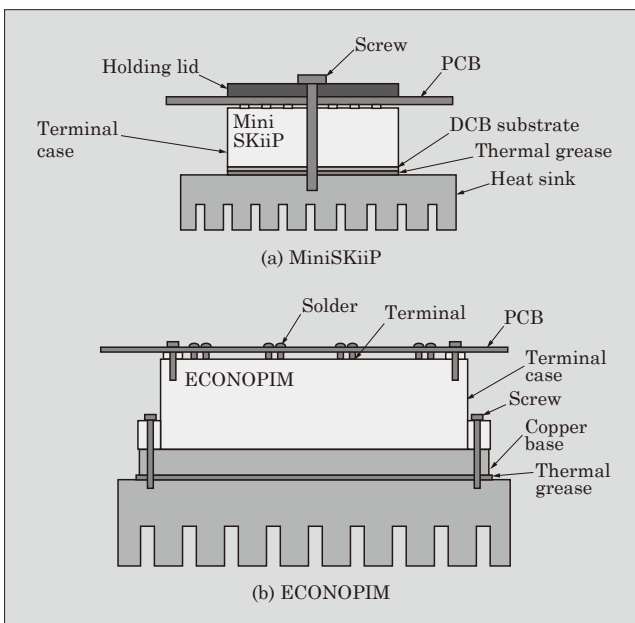


Fig.2 Cross-sectional views of modules mounted on inverter

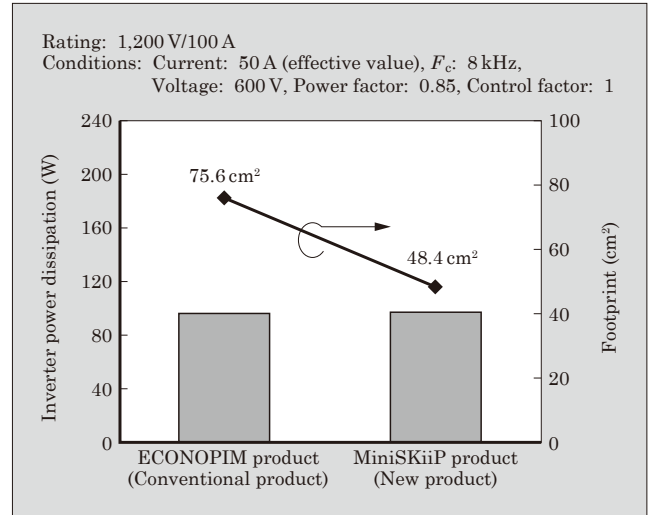


Fig.3 Inverter power dissipation and module footprint

or after mounting the module on the heat sink. The MiniSKiiP mounting technology described above simplifies the assembly of inverters by reduction of screwing worktime and soldering worktime.

1.4 Reduction of power dissipation

Figure 3 shows a comparison of inverter power dissipation by the inverter circuit against the module footprint of a MiniSKiiP and an ECONOPIM module with a 1,200 V/100 A rating. MiniSKiiP achieves a reduction of the module's footprint compared to the ECONOPIM with similar low loss.

2. Background Technologies

MiniSKiiP products realize great downsizing by high-density mounting with spring contact structure and optimized insulation gel.

2.1 High-density mounting

Figure 4 shows the internal structures of the MiniSKiiP and ECONOPIM products. With ECONOPIM products, the limiting factor for package size reduction is the required area on the direct copper bonding (DCB) substrate for the aluminum wire bonding to connect the DCB substrate to main terminals. For MiniSKiiP in comparison the main terminals are directly connected to the DCB allowing the greatly reduced footprint.

As a result, significant miniaturization has been achieved.

2.2 Spring contact structure

MiniSKiiP products further advantages are realized for the inverter assembly process by realizing solderless assembly using spring contact structure for the terminal connections.

Figure 5 shows a cross-sectional view after PCB mounting.

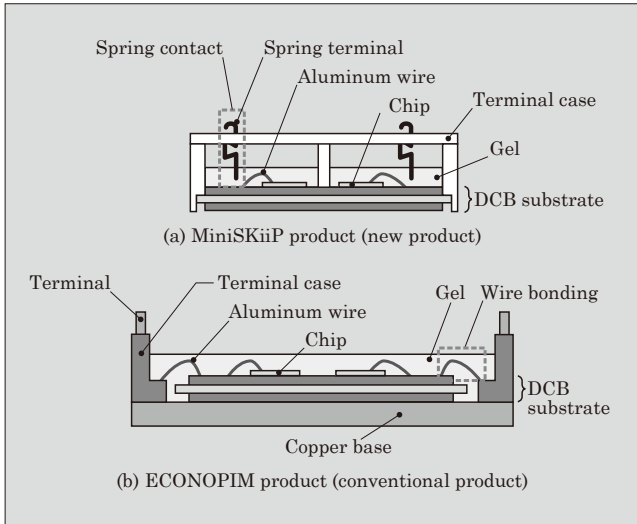


Fig.4 Internal structure

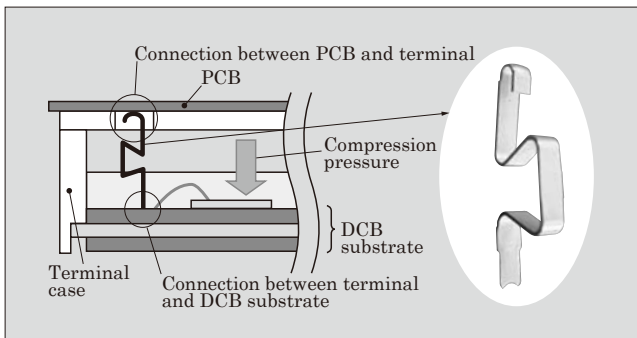


Fig.5 Cross-sectional view after PCB mounting

By tightening the main screw, the force applied on the PCB is compressing the spring establishing a stable connection while at the same time the MiniSKiiP modules is mounted to the heat sink.

2.3 Optimization of insulating material

While with ECONOPIM products, the creepage distance is secured considering the rated isolation voltage. With MiniSKiiP modules, the decreased creepage distance related to the downsizing concerns about the decrease of an isolation voltage.

These concerns were solved by changing the commonly used isolation gel to a newly developed gel. By applying this new gel, MiniSKiiP realizes a highly reliable package characteristics ensuring equivalent or higher voltage withstand capabilities comparing to the ECONOPIM packages.

Launch time

April 2015

Product Inquiries

Module Technology Department, Business Planning Division, Electronic Devices Business Group, Fuji Electric Co., Ltd.
Phone: +81-263-25-2943

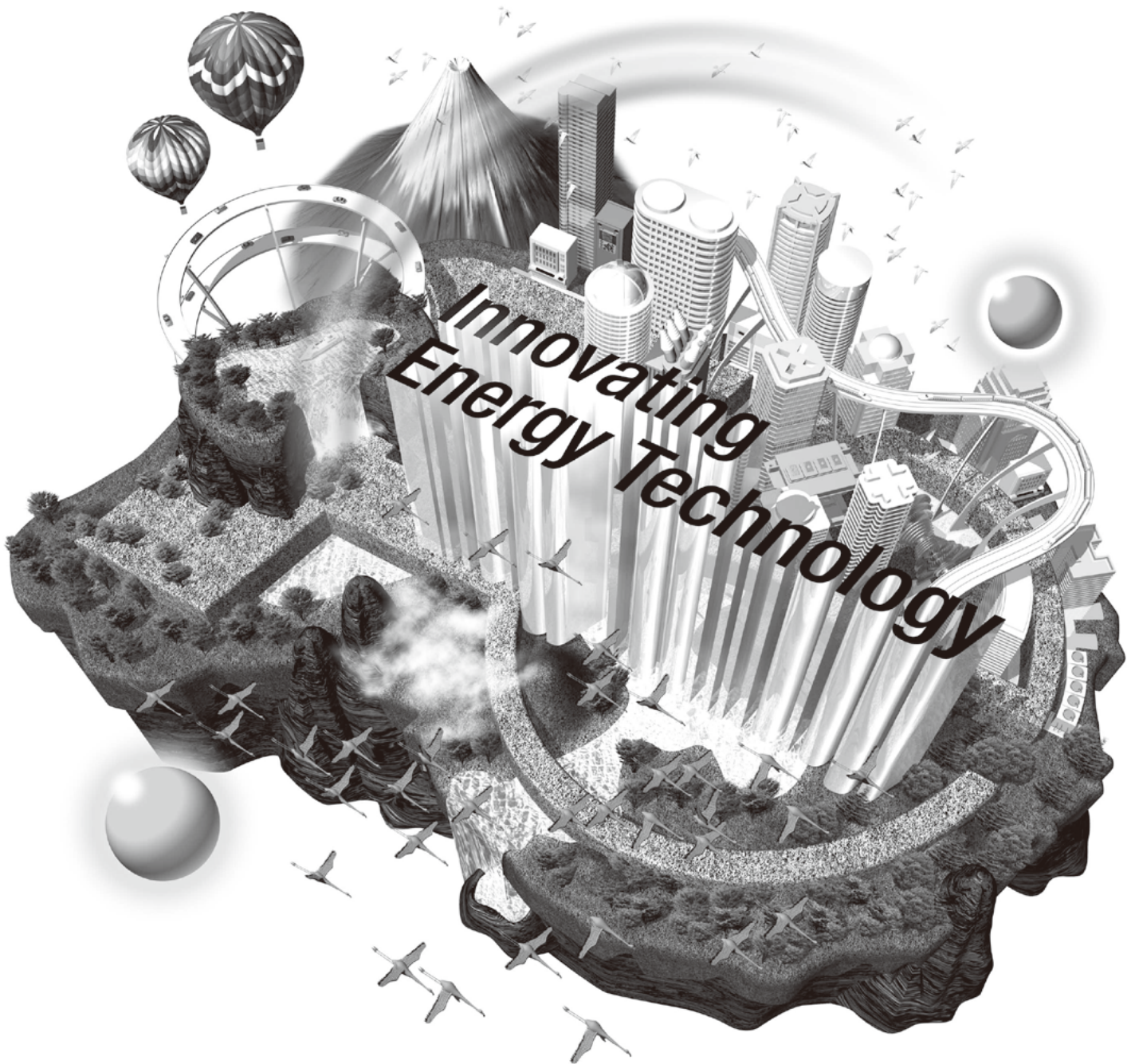
Integration of the Future

Fuji Electric's power semiconductors densely containing our unique power electronics technology and possibility of application. We have been improving these key devices to have a high withstanding voltage, high capacitance, low power loss, and compact & light-weight package. The key devices have vigorously playing active parts in the clean energy field including photovoltaic and wind power generation, the energy conservation field, demanded in the industry and the home, and the traffic field including hybrid and electric vehicles. Moreover, we have been developing the next generation power semiconductors of higher performance using new material SiC. Fuji Electric will continue to renovate energy technologies and contribute to realize a safe, secure and sustainable society.



Fuji Electric's power semiconductors

Innovating Energy Technology



Through our pursuit of innovation in electric and
thermal energy technology,
we develop products that maximize energy efficiency and
lead to a responsible and sustainable society.

Overseas Subsidiaries

* Non-consolidated subsidiaries

America

Fuji Electric Corp. of America

Sales of electrical machinery and equipment, semiconductor devices, drive control equipment, and devices

Tel +1-732-560-9410

URL <http://www.americas.fujielectric.com/>

Fuji Electric Brazil-Equipamentos de Energia Ltda *

Sales of inverters, semiconductors, and power distribution

Tel +55-11-2283-5991

URL <http://www.americas.fujielectric.com/portugues>

Asia

Fuji Electric Asia Pacific Pte. Ltd.

Sales of electrical distribution and control equipment, drive control equipment, and semiconductor devices

Tel +65-6533-0014

URL <http://www.sg.fujielectric.com/>

Fuji Electric (Thailand) Co., Ltd. *

Sales and engineering of electric substation equipment, control panels, and other electric equipment

Tel +66-2-210-0615

Fuji Electric Manufacturing (Thailand) Co., Ltd.

Manufacture and sales of inverters (LV/MV), power systems (UPS, PCS, switching power supply systems), electric substation equipment (GIS) and vending machines

Tel +66-2-5292178

Fuji Electric Vietnam Co.,Ltd. *

Sales of electrical distribution and control equipment and drive control equipment

Tel +84-4-3935-1593

Fuji Furukawa E&C (Vietnam) Co., Ltd. *

Engineering and construction of mechanics and electrical works

Tel +84-4-3755-5067

PT. Fuji Electric Indonesia *

Sales of inverters, servos, UPS, tools, and other component products

Tel +62 21 398-43211

Fuji Electric India Pvt. Ltd. *

Sales of drive control equipment and semiconductor devices

Tel +91-22-4010 4870

URL <http://www.fujielectric.co.in>

Fuji Electric Philippines, Inc.

Manufacture of semiconductor devices

Tel +63-2-844-6183

Fuji Electric Semiconductor (Malaysia) Sdn. Bhd.

Manufacture of semiconductor devices

Tel +60-4-494-5800

URL <http://www.fujielectric.com.my/>

Fuji Electric (Malaysia) Sdn. Bhd.

Manufacture of magnetic disk and aluminum substrate for magnetic disk

Tel +60-4-403-1111

URL <http://www.fujielectric.com.my/>

Fuji Furukawa E&C (Malaysia) Sdn. Bhd. *

Engineering and construction of mechanics and electrical works

Tel +60-3-4297-5322

Fuji Electric Taiwan Co., Ltd.

Sales of semiconductor devices, electrical distribution and control equipment, and drive control equipment

Tel +886-2-2511-1820

Fuji Electric Korea Co., Ltd.

Sales of power distribution and control equipment, drive control equipment, rotators, high-voltage inverters, electronic control panels, medium- and large-sized UPS, and measurement equipment

Tel +82-2-780-5011

URL <http://www.fujielectric.co.kr/>

Fuji Electric Co.,Ltd. (Middle East Branch Office)

Promotion of electrical products for the electrical utilities and the industrial plants

Tel +973-17 564 569

Fuji Electric Co., Ltd. (Myanmar Branch Office)

Providing research, feasibility studies, Liaison services

Tel +95-1-382714

Representative office of Fujielectric Co., Ltd. (Cambodia)

Providing research, feasibility studies, Liaison services

Tel +855-(0)23-964-070

Europe

Fuji Electric Europe GmbH

Sales of electrical/electronic machinery and components

Tel +49-69-6690290

URL <http://www.fujielectric-europe.com/>

Fuji Electric France S.A.S

Manufacture and sales of measurement and control devices

Tel +33-4-73-98-26-98

URL <http://www.fujielectric.fr/>

China

Fuji Electric (China) Co., Ltd.

Sales of locally manufactured or imported products in China, and export of locally manufactured products

Tel +86-21-5496-1177

URL <http://www.fujielectric.com.cn/>

Shanghai Fuji Electric Switchgear Co., Ltd.

Manufacture and sales of switching equipment, monitoring control appliances, and related facilities and products

Tel +86-21-5718-1234

URL <http://www.fujielectric.com.cn/sfswgr/>

Shanghai Fuji Electric Transformer Co., Ltd.

Manufacture and sales of molded case transformers

Tel +86-21-5718-7705

URL <http://www.fujielectric.com.cn/sfswgr/>

Wuxi Fuji Electric FA Co., Ltd.

Manufacture and sales of low/high-voltage inverters, temperature controllers, gas analyzers, and UPS

Tel +86-510-8815-2088

Fuji Electric (Changshu) Co., Ltd.

Manufacture and sales of electromagnetic contactors and thermal relays

Tel +86-512-5284-5642

URL <http://www.csfe.com.cn/>

Fuji Electric (Zhuhai) Co., Ltd.

Manufacture and sales of industrial electric heating devices

Tel +86-756-7267-861

<http://www.fujielectric.com.cn/fez/>

Fuji Electric (Shenzhen) Co., Ltd.

Manufacture and sales of photoconductors, semiconductor devices and currency handling equipment

Tel +86-755-2734-2910

URL <http://www.sz.fujielectric.com.cn/FUJIWebSite/index.html>

Fuji Electric Dalian Co., Ltd.

Manufacture of low-voltage circuit breakers

Tel +86-411-8762-2000

Fuji Electric Motor (Dalian) Co., Ltd.

Manufacture of industrial motors

Tel +86-411-8763-6555

Dailan Fuji Bingshan Vending Machine Co.,Ltd.

Development, manufacture, sales, servicing, overhauling, and installation of vending machines, and related consulting

Tel +86-411-8754-5798

<http://www.fushibingshan.com/index.html>

Fuji Electric (Hangzhou) Software Co., Ltd.

Development of vending machine-related control software and development of management software

Tel +86-571-8821-1661

URL <http://www.fujielectric.com.cn/fhs/cn/>

Zhejiang Innovation Fuji Technology Co., Ltd. *

Design, development, and services pertaining to software

Tel +86-571-8827-0011

URL <http://www.fujielectric.com.cn/sif/>

Fuji Electric FA (Asia) Co., Ltd.

Sales of electrical distribution and control equipments

Tel +852-2311-8282

URL <http://www.fea.hk/>

Fuji Electric Hong Kong Co., Ltd.

Sales of semiconductor devices and photoconductors

Tel +852-2664-8699

URL <http://www.sz.fujielectric.com.cn/hkeng/company/index.htm>

Hoei Hong Kong Co., Ltd.

Sales of electrical/electronic components

Tel +852-2369-8186

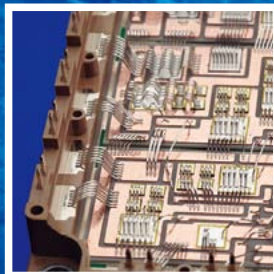
URL <http://www.hoei.com.hk/>

Innovating Energy Technology

Through our pursuit of innovation in electric and thermal energy technology, we develop products that maximize energy efficiency and lead to a responsible and sustainable society.



Corrosion Resistant, Material, and Hot Water Utilization Technology
Geothermal Power Plants



Device Technology
Power Devices (IGBT)



Power Electronics Technology
Power Conditioning Systems (PCS)
for Megasolar Plants



Power Electronics Technology
Inverters



Power Electronics Technology
Uninterruptible Power Supply
Systems (UPS)



Heat Exchange and Refrigerant Control Technology
Hybrid Heat Pump
Vending Machines

F Fuji Electric